2023 Trabecular Meshwork Study Club

December 7 – 9, 2023

Hilton near Duke

3800 Hillsborough Rd, Durham, NC

Table of Contents

2023 Agenda

Thursday, December 7th		
6:30PM – 8:30PM - Opening Reception, at the Hilton near Duke, Durham, NC		
Friday, December 8th		
8:00	Samples, John	Introduction
I. Proteomic and Transcriptomics of the TM — Markus Kuehn, moderator		
8:15	Elliott, Michael	1. Proteomic Analysis of the Caveolae Interactome in Human Trabecular Meshwork Cells
8:30	McLellan, Gillian	2. Transcriptomic profiling of laser capture micro-dissected trabecular meshwork reveals early molecular effects of LTBP2 mutation prior to glaucoma development
8:45	Keller, Kate	3. Profiling IOP-responsive genes in anterior and posterior tissues in the CEI glaucoma model
9:00	Balasubramanian, Ravethi	4. Development of the Schlemm's canal and the trabecular meshwork: Insights from single cell RNA sequencing
II. Schlemm's Canal – Paloma Liton, moderator		
9:15	Thomson, Ben	5. Lymphatic characteristics of the Schlemm's canal endothelium
9:30	Fang, Raymond	6. In Vivo Optical Coherence Tomography for Noninvasive Imaging of Collector Channels
9:40	Ethier, Ross	7. An assay for studying Schlemm's canal inner wall mechanobiology
9:55 – 10:40 Break		
II. Schlemm's Canal, continued – Paloma Liton, moderator		
10:40	Singh, Ayushi	8. Identifying cellular and nuclear changes in Schlemm's canal cells interacting with glaucomatous trabecular meshwork cells in a 3D ECM hydrogel co-culture model
10:50	Herberg, Samuel	9. Targeting YAP/TAZ mechanosignaling to ameliorate stiffness-induced Schlemm's canal cell pathobiology
III. Segmental outflow – Kate Keller, moderator		
11:05	Reina-Torres, Ester	10. VEGF expression is elevated in high-flow regions of mouse trabecular meshwork
11:20	Peters, Donna	11. Digital Spatial Profiling of Segmental Outflow Regions in Trabecular Meshwork Reveals a Role for ADAM15
11:35	Li, Hoi Lam	12. Segmental Uveoscleral Outflow in Monkey Eyes
11:45	McDowell, Colleen	13. Nerve innervation of high and low flow regions of the TM and Schlemm's canal.

12:05 – 1:35 Lunch		
IV. Stem cells – Kate Keller, moderator		
1:35	Kelley, Mary	14. RNA Seq Analysis of Expression Differences of Human TM Cells and TM Insert Stem Cells
1:50	Kuehn, Markus	15. Reduced abundance of trabecular meshwork stem cells (TMSC) in human donor eyes with POAG
2:05	Du, Yiqin	16. Activation of Endogenous Trabecular Meshwork Stem Cells
V. Animal models – Gillian McLellan, moderator		
2:20	Zhang, Hao	17. Freeform visible-light OCT to quantify anterior chamber volume in mice.
2:35	Kitzhatil, Krish	18. A role for the arginine transporter SLC7A1 in regulating aqueous humor outflow
2:50	Nair, Sai	19. Post GWAS Approaches: From Association to Function of IOP Genes"
3:05	Liton, Paloma	20. Autophagy deficiency protects against ocular hypertension in an experimental and spontaneous glaucoma mouse models
3:20	West-Mays, Judy	21. Testing of IOP lowering drugs in a mouse model of glaucoma
3:35	Gong, Haiyan	22. Investigation of the morphological changes in the trabecular outflow pathway associated with thrombospondin-1-induced outflow facility decrease in porcine eyes
3:50 – 4:35 Break		
VI. TM Biomechanics – Ross Ethier, moderator		
4:35	Karimi, Alireza	23. Dynamic 3D Traction Force in Normal and Glaucomatous Human TM Cells
4:50	McDonnell, Fiona	24. The Effects Of Mechanical Stimuli On Trabecular Meshwork Extracellular Vesicles
5:05	Krizaj, David	25. TRPV4 and IOP: What is going on?

6:00	**Depart for Group Dinner at Parazide, 2200 W Main St, Durham.**

Saturday, December 9th		
VII. Keynote		
8:00	Borras, Terete	A journey from … DNA Reassociation Kinetics to … Gene Therapy of Glaucoma
VIII. TM Cell Signaling and Regulation – Donna Peters, moderator		
8:45	Mao, Weiming	26. Deciphering the role and origin of cross-linked actin networks in the trabecular meshwork

9:00	Russell Randall, Karen	27. Opioid Receptor-Mediated Mechanisms in Maintaining IOP
9:15	Liu, Yutao	28. Estrogen Receptors, Biomechanical Factors, and Trabecular Meshwork
9:30	Rudzitis, Christopher	29. Signaling cytokines, mechanochannels, and ocular hypertension.
9:40	Battacharya, Sanjoy	30. Metabolites of Aqueous humor and deposit formation
9:55	Rao, Vansanth	31. Role of Dysregulated Glypicans in the Pathobiology of Ocular Hypertension
10:10 – 10:55 Break		
IX. White paper discussion #1		
10:55	Acott, Ted	White Paper #3: Consensus recommendations for ex vivo intraocular pressure regulation studies – for final discussion
11:45 – 1:15 Lunch		
X. Clinical – Shan Lin, moderator		
1:15	Lieberman, Raquel	32. Targeted degradation of mutant myocilin with tailored antibodies
1:30	Roddy, Gavin	33. Transgene expression of Stanniocalcin-1 for sustained IOP reduction
1:45	Willoughby, Colin	34. Preliminary Evaluation of NOX4 Inhibition to Prevent FibROSis in the TM
2:00	Toris, Carol	35. Successes and failures of novel glaucoma drainage devices; Preclinical studies of outflow facility
2:15-3:00 Break		
XI. Clinical Laboratory - John Samples, moderator		
3:00	Challa, Pratap	36. Clinical Glaucoma for scientists, Part I
3:15	Asrani, Sanjay	37. Clinical Glaucoma for scientists, part II
3:30	Fellman, Ronald	38. What Glaucoma doctors want meshworkers to know about the canal
3:45	Danias, John	39. The role of tissue plasminogen activator in regulating outflow
4:00	Steele, Cynthia	40. Overcoming Barriers with Intracameral Drug Delivery
XII. White paper discussion #2		
4:15	Toris, Carol	White Paper #4: Consensus recommendations for tonography methods to assess outflow facility – draft for comments
	Dan Stamer & John Samples	Closing comments, evaluation & stipends

Sunday, December 10th
9:00-10:30AM: Optional perfusion demonstration at the lab.

I. Proteomic and Transcriptomics of the TM

1. Proteomic Analysis of the Caveolae Interactome in Human Trabecular Meshwork Cells

Michael H. Elliott[1], Nikolai P. Skiba[2], Olawale Bankole[1], Michael De Ieso[2] and W. Daniel Stamer[2]

[1] Dept. of Ophthalmology, Dean McGee Eye Institute, Oklahoma City, OK, USA
[2] Dept. of Ophthalmology, Duke Eye Center, Duke University, Durham, NC, USA

Purpose: Variants at the *CAV1* gene locus, which codes for the caveolae scaffolding protein, caveolin-1 (CAV1), are associated with risk of primary open angle glaucoma (POAG) and with elevated intraocular pressure (IOP). Caveolae domains are common features of many cells and the CAV1 protein differentially scaffolds a wide array of proteins in cell-specific contexts. Caveolae are abundant features of resident cells in the conventional outflow tract, including the trabecular meshwork (TM) where it has been implicated in control of contractile tone and cell adhesion, *in vitro*. Ablation of CAV1 (and caveolae) in mice, both globally and specifically in the TM, results in IOP elevation and reduced outflow facility. However, the molecular machinery connecting caveolae to TM contractility/ECM production and, by implication, to IOP is currently unknown. As a first step in addressing this knowledge gap, we set out to define the protein landscape of caveolae in TM.

Methods: To define the CAV1 interactome in human TM cells, we immunoprecipitated CAV1 from three authenticated human TM cell strains (HTM 86, 150, 151) using highly specific CAV1 antibody. Control immunoprecipitations using normal rabbit IgG were done in parallel to evaluate specificity. We first validated the immunoprecipitation and immune complex elution efficiencies by immunoblot analysis. We then proceeded to evaluate CAV1 immune complexes by unbiased, quantitative mass spectrometry (Mass Spectrometry/Molecular Biology Core Module at Duke University Eye Center). Positive interacting proteins (≥ 2 peptides) were compared between CAV1 and control IgG immunoprecipitations to determine proteins significantly enriched in CAV1 immune complexes. Interactome maps were generated using STRING databases (https://string-db.org/). To validate the mass spectrometry data, we assessed putative CAV1-interacting proteins by immunoblot analyses of CAV1 immune complexes.

Results: CAV1 was quantitatively precipitated from human TM cell lysates (50-120 µg of total protein) and efficiently eluted for mass spectrometric analyses. Using the most stringent criteria (≥2 peptides; ≥2-fold enrichment; ANOVA $p<0.05$), we identified 55 interacting proteins including known, bona fide caveolae proteins (CAV2, PTRF/CAVIN1, PRKCDBP/CAVIN3, EHD2), known lipid raft proteins (FLOT2, STOM), and a key protein that links caveolae to actin stress fibers (FLNA). We also identified several novel interactions relevant to mechanobiology including interaction with myosin phosphatase rho-interacting protein (MPRIP), desmosomal proteins (DSP,

DSG1), and an ECM remodeling protein (LOX). We confirmed the interaction with PTRF/CAVIN1 and EHD2 by immunoblotting.

Conclusion: The CAV1 interactome from human TM cells is enriched in proteins involved in caveolae biogenesis, protein localization to lipid rafts, receptor-mediated endocytosis, cell-cell adhesion, and cytoskeletal protein binding. These results provide the framework for the future studies designed to evaluate the impact of mechanical stimulation on the mechanically-sensitive caveolae interactome.

Support: R01EY028608, P30EY005722, P30EY021725, R01EY022359, and Research to Prevent Blindness.

2. Transcriptomic profiling of laser capture micro-dissected trabecular meshwork reveals early molecular effects of *LTBP2* mutation prior to glaucoma development.

McLellan, Gillian J.[1,2], Torné Escudé, Odalys[1,2], Kiland, Julie A.[2], Oikawa, Kazuya[1,2].

[1] Surgical Sciences - School of Veterinary Medicine, University of Wisconsin-Madison, Madison, WI, USA.
[2] Ophthalmology and Visual Sciences, University of Wisconsin-Madison School of Medicine and Public Health, Madison, WI, USA.

Introduction: Mutations in *LTBP2* are implicated in the pathogenesis of various forms of human glaucoma ranging from primary and secondary pediatric glaucoma, to adult-onset open angle glaucoma. Importantly, LTBP2 (Latent Transforming Growth Factor-β-Binding Protein 2) is highly and preferentially expressed in ocular tissues critical to IOP regulation, notably the TM and ciliary epithelium. Uniquely among LTBP isoforms, LTBP2 does not bind TGFβ directly and the developmental, cellular, and molecular mechanisms responsible for elevated IOP in humans bearing *LTBP2* mutations, remain unresolved. Based on published work in other tissues, reports of differential expression under glaucoma conditions in ocular tissues and *in vitro*, and preliminary data, we formulated a **central hypothesis** that perturbation of LTBP2 expression contributes to glaucoma by modifying outflow pathway development and homeostasis. A spontaneous, fully penetrant, recessively inherited genetic model of glaucoma in cats, with causal mutation in *LTBP2*, represents the only currently known large animal homolog of inherited glaucoma in humans and is maintained in a viable colony for translational research. Congenital morphologic abnormalities have not been identified in the trabecular meshwork (TM) and distal outflow pathway of neonates in our spontaneous feline model of glaucoma due to *LTBP2* mutation. IOP elevation becomes evident within the first few months of life and is associated with progressive ECM and TM cell pathology and distal outflow vessel collapse in this model. In previous studies we identified the earliest detectable pathology by electron microscopy in 2 week old cats. This consisted of subtle attenuation of elastic fibers, accumulation of microfibrils and TM cell swelling.

Purpose: To elucidate molecular mechanisms responsible for this post-natal developmental pathology. Transcriptomic profiling by RNAseq affords an unbiased approach to discovery of novel mechanisms and interactions. As there can be substantial sub-regional heterogeneity in pathology and gene expression within the outflow pathways, we elected to use laser capture microdissection (LCM) to reduce the likelihood of missing subtle and/or highly localized differences in gene expression that could still have great pathological significance.

Methods: For LCM, two randomly selected quadrants were dissected from one eye under nuclease free conditions for each of four 2 week-old *LTBP2* homozygous mutant and 4 wild-type age-matched cats immediately following humane euthanasia. Tissues were cryoembedded in optimal cutting temperature (OCT) compound and stored at -80°C prior to sectioning at 10µm onto nuclease-free polyethylene naphthalate (PEN) membrane slides (Zeiss). A total of 48 sections were obtained from each eye, and 3 sections mounted on each slide were stained with the Arcturus HistoGene™ LCM frozen section staining kit (ThermoFisher). Trabecular meshwork was selected under 10X objective, UV-laser dissected and catapulted into nuclease free adhesive caps of 500µl microcentrifuge tubes (Zeiss) using the Palm MicroBeam system with motorized RoboStage (Zeiss). RNA was extracted and gDNA eliminated by RNeasy Plus Micro Kit (Qiagen). Our settings and protocol were optimized for collagenous tissue dissection and repeated LCM avoided. LCM-derived samples were pooled from multiple tissue sections of individual cats, but not between cats, to maximize the number of biological replicates (4 per condition) and ensure adequate power for robust downstream analyses. Quantity, integrity and purity of RNA was assessed by Eukaryote Total RNA Pico-Chip / Bioanalyzer 2100 (Agilent Technologies). Only high-quality samples with RIN ≥6 (RIN ≥7 from adjacent tissues); distinct 28S rRNA and 18S rRNA electropherogram peaks, and RNA quantity ≥2000pg/ µl) was used in downstream applications. UW-Madison's Biotechnology Center Gene Expression Center conducted the library prep and RNAseq. Briefly, libraries were constructed using the SMART-Seq v4 Ultra Low Input RNA Kit for Sequencing (Takara Bio; Kusatsu, Japan) and sequenced on an Illumina NovaSeq 6000 platform (Illumina, Inc.) to obtain 150 bp strand-specific paired-end reads with approximately 33 million read depth per sample on average. Libraries were normalized and multiplexed across lanes (to limit batch effects) for sequencing Generated raw reads were quality-filtered by Skewer version 0.2.2. Trimmed reads were mapped to Felis catus reference genome (NCBI RefSeq assembly GCF_018350175.1) using STAR version 2.7.11 followed by estimation of transcript abundances using RSEM version 1.3.3 and DESeq2 version 1.39 was used to detect differentially expressed genes (DEGs) between groups, with false discovery rate (FDR)≤ 0.05 considered significant. To provide a functional context for the DEGs identified, we utilized a functional enrichment analysis on g:Profiler by gene ontology (GO) terms, Kyoto Encyclopedia of Genes and Genomes (KEGC), Reactome and WikiPathways. As a validation step, RNAscope in situ hybridization (ACD Biotechne) used custom, commercially available feline probes.

Results: Laser capture microdissection of feline trabecular meshwork from frozen tissue sections yielded acceptable quality and quantity of RNA for downstream applications (Fig.1). Initial bioinformatic analyses have identified a total of 67 DEGs in the TM of *LTBP2* mutant cats relative to normal, wild-type age-matched cats. Of these 36/67 (54%) were upregulated and 31/67 were downregulated (46%), and 49% of expression changes were less than two-fold. Among the upregulated DEGs,

overrepresented biological processes included anatomical structure morphogenesis and development, regulation of cell communication, smooth muscle and lymphatic endothelial cell migration, cell differentiation and organic anion transport. Over-represented molecular functions of upregulated DEGs included gap junction hemi-channel activity, store-operated calcium channel activity and protein binding. On functional enrichment analysis, downregulated DEGs were involved in cytoplasm, extracellular region, fibronectin binding, regulation of cell proliferation, calcium ion binding, phospholipid-hydroperoxide glutathione peroxidase activity and benzaldehyde dehydrogenase (NAD+ and NAD(P)+) activity, collagen binding, prostaglandin F receptor activity, angiotensin type I and II receptor activity, and the lysosome.

Conclusions: We have developed and optimized a robust and reproducible method for LCM of highly collagenous TM tissue from large eyes, enabling RNA isolation of sufficient quality and quantity for downstream transcriptomic approaches. Applying these methods across different time-points in post-natal development in this large animal glaucoma model will yield further insight into the role of LTBP2 in development and homeostasis of the proximal aqueous humor outflow pathway.

Support: An unrestricted award to the University of Wisconsin-Madison Department of Ophthalmology and Visual Sciences from Research to Prevent Blindness; an award to Odalys Torne from La Caixa Foundation and NIH Grants R21 EY034373, Vision Research Core grant P30 EY016665, and Shared Instrumentation grant S10 OD026957. Satoshi Kinoshita prepared cryosections and membrane slides in the Translational Research Initiatives in Pathology Lab, which receives support from the University of Wisconsin Carbone Cancer Center Grant P30 CA014520.

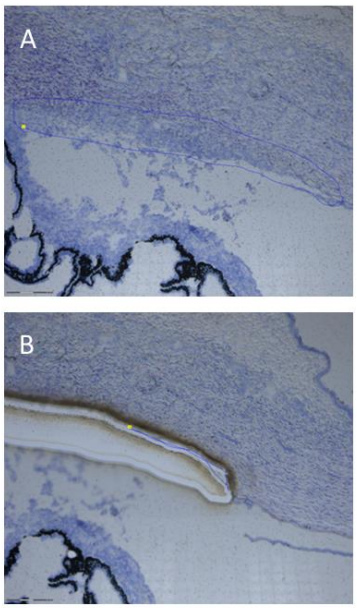

Figure 1: (A) In laser capture microdissection, the TM region is delineated as the region of interest (thin blue line) before (B) the TM tissue is cut from the adjacent fibrous sclera by UV laser, catapulting it into the collection tube cap. (C) Representative RNA sample quality (pooled sample from multiple tissue sections)

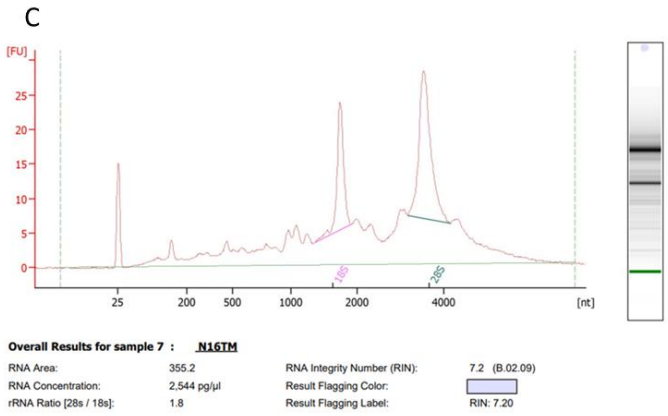

3. Profiling IOP-responsive genes in anterior and posterior tissues in the CEI glaucoma model

Kate E. Keller, Diana C. Lozano, Yong-Feng Yang, Eliesa Ing, William O. Cepurna, John C. Morrison

Casey Eye Institute, Oregon Health & Science University, 3181 SW Sam Jackson Park Road, Portland, OR 97239.

Purpose: The rat controlled elevation of intraocular pressure (CEI) model is used to study *in vivo* responses to defined intraocular pressures (IOP). In this model, a cannula is placed in the anterior chamber and fluid is delivered to elevate IOP to a defined level and duration in anesthetized rats over several hours. Importantly, since the angle is open, IOP elevation stretches/distorts the trabecular meshwork (TM), mimicking the responses found in glaucoma patients. In this study, we use Nanostring technology to investigate *in vivo* IOP-related gene responses in the TM and optic nerve head (ONH) simultaneously from the same animals.

Methods: An equal number of male and female rats were subject to CEI for 8-hours. Rat IOPs normally range from 15 to 30 mmHg during a 24-hour period, with a mean IOP of ~20 mmHg. Therefore, IOPs simulating mean IOP (CEI-20; normotensive; n=11), or 2.5x IOP (CEI-50; elevated IOP; n=12) were chosen. Naïve animals (n=12), receiving no anesthesia or surgical interventions, served as additional controls. After CEI, TM and ONH tissues were immediately dissected and RNA was isolated with TriZol. Samples were processed with the Nanostring *nCounter PanCancer Immune Profiling Panel*, following the low input RNA protocol. This panel contains 770 genes related to immune responses, fibrosis, and cytokine signaling. Post-processing, raw count data was uploaded to Rosalind® for differential expression analyses. Samples were excluded if they had low image quality (<0.8), high binding density (>1), or if housekeeping genes had zero counts. For TM, three comparisons were made: “CEI-50 vs. CEI-20”, “CEI-50 vs. naïve”, and “CEI-20 vs. naïve”. For ONH, a previous RNA-seq study showed no significant gene responses in CEI-20 vs. naïve, so only “CEI-50 vs. naïve” ONH samples were compared by Nanostring.

Results: Mean RNA concentration was 61 ng/TM and 60 ng/ONH. For TM, genes significant in CEI-50 comparisons were considered IOP-responsive TM genes, whereas genes in the CEI-20 vs. naïve comparison were likely related to cannulation or anesthesia. Forty-six IOP-related genes were found to be significant in “CEI-50 vs. CEI-20” and “CEI-50 vs. naïve” groups, with 15 genes common to both groups. These 15 genes were uploaded to ShinyGO bioinformatics software and the Notch and TGFβ pathways were among the most up- and down-regulated KEGG pathways, respectively. For ONH, 22 significantly regulated genes were identified in the “CEI-50 vs. naïve” comparison. Several of these genes (*Angptl4, Cebpb, Edn1, Myd88, Nfil3, Slc2a1,* and *Srebf1*) were regulated in the same direction between this Nanostring

study and the published ONH RNA-seq study. ShinyGO analysis identified ‘defense response’ and ‘immune response’ as two significantly affected biological process pathways.

Conclusions: In response to CEI-50 for 8-hours, we identified IOP-related gene responses in both the TM and the ONH. In the TM, Notch is a conserved pathway, which plays an important role in cell-cell communication and mechanotransduction. Downregulation of TGFβ pathway genes suggest that TM responses may be protective by preventing TGFβ-induced ECM synthesis. For ONH, the initial response to elevated IOP is also likely protective, with astrocytes likely playing a key role in these gene responses.

Funding: This study was supported by NIH/NEI grants R21 EY033073 (KEK), R01 EY019634 (KEK), R01 EY010145-17S1 (DCL), R01 EY010145 (JCM), P30 EY010572 (OHSU), and by unrestricted departmental funding from Research to Prevent Blindness (New York, NY).

4. Development of the Schlemm's canal and the trabecular meshwork: Insights from single cell RNA sequencing

Revathi Balasubramanian*[1], Nicholas G Tolman*[1,3], Taibo Li*[2], Violet Bupp-Chickering[1], Aakriti Bhandari[4], Sally Zhou[5], John Peregrin[1], Christa Montgomery[1], Jiang Qian[6], Simon W.M. John[1,7].

[1] Dept. of Ophthalmology, Columbia University Irving Medical Center, New York, NY
[2] Dept. of Molecular Biology and Genetics, Johns Hopkins University, Baltimore, MD
[3] Graduate School of Biomedical Sciences, Tufts University School of Medicine, Boston, MA
[4] Neuroscience Graduate Program, University of Utah, Salt Lake City, UT
[5] SUNY Downstate Health Sciences University, New York, NY
[6] Dept. of Ophthalmology, Johns Hopkins School of Medicine, Baltimore, MD
[7] Zuckerman Mind Brain Behavior Institute, Columbia University, New York, NY

Purpose: Schlemm's canal (SC) and trabecular meshwork (TM) play a central role in ocular physiology. SC develops from blood vessels through a process recently described as canalogenesis. TM develops from migrating neural crest cells. Impaired SC and TM development has implications in regulation of ocular physiology and congenital glaucoma. The transcriptomic control of SC and TM development is unknown. It is essential that we understand the underlying biology of normal development of SC and TM to understand how genetic changes in disease impact these structures in congenital glaucoma.

Method: Recent advances in genomics and sequencing have enhanced our understanding of the interplay between signaling networks and gene regulation during ocular development. Single cell RNA sequencing allows for complex assessment of inter-cellular and intra-cellular dynamics during development. We have generated single cell profiles for over 290,000 cells across multiple developmental ages – postnatal days P2, P4, P6, P10, P14, P21 and P60, that are crucial for SC and TM development.

Results: We observe dynamic populations of cells charting the course of SC and TM development. We identify the developmental trajectory of vascular progenitors and changes in key gene expression leading to SC development and the specification of inner and outer wall endothelial cells of SC. Pathway analysis and predicted dynamic cellular crosstalk highlights the importance of signaling between SC and the adjacent TM. We identify several novel interaction partners between SC and TM during development, opening up further avenues of investigation.

Conclusions: Single cell RNA sequencing demonstrates the importance of intercellular signaling between SC and TM and its influence on their normal

development. Insights gained from normal development will inform us about genetic abnormalities underlying congenital glaucoma.

Funding: BrightFocus Foundation NGR G2021007S (RB), partial support from National Eye Institute grants R01EY032507 (SJ), R01EY032062 (SJ) and R01EY029548 (JQ).

II. Schlemm’s Canal

5. Lymphatic characteristics of the Schlemm's canal endothelium

Hoi-Lam Li[1], Elysse Brookins[2], Hayian Gong[1], Mark Johnson[3] and Benjamin R. Thomson[2]

[1] Department of Ophthalmology, Boston University School of Medicine, Boston MA
[2] Feinberg Cardiovascular and Renal Research Inst and Department of Ophthalmology Northwestern University Feinberg School of Medicine, Chicago IL
[3] Northwestern University McCormick School of Engineering, Evanston IL

Purpose: As aqueous humor leaves the eye through the iridocorneal angle, it passes through either the trabecular (conventional) outflow pathway, comprised of the trabecular meshwork and Schlemm's canal, or uveoscleral (unconventional) routes. Although the majority of outflow occurs through the conventional route [2], most current glaucoma drugs target the unconventional pathway or reduce production of aqueous humor, leaving an important niche for new approaches directed at the conventional route. This includes broadly active drugs that increase conventional outflow such as Rho kinase inhibitors as well as more specific drugs targeting the trabecular meshwork and Schlemm's canal. However, despite the potential value of specific therapies, it has proven challenging as many of the genes and pathways critical for canal and trabecular meshwork function are widely expressed. Accordingly, it is critical to identify unique phenotypes and patterns of protein expression that underlie canal and meshwork function and can be used to direct targeted therapy. At the molecular level, the endothelium lining Schlemm's canal is said to exhibit a "hybrid" identity, incorporating aspects of lymphatic and blood vascular endothelial phenotypes [3]. Similar hybrid phenotypes have been identified elsewhere in the body in endothelia with unique fluid handling tasks, including the renal ascending vasa recta, penile cavernous sinusoids, and placental spiral arteries, suggesting that targeting the "lymphatic" aspects of canal biology may be an effective strategy for IOP-lowering therapy. However, our understanding of this hybrid phenotype is largely derived from mouse eyes, and there have been conflicting reports regarding expression of lymphatic genes in the human Schlemm's canal. While compelling, human RNA seq datasets contain limited numbers of Schlemm's canal endothelial cells, and high-quality tissue for analysis is challenging to obtain. Here, we set out to fully characterize the lymphatic-like "hybrid" phenotype in human Schlemm's canal, to determine if these characteristics are shared with the mouse and guide potential future therapeutic targeting.

Methods: Fresh human corneal rims were received from CorneaGen (Boston MA). The rims were fixed with 4% paraformaldehyde and processed for cryosectioning. Immunostaining was then used interrogate the "lymphatic like" phenotype of human Schlemm's canal. To further determine the role of this lymphatic transcriptional program in SC identity, siRNA knockdown of the master lymphatic transcription factor

PROX1 followed by RNA seq was then performed in primary human Schlemm's canal endothelial cells obtained from non-glaucomatous donor eyes.

Results: Immunostaining of human tissue sections confirmed that the lymphatic-like phenotype described in mouse is conserved in the human SC. In primary human Schlemm's canal endothelial cells, PROX1 expression was detected in 2 out of 3 lines tested. In both of these lines, PROX1 knockdown led to reduced expression of lymphatic genes including FLT4, confirming that PROX1 is central to maintaining the lymphatic-like phenotype in canal endothelial cells. Interestingly, PROX1 knockdown also resulted in marked reduction of AQP1, encoding the water channel aquaporin 1.

Conclusions: The hybrid lymphatic-like phenotype that has been well-characterized in mouse SC appears to be well-conserved in human eyes and is likely driven by the transcription factor PROX1. In addition, our data suggests that AQP1 regulation by PROX1 may occur in SC.

Financial support: The work described here was primarily supported by a Northwestern University Catalyst award to Mark Johnson. The Thomson lab also receives support from R01 EY032609 and a Brightfocus Foundation new investigator grant in macular degeneration research.

References

1. Tanna, A.P. and M. Johnson, *Rho Kinase Inhibitors as a Novel Treatment for Glaucoma and Ocular Hypertension.* Ophthalmology, 2018.
2. Johnson, M., J.W. McLaren, and D.R. Overby, *Unconventional aqueous humor outflow: A review.* Experimental Eye Research, 2017. **158**(Supplement C): p. 94-111.
3. Kizhatil, K., et al., *Schlemm's Canal Is a Unique Vessel with a Combination of Blood Vascular and Lymphatic Phenotypes that Forms by a Novel Developmental Process.* PLoS Biol, 2014. **12**(7): p. e1001912.

6. In Vivo Optical Coherence Tomography for Noninvasive Imaging of Collector Channels

Raymond Fang[1], Pengpeng Zhang[2], Tingwei Zhang[1], Daniel Kim[3], Edison Sun[1], Roman Kuranov[1], Junghun Kweon[1], Alex Huang[4], and Hao F. Zhang[1]

[1] Department of Biomedical Engineering, Northwestern University, Evanston IL
[2] Department of Mechanical Engineering, Northwestern University, Evanston IL
[3] Department of Chemical Engineering, Northwestern University, Evanston IL
[4] Department of Ophthalmology, University of California San Diego, San Diego CA

Purpose: Primary open-angle glaucoma, the leading cause of irreversible blindness worldwide, is caused by increased fluid resistance within the conventional aqueous humor outflow pathways (the conventional outflow pathway consists of the trabecular meshwork (TM), Schlemm's Canal (SC), collector channels (CC), and distal vasculature). Although up to half of aqueous outflow resistance is distal to the TM, the main cause of post-trabecular aqueous outflow resistance is still debated. It has been demonstrated that CCs have a crucial role in regulating distal outflow resistance. To better understand the anatomy and physiology of collector channels, we developed a robotic visible-light optical coherence tomography (vis-OCT) for imaging the CCs *in* vivo. We imaged CCs around the entire conventional outflow pathway and investigated their response *in vivo* to perturbations in the eye.

Methods: We designed a robotic anterior segment vis-OCT to image the CCs around the full circumference of mouse eyes. First, we volumetrically reconstructed the conventional outflow pathway around the globe and identified the locations of collector channels. Following data acquisition, we developed a customized reconstruction algorithm utilizing graph theory to digitally resample the volumetric data from the SC to CC to the pathway distal to CC. For each CC, we measured the width of the channel as well as characterized its morphology. Changes in CC size and morphology were tracked following topical 1% pilocarpine administration and intraocular pressure (IOP) modulation.

Results: For a sample of 6 C56BL/6 mice, we identified 33.7 ± 6.5 total CC. Upon increases in IOP, we observed decreased size of CC lumen size. Additionally, we observed segmental differences in CC morphology and the number of CC in the eye, with the quadrant with the most CC having 2.3 ± 0.6 times the number of CC as compared to the quadrant with the least CC. On average, the largest quadrant had 2.13 ± 0.41 times the volume of the smallest quadrant. Finally, we found a wide variety in CC morphology, with some CCs nearly collapsed and others having a wide diameter.

Conclusion: We were able to reconstruct CC around the eye using our robotic anterior segment vis-OCT system. Overall, this suggests that vis-OCT can assist us in better understanding how CC regulates distal outflow resistance *in vivo*.

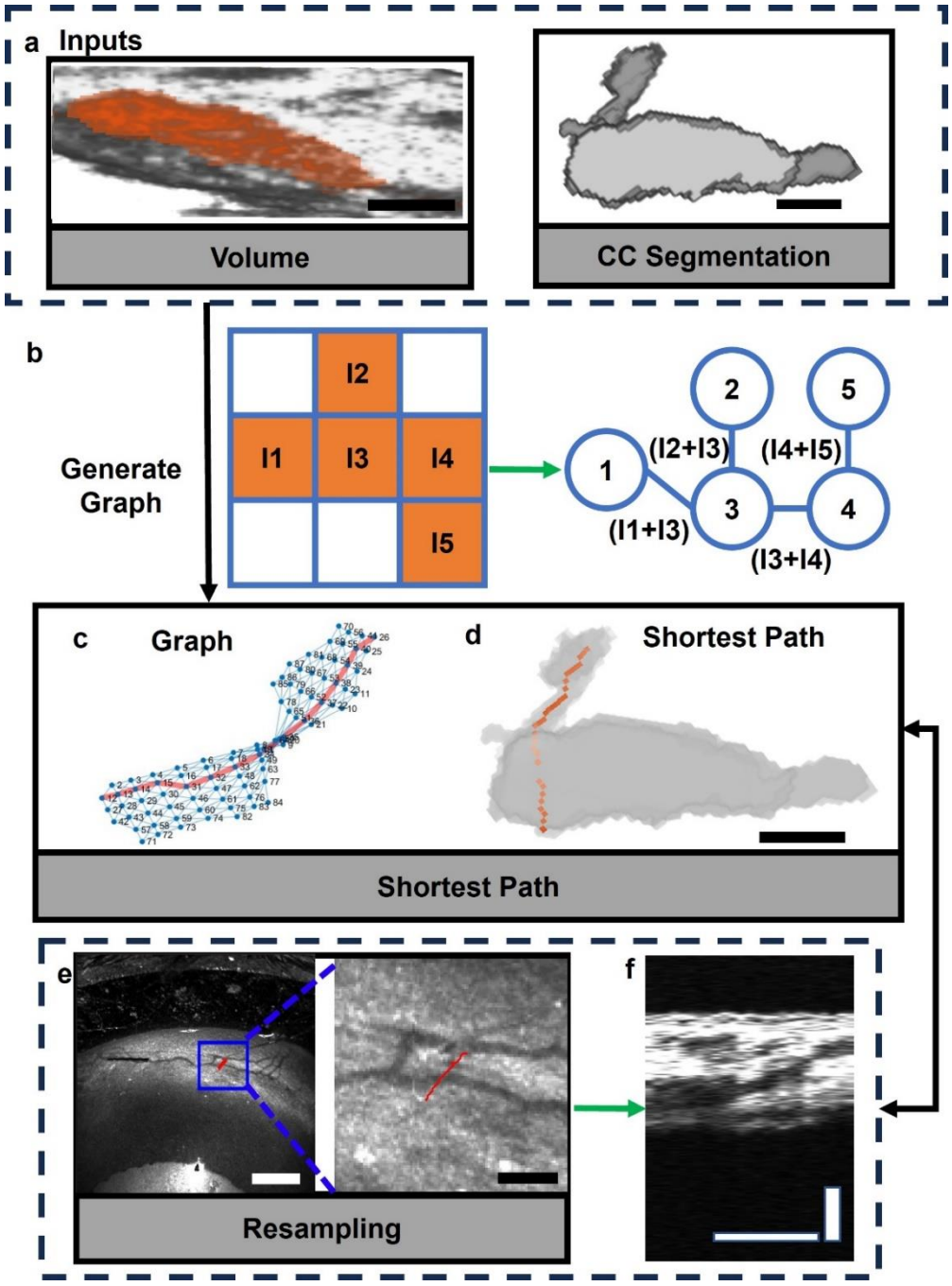

Figure. 1: Methodology for digital reconstruction of collector channels. *a) Inputs to digital reconstruction algorithm. Volumetric structural data and segmentations for each CC were taken as inputs. Scale bars are 50 μm. b) The segmentation for each CC was represented as a graph, with each pixel in the segmentation represented as a node. c) A sample graph for the segmentation in a single B-scan with the shortest path between end nodes highlighted in red. d) The shortest path in 3D inside the segmented CC and SC. The scale bar is 50 μm. e) The structural data is resampled following the shortest path found in the graph. Scale bars are 400 and 100 μm respectively. f) Resampled CC. The scale bar is 50 μm in each direction.*

7. An assay for studying Schlemm's canal inner wall mechanobiology

C. Ross Ethier[1], Seyed Mohammad Siadat[1,2], Haiyan Li[1], Jacques A. Bertrand[3], Babak N. Safa[1], M. Reza Bahrani Fard[1], Brigid Millette[1], A. Thomas Read[1], Kristin M. Perkumas[4], W. Daniel Stamer[4], Darryl R. Overby[3]

[1] Wallace H. Coulter Department of Biomedical Engineering, Georgia Tech/Emory, Atlanta, GA
[2] Department of Bioengineering, Northeastern University, Boston, MA
[3] Department of Bioengineering, Imperial College London, London, , UK
[4] Department of Ophthalmology, Duke Eye Center, Duke University, Durham, NC

Purpose: Aqueous humor transits the inner wall of Schlemm's canal (SC) by passing through pores, thought to modulate total outflow resistance, and SC pore density is reduced in glaucoma (Johnson et al. 2002). Despite the importance of inner wall pores, little is understood about the factors controlling their formation, other than that they are induced by cellular stretch (Braakman et al. 2014). Here, we introduce a novel assay designed to study intracellular (I-pore) formation in cultured SC cells and which complements an assay based on substrate stretch (Braakman et al. 2014).

Methods: Primary human SC cells from normal and glaucomatous donors were isolated and characterized (Stamer et al. 1998). Carboxyl ferromagnetic beads (diameter: 4.0-4.9 µm, Spherotech) were randomly seeded onto a biotinylated gelatin substrate in a multiwell format, after which SC cells were seeded on top, and allowed to attach and cover the beads for several hours. Fluorescently labeled streptavidin (Figure 1, green) was then added to the media overlying the cells for 5 min and washed away, after which a second fluorescently labelled streptavidin (Figure 1, purple) was added to the media while a magnet was simultaneously positioned above the cells (applied force: ~460 pN). Any pores that formed would allow access of the streptavidin to the biotinylated substrate under the cell, thereby creating fluorescent "dots" at pore locations (Braakman 2014). We investigated pores using scanning electron microscopy (SEM) and fluorescence microscopy.

Results: By SEM imaging we confirmed the cells overlay the beads (Figure 2). In some cells, no pores formed over the bead, while in others, pores remarkably similar to I-pores in *post mortem* tissue could be observed (Figure 2). Artifactual cracks suggested that the cells were under significant tension. Fluorescent imaging confirmed pore formation; importantly, pores were seen to form both prior to application of a magnetic field (here referred to as "Type I pores"), and after magnetic field delivery ("Type II pores"). Quantification showed Type I pores forming over 10.30 ± 4.48% of beads (mean ± standard deviation; n=5 normal cell strains), while magnetic force increased pore count (Type II pores) by 2.83 ± 1.99-fold. There was a tendency

towards fewer pores in glaucomatous cells (n=2 glaucomatous cell strains), but this difference did not reach statistical significance for the small number of glaucomatous cell strains studied to date.

Conclusions: By replicating the basal-to-apical force experienced by SC cells *in vivo* we successfully induced transcellular pores in cultured SC cells. Intriguingly, pores were formed even without magnetic force, likely due to significant tension generated within the cell and the associated local deformations as the cell extends itself over the bead. This assay shows promise for understanding the mechanobiology of transcellular pore formation in SC cells.

Financial Support: BrightFocus Foundation, NIH NEI R21, Georgia Research Alliance.

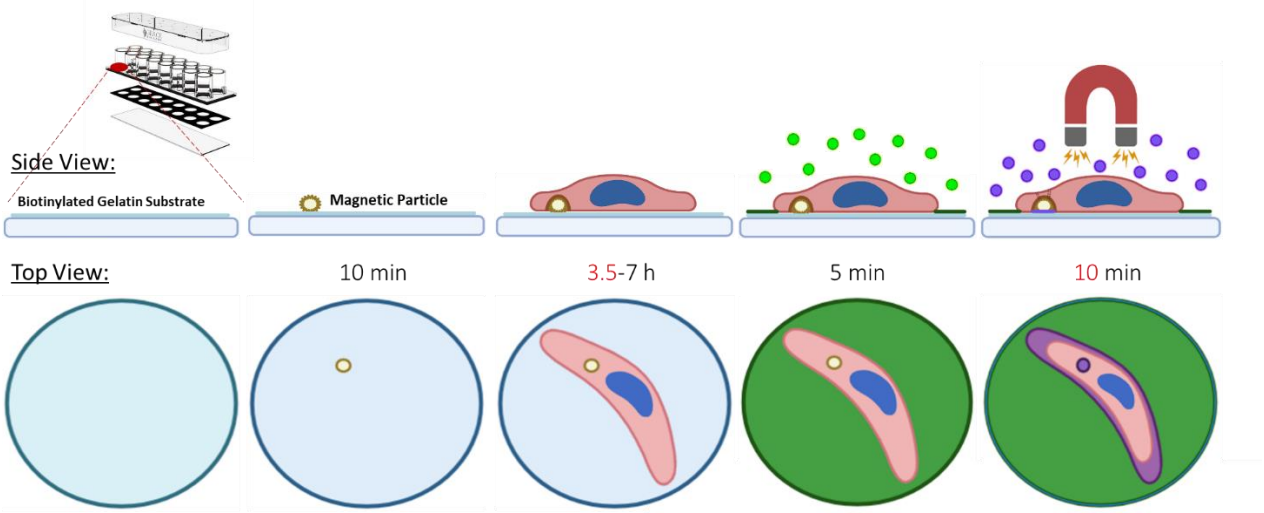

Figure 1: *Schematic overview of the pore formation and detection assay. Fluorescent dyes irreversibly bind to the biotin substrate at locations not covered by subconfluent cells, as well as at pore locations. Thus, pores labelled green (Type I pores) are those that form without application of basal-to-apical magnetic force, while pores labelled purple (Type II pores) form after magnetic force delivery.*

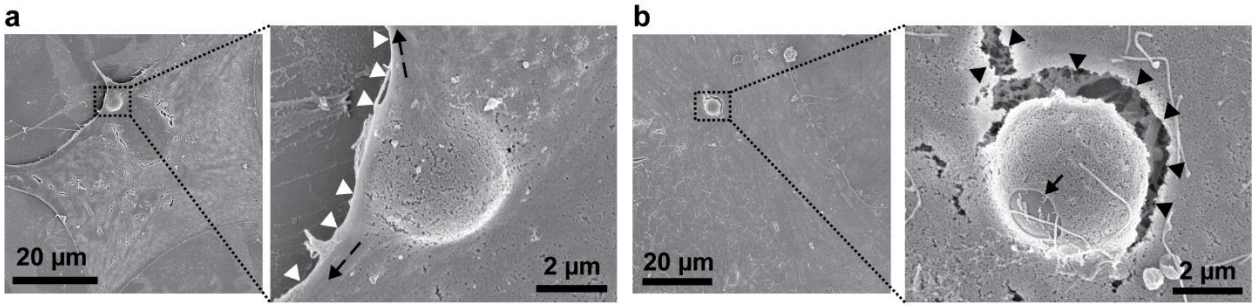

Figure 2: *SEM images showing SC cells overlying beads.* ***(a)*** *A bead is visible, but no pore appears to have formed.* ***(b)*** *A pore has formed over the bead (arrow). Note the artifactual cracking (arrowheads), typically associated with the SEM preparation process, suggestive of significant tension within the cell.*

References

1. Braakman, Sietse T. 2014. “Biomechanical Regulation of Permeability in Schlemm’s Canal Endothelium with Respect to Glaucoma.” Ph.D. thesis, London: Imperial College London. https://doi.org/10.25560/34396.
2. Braakman, Sietse T., Ryan M. Pedrigi, A. Thomas Read, James A.E. Smith, W. Daniel Stamer, C. Ross Ethier, and Darryl R. Overby. 2014. “Biomechanical Strain as a Trigger for Pore Formation in Schlemm’s Canal Endothelial Cells.” *Experimental Eye Research* 127: 224–35. https://doi.org/10.1016/j.exer.2014.08.003.
3. Johnson, Mark, D Chan, A T Read, C Christensen, A Sit, and C. Ross Ethier. 2002. “The Pore Density in the Inner Wall Endothelium of Schlemm’s Canal of Glaucomatous Eyes.” *Investigative Ophthalmology and Visual Science* 43 (9): 2950.
4. Stamer, W Daniel, Bruce C Roberts, David N Howell, and David L Epstein. 1998. “Isolation, Culture, and Characterization of Endothelial Cells from Schlemm’s Canal.” *Investigative Ophthalmology and Visual Science* 39 (10): 9.

8. Identifying nuclear and cytoskeletal changes in Schlemm's canal cells interacting with glaucomatous trabecular meshwork cells in a 3D ECM hydrogel co-culture model

Ayushi Singh[1,2], Suhani Patel[1], Rajanya Ghosh[1,3], Ana N. Strat[1,4], Kristin M. Perkumas[5], W. Daniel Stamer[5,6], Kate E. Keller[7], Yutao Liu[8], Preethi S. Ganapathy[1,4], Samuel Herberg[1,2,3]

[1] Departments of Ophthalmology and Visual Sciences, [2] Cell and Developmental Biology, [3] Biochemistry and Molecular Biology, and [4] Neuroscience and Physiology, SUNY Upstate Medical University, Syracuse, NY, USA
[5] Departments of Ophthalmology, Duke Eye Center, and [6] Biomedical Engineering, Duke University, Durham, NC, USA
[7] Department of Ophthalmology and Casey Eye Institute, Oregon Health and Science University, Portland, OR, USA
[8] Department of Cellular Biology and Anatomy and Culver Vision Discovery Institute, Augusta University, Augusta, GA, USA

Purpose: In the conventional outflow pathway, the Schlemm's canal (SC) inner wall endothelium interfaces with the trabecular meshwork (TM). Cellular interactions between SC and TM cells, and their extracellular matrix (ECM), are critical for maintaining outflow function and intraocular pressure homeostasis. The biomechanical changes occurring within this specific microenvironment are responsible for increased resistance to aqueous outflow in ocular hypertensive glaucoma. Notably, the TM undergoes fibrotic-like remodeling and stiffening. SC cells in the diseased outflow tract are thus exposed to increased biomechanical stress from the pathologically-altered TM. However, there is a fundamental lack of understanding how glaucomatous TM cells and their modified ECM influence SC cell behavior. In this study, we investigate the role of glaucomatous cellular and biomechanical TM stimuli on driving SC cell nuclear and cytoskeletal alterations using a novel SC/TM cell co-culture hydrogel model (**Fig. 1**).

Methods: Primary normal SC cells were plated as monolayers on photo-crosslinked ECM hydrogels (collagen type I, elastin-like polypeptide, and hyaluronic acid) encapsulated with age-matched normal TM (NTM) or glaucomatous TM (GTM) cells. Normal and glaucomatous SC cells grown atop acellular ECM hydrogels served as controls to benchmark the induced changes. The SC cell nuclear and cytoskeletal phenotypes were assessed using immuno-stained confocal Z-stacks. Chromatin condensation was quantified using a Sobel edge detection algorithm in MATLAB. Changes in SC cell mRNA expression of histone deacetylases were determined using quantitative polymerase chain reaction. Genome-wide expression profiling of SC cells was performed using 100 bp paired-end RNA sequencing using Illumina NextSeq2000.

Results: SC cells atop GTM hydrogels showed decreased nuclear number compared to NTM hydrogels ($p<0.05$), approximating glaucomatous SC cell controls. Furthermore, SC cells on GTM hydrogels exhibited decreased nuclear volume compared to NTM hydrogels ($p<0.05$), with nuclei morphologically transitioning into a flattened oblate shape ($p<0.0001$) compared to an elongated prolate shape on NTM hydrogels. A comparable trend was observed in glaucomatous SC cells relative to normal SC cells. Moreover, SC cells on GTM hydrogels showed increased chromatin condensation ($p<0.001$) compared to SC cells on NTM hydrogels. This correlated with increased HDAC2 mRNA expression ($p<0.0001$) in SC cells atop GTM hydrogels compared to NTM hydrogels, suggesting potential alterations in the epigenetic landscape, again behaving similarly to glaucomatous SC cell controls. Ongoing RNA sequencing analyses are expected to shed further light on and expand these preliminary observations. Lastly, a pattern of markedly disordered (i.e., multimodal) F-actin stress fiber distribution was observed in SC cells on GTM hydrogels, approximating that of glaucomatous SC cell controls, compared to an aligned (i.e., unimodal) distribution in SC cells on NTM hydrogels.

Conclusion: Our data suggest that the presence of GTM cells in absence of other disease-associated exogenous stimuli are sufficient to induce a glaucoma-like phenotypic conversion of normal SC cells, uniquely facilitated by the biomimetic SC/TM cell co-culture hydrogel model.

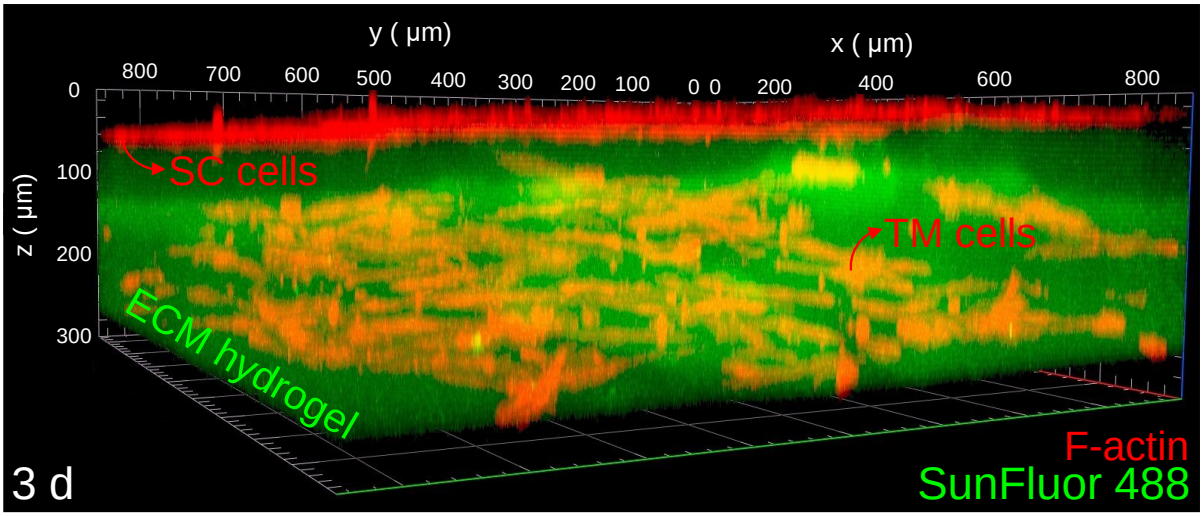

Figure 1: Engineered SC/TM cell co-culture hydrogel makeup by confocal fluorescence microscopy. *SC cells were cultured as a monolayer atop the TM cell-encapsulated ECM hydrogel to simulate the native SC/TM interface. A cytocompatible fluorophore was added prior to photocrosslinking to clearly demarcate the hydrogel boundaries.*

9. Targeting YAP/TAZ mechanosignaling to ameliorate stiffness-induced Schlemm's canal cell pathobiology

Haiyan Li[1,2,†], Megan Kuhn[3], Ruth A. Kelly[3], Ayushi Singh[1,2], Kavipriya Kovai Palanivel[1], Izzy Salama[1], Michael L. De Ieso[3], W. Daniel Stamer[3,4], Preethi S. Ganapathy[1,5,], Samuel Herberg[1,2,6]

[1]Departments of Ophthalmology and Visual Sciences, [2]Cell and Developmental Biology, [5]Neuroscience and Physiology, and [6]Biochemistry and Molecular Biology, SUNY Upstate Medical University, Syracuse, NY, USA

Departments of [3]Ophthalmology, Duke Eye Center and [4]Biomedical Engineering, Duke University, Durham, NC, USA

[†]Present address: Wallace H. Coulter Department of Biomedical Engineering, Georgia Institute of Technology & Emory University, Atlanta, GA, USA

Purpose: Pathological alterations in the biomechanical properties of the Schlemm's canal (SC) inner wall endothelium and its immediate vicinity are strongly associated with ocular hypertension in glaucoma due to decreased outflow facility. Specifically, the underlying trabecular meshwork is substantially stiffer in glaucomatous eyes compared to that from normal eyes. This raises the possibility of a critical involvement of mechanotransduction processes in driving SC cell dysfunction. Yes-associated protein (YAP) has emerged as a key contributor to glaucoma pathogenesis. However, the molecular underpinnings of SC cell YAP/TAZ (transcriptional coactivator with PDZ binding motif) mechanosignaling in response to glaucomatous extracellular matrix (ECM) stiffening are not well understood.

Methods: Using a novel biopolymer hydrogel that facilitates dynamic and reversible stiffness tuning, we investigated how ECM stiffening modulates YAP/TAZ activity in primary human SC cells, and whether disruption of YAP/TAZ mechanosignaling attenuates SC cell pathobiology and increases *ex vivo* outflow facility.

Results: We demonstrated that ECM stiffening drives pathological YAP/TAZ activation and cytoskeletal reorganization in SC cells, which was fully reversible by matrix softening in a distinct time-dependent manner. Furthermore, we showed that pharmacologic or genetic disruption of YAP/TAZ mechanosignaling abrogates stiffness-induced SC cell dysfunction involving altered cytoskeletal and ECM remodeling. Lastly, we found that perfusion of the clinically-used, small molecule YAP/TAZ inhibitor verteporfin (without light activation) increases *ex vivo* outflow facility in normal mouse eyes. This was associated with decreased alpha smooth muscle actin expression in the SC inner wall and underlying TM.

Conclusions: Our data provide new evidence for a pathologic role of aberrant YAP/TAZ mechanosignaling in SC cell dysfunction and suggest that YAP/TAZ inhibition has therapeutic value for treating ocular hypertension in glaucoma.

III. Segmental Outflow

10. VEGF expression is elevated in high-flow regions of mouse trabecular meshwork.

Ester Reina-Torres & Darryl R. Overby

Dept. of Bioengineering, Imperial College London, London, UK

Purpose: Aqueous humour drainage through the trabecular meshwork (TM) is non-uniform or segmental, with some regions of the TM exhibiting greater local filtration than others. We have recently shown that segmental outflow patterns are dynamic (Reina-Torres, *et al. EER*, 2022), redistributing over a time scale of a few days in living mice. This redistribution implies some regulatory mechanism governing segmental outflow. We hypothesise that VEGF, which modulates outflow resistance (Reina-Torres, *et al. IOVS*, 2017), controls the distribution segmental outflow. We test this hypothesis by comparing segmental patterns and VEGF-A expression.

Methods: Segmental outflow patterns were labelled in live C57BL/6J mice (n = 4 eyes) by intracameral injection of fluorescent tracer microparticles (0.2 µm; 10^{11} particles/ml) under anaesthesia. After 6 hours, eyes were enucleated following humane culling and fixed overnight in 4% PFA. The anterior segments were dissected and immunolabelled for VEGF-A. Sagittal 100µm cryosections through the iridocorneal angle were imaged by confocal microscopy around the TM circumference (27 to 47 sections per eye). From each cryosection, 15 consecutive confocal slices (0.5 µm; 40x) were selected for analysis. A polygon was drawn to include all tracer fluorescence within the TM and to create a 3D mask. We calculated the sum intensity of tracer and VEGF-A immunolabelling within the mask for each cryosection to correlate both variables, an ANCOVA analysis was done to account for differences between eyes. We also normalised and lumped data from the highest, middle and lowest thirds of tracer intensity and compared VEGF-A labelling between these groups using one-way ANOVA with a post-hoc Tukey test.

Results: The correlation between tracer and VEGF-A signal intensities was highly significant ($p < 0.001$), although there were significant differences in the slope of the tracer-VEGF relationship between eyes ($p < 0.001$). VEGF-A expression was significantly different between segmental regions exhibiting high, medium, and low tracer intensity ($p < 0.001$).

Conclusions: VEGF-A expression in the TM coincides with the distribution of segmental outflow. As VEGF-A is known to increase outflow facility (Reina-Torres, *et al. IOVS*, 2017), this raises the possibility that VEGF expression by TM cells is acting as a paracrine regulator of local outflow conductivity to control segmental outflow.

Financial Support: BrightFocus Foundation fellowship (G2021004F).

11. Digital Spatial Profiling of Segmental Outflow Regions in Trabecular Meshwork Reveals a Role for ADAM15

Jennifer A. Faralli[1], Mark S. Filla[1], Yong-Feng Yang[2], Ying Ying Sun[2], Kassidy Johns[1], Kate E. Keller[2], and Donna M. Peters[1,3]

[1] Depts. of Pathology & Laboratory Medicine and Ophthalmology & Visual Sciences[3] University of Wisconsin, Madison, WI
[2] Casey Eye Institute, Oregon Health & Science University, Portland, OR

Purpose: In this study we used a spatial transcriptomics approach to identify genes specifically associated with either high or low outflow regions in the trabecular meshwork (TM) that could potentially affect aqueous humor outflow in vivo.

Methods: High and low outflow regions were identified and isolated from organ cultured human anterior segments perfused with fluorescently-labeled 200 nm FluoSpheres. The NanoString GeoMx Digital Spatial Profiler (DSP) platform was then used to identified genes in the paraffin embedded tissue sections from within those regions.

Results: These transcriptome analyses revealed that 16 genes were statistically upregulated in high outflow regions and 57 genes were statistically downregulated in high outflow regions when compared to low outflow regions. Gene ontology enrichment analysis indicated that the top three biological categories of these differentially expressed genes were ECM/cell adhesion, signal transduction, and transcription. Among the ECM/cell adhesion genes that showed the largest differential expression (Log2FC ±1.5) were *ADAM15, BGN, LDB3*, and *CRKL*. ADAM15 which is a metalloproteinase that can bind integrins was upregulated in high outflow regions. *BGN* which encodes for the proteoglycan biglycan was downregulated. *LDB3* and *CRKL* which are two genes associated with integrin signaling were also downregulated. Immunolabeling studies supported the differential expression of ADAM15 and showed that it was specifically upregulated in high outflow regions along the inner wall of Schlemm's canal and in the juxtacanalicular region of the TM. In addition, to these genes the studies showed that genes for decorin, another small leucine-rich proteoglycan and the α8 integrin subunit were enriched in high outflow regions.

Conclusion: These studies identify several novel genes that could be involved in segmental outflow, thus demonstrating that digital spatial profiling could be a novel approach for understanding segmental flow through the TM. Furthermore, this study suggests that changes in the expression of genes involved in regulating the activity and/or organization of the ECM and integrins in the TM are more likely to be key players in segmental outflow.

12. Segmental Uveoscleral Outflow in Monkey Eyes

Hoi-Lam Li[1], Shan Fan[3], Carol B. Toris[3,4], Haiyan Gong[1,2]

[1] Dept. of Ophthalmology, Boston University Chobanian & Avedisian School of Medicine, Boston, MA, USA
[2] Dept. of Anatomy and Neurobiology, Boston University Chobanian & Avedisian School of Medicine, Boston, MA, USA
[3] Dept. of Ophthalmology and Visual Science, University of Nebraska Medical Center, Omaha, NE, USA
[4] Dept. of Ophthalmology and Visual Sciences, The Ohio State University, Columbus, OH, USA

Purpose: While segmental trabecular outflow has been observed in various species (1-7), segmental uveoscleral outflow was first reported recently in normal mouse eyes by our research group (8). In the mouse study, we found no correlation between the overall segmental flow patterns in both outflow pathways. However, the existence of the segmental flow pattern in unconventional outflow and its correlation with conventional outflow in other species remain unknown. This study aimed to investigate the flow pattern along the uveoscleral outflow pathway and its correlation with trabecular outflow in monkey eyes.

Methods: This study examined the normal eyes of three adult female cynomolgus macaques. Intraocular pressure (IOP) of each monkey eyes were measured. After administering anesthesia with ketamine (10 mg/kg) a fixed volume of tracer (50 µl) was injected into the anterior chamber. The tracers were allowed to diffuse and reach the outflow systems for 45 minutes and the eyes were fixed with 4% paraformaldehyde (PFA) *in situ* for 30 minutes and then enucleated. After euthanasia and marking the 12 o'clock location on the globes, the eyes were further immersion-fixation with 4% PFA for 48 hours. The eyes were transferred to saline solution and shipped from University of Nebraska Medical Center to Boston University for imaging analysis. The eyes were dissected into 12 radial segments based on clock hours. Images of both sides of each segment were captured by a confocal microscope after nuclear counter-staining and analyzed using ImageJ. Eyes without tracer injection were used as the negative control.

Results: The average IOP of the three monkey eyes was 18.8±1.5 mmHg. We observed a segmental uveoscleral outflow (Figure 1A) where the tracer intensity was highest on the superior side (at 11 o'clock) and lowest on the nasal side (at 4 o'clock). Concurrently, in the trabecular outflow pathway (Figure 1B), the tracer intensity was highest in the nasal side (at 2 o'clock) and lowest in the inferior temporal region (at 8 o'clock). Overall flow patterns in both outflows were uncorrelated with four different tracer patterns: 1) Low flow in both outflow pathways (Figure 2A); 2) High flow in both outflow pathways (Figure 2B); 3) High flow mainly in the conventional outflow pathway

(Figure 2C); and 4) High flow mainly in the unconventional outflow pathway (Figure 2D).

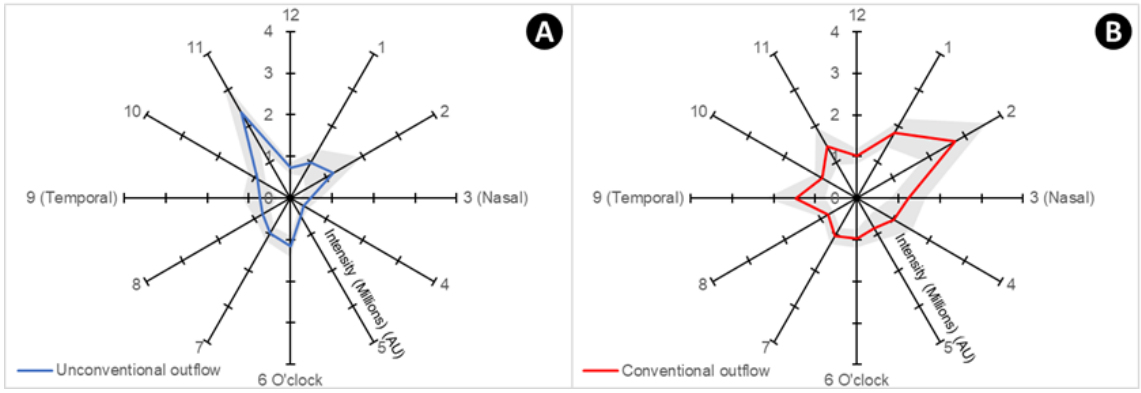

***Figure 1**: Tracer distribution in both outflow pathways: The mean tracer intensity at each clock hour position in (A) unconventional; and (B) conventional outflow.*

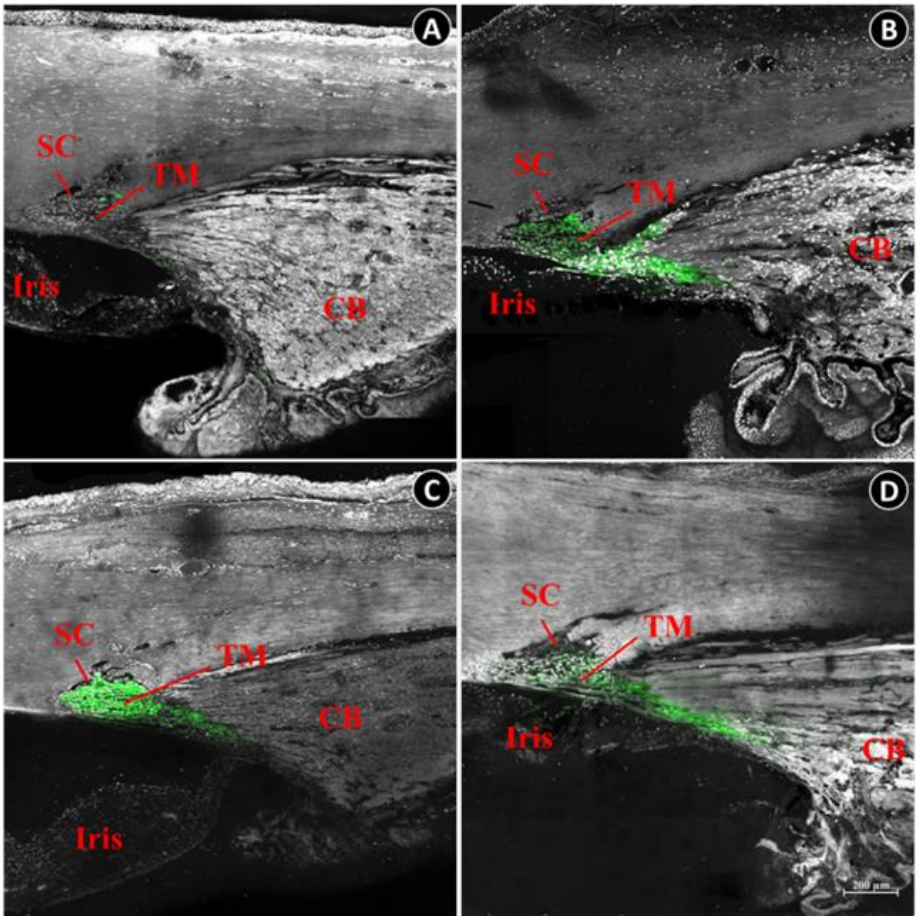

***Figure 2**: Four outflow patterns: (A) Low flow in both outflow pathways; (B) High flow in both outflow pathways; (C) High flow mainly in the conventional outflow pathway; and (D) High flow mainly in the unconventional outflow pathway. Gray color: nuclear counter-staining with DAPI; Green color: tracer; SC: Schlemm's canal; TM: trabecular meshwork; CB: ciliary body.*

Conclusion: We identified segmental flow patterns in the uveoscleral outflow pathway in monkey eyes, which were independent of the segmental flow patterns in the trabecular outflow pathway. Our results reveal that unconventional outflow is segmental in both mouse and monkey eyes. Future studies of segmental unconventional outflow patterns in human eyes will provide better understanding of the optimal location for the placement of drainage devices and drug delivery systems targeting the unconventional outflow pathway.

Financial Support: This research was funded by the BrightFocus Foundation Grant G2022013S, The Rifkin Family Glaucoma Research Fund, and Massachusetts Lion Research Fund.

References:

1. Raghunathan V, Nartey A, Dhamodaran K, Baidouri H, Staverosky JA, Keller KE, et al. Characterization of extracellular matrix deposited by segmental trabecular meshwork cells. Exp Eye Res. 2023;234:109605.
2. Huang AS, Penteado RC, Saha SK, Do JL, Ngai P, Hu Z, et al. Fluorescein Aqueous Angiography in Live Normal Human Eyes. J Glaucoma. 2018;27(11):957-64.
3. Huang AS, Saraswathy S, Dastiridou A, Begian A, Legaspi H, Mohindroo C, et al. Aqueous Angiography with Fluorescein and Indocyanine Green in Bovine Eyes. Transl Vis Sci Technol. 2016;5(6):5.
4. Cha EDK, Xu J, Gong L, Gong H. Variations in active outflow along the trabecular outflow pathway. Exp Eye Res. 2016;146:354-60.
5. Vranka JA, Bradley JM, Yang YF, Keller KE, Acott TS. Mapping molecular differences and extracellular matrix gene expression in segmental outflow pathways of the human ocular trabecular meshwork. PLoS One. 2015;10(3):e0122483.
6. Swaminathan SS, Oh DJ, Kang MH, Ren R, Jin R, Gong H, et al. Secreted protein acidic and rich in cysteine (SPARC)-null mice exhibit more uniform outflow. Invest Ophthalmol Vis Sci. 2013;54(3):2035-47.
7. Keller KE, Bradley JM, Vranka JA, Acott TS. Segmental versican expression in the trabecular meshwork and involvement in outflow facility. Invest Ophthalmol Vis Sci. 2011;52(8):5049-57.
8. Li H-L, Ren R, Gong H. Uveal outflow is segmental. Investigative Ophthalmology & Visual Science. 2023;64(8):1889-.

13. Nerve innervation of high and low flow regions of the trabecular meshwork and Schlemm's canal

Colleen M. McDowell, Timur Mavlyutov

Department of Ophthalmology and Visual Sciences, University of Wisconsin-Madison, Madison, WI

Purpose: Increased stiffness in the juxtacanicular tissue of the TM and the underlying basement membrane of the inner wall of SC has been identified as the region contributing the greatest resistance to aqueous humor (AH) outflow. The extracellular matrix (ECM) stiffness is dependent on the type of ECM proteins present, the degree of covalent crosslinking present and the 3-D organization of the ECM proteins in the matrix. In addition, the AH outflow pathway through the TM and SC is known to have regions of both high and low-flow, with high-flow regions containing significantly less ECM proteins compared to the low flow regions. Increased areas of low-flow regions increase risk for higher IOP; however, the mechanism of how high and low-flow regions are developed and regulated is unknown. Sensory neurons have previously been shown to innervate the TM and SC. Importantly, CGRP positive C-fibers were shown to be the major type of sensory neurites innervating the TM and SC; however, the functional significance has not been elucidated. Afferent neurons are known upon activation to secrete CGRP locally, which activates surrounding cells, and CGRP receptors are known to be expressed in the TM and SC cells. It has previously been shown in other cell types that CRGP can modulate ECM protein expression and remodeling as well as enhance phagocytosis. It is well known the ECM composition of the outflow pathway effects tissue stiffness and AH flow, and the phagocytotic properties of TM cells are important to tissue homeostasis, with suppression of phagocytosis in TM cells resulting in decreased ECM digestion and elevated IOP. The goal of this project was to determine whether CGRP positive neurites innervating the TM and SC are involved in the formation of high and low-flow regions and TM function.

Methods: High and low-flow regions of the TM and SC were determined in 9-month-old wild-type C57BL/6J mice using yellow-green fluorescent tracer latex beads (0.02 µm). The fluorescent beads were injected intracamerally with a 35G needle at a rate 4 nL/s using a syringe pump controller for 45 min, eyes were then harvested and processed for anterior segment flat mounts. Tissue was co-labeled with antibodies against CGRP (afferent neurons), CALCRL (CGRP receptor), and PECAM1 (SC endothelium), and imaged by confocal microscopy to acquire tiled Z-stacks of entire outflow area of each injected eye. Density of CGRP neurites in both high and low-flow regions was determined by volumetric analysis in ImageJ. Primary human TM cells in culture were exposed to fluorescently labeled beads (0.02 µm size) with or without CGRP (0.1 nM-5mM) for 24 hours. Cells were washed, fixed, and processed for immunocytochemistry. Phagocytosed fluorescent beads were imaged and quantified using ImageJ analysis.

Results: Both high and low flow regions were identified in wild-type C57BL/6J mice. There was significantly more CGRP positive neurites per square area of high-flow

regions compared to no flow and low flow regions ($p<0.05$, n=8 eyes). The CGRP receptor, CALCRL, is expressed in both TM and SC cells and there is significantly more CALCRL expression in high-flow regions compared to no flow and low flow regions ($p<0.01$, n=4 eyes). CGRP (1μM) significantly increased phagocytosis in primary TM cells in culture compared to untreated controls, while Substance P treated cells had no significant differences in phagocytosis.

Conclusion: These data suggest that the innervation of CGRP positive C-fibers in the TM and SC may influence the development and regulation of high and low-flow regions of aqueous humor outflow.

IV. Stem Cells

14. RNA Seq Analysis of Expression Differences of Human TM Cells and TM Insert Stem Cells

Mary J. Kelley[1], Yutao Liu[3], Andrew Ashford[2], Mini Aga[1], John R. Samples[4] and Ted S. Acott[1]

1. Dept. of Ophthalmology, Oregon Health & Sciences University, Portland, OR, USA
2. Dept. of Molecular and Medical Genetics, Oregon Health & Science University, Portland, OR, USA
3. Depts. Of Cellular Biology and Anatomy, Center for Biotechnology & Genomic Medicine, Augusta University, Augusta, GA, USA
4. Dept. of Ophthalmology, Washington State University Elson S. Floyd College of Medicine, Spokane, WA, USA

Purpose: The goal of this study is to investigate a population of trabecular meshwork (TM) stem cells, located in the "Insert" region beneath Schwalbe's line. This population is thought to contribute to the maintenance of the cells of the aqueous humor outflow pathway. With aging and particularly in glaucoma, TM cellularity is reduced and this diminishes normal intraocular pressure (IOP) homeostasis. IOP elevation often results in progressive glaucomatous optic nerve damage and vision loss. Our hypothesis states that disparities in gene expression patterns of TM insert stem cells and mature TM cells will elucidate key functional differences of these two cell types and can be used to push cellularity increases.

Methods: The TM Insert and the filtering TM were surgically dissected from paired aged normal human eyes and the total RNA from each was used for RNASeq. The data were analyzed with optimal bioinformatics and pathway programs**.**

Results: In our analysis of differential gene expression between the dissected Insert region and the filtering TM using RNASeq data from normal eyes, we identified 2250 transcripts preferentially expressed in the Insert, with 3,040 preferentially expressed in the TM, and 11,245 shared by both tissues. Additionally, this investigation uncovered distinctions in key signaling pathways associated with IOP homeostasis, mechanical stretch/distortion responses, TNF-a and IL-1 signaling, glycol-related genes, and alternative splicing within the signaling components of TM and Insert. Specifically, for IOP homeostasis, we detected differences in the expression of 3 of the 6 isoforms of MMP2, 1 isoform variation for MMP14, and one of 4 isoforms of EIF4E3. These differences were consistently higher within the TM compared to the Insert. In terms of mechanical stretch responses, notable fold changes were revealed in the extracellular matrix (ECM) transcripts within both TM and TM Insert cells. Furthermore, our study found that TNF-alpha and IL-1 signaling pathways post-laser trabeculoplasty showed that one or more isoforms exhibited greater expression in the Insert in contrast to the TM, while other pathway components were more highly expressed in TM rather than Insert cells. Lastly, we also determined distinct fold

changes in glyco-related genes and in alternative splicing events between transcripts originating from TM and TM Insert stem cells.

Conclusions: These results should clarify the nuanced molecular differences underlying the functional differences between the TM and the Insert. These differences will highlight critical implications for advancing our knowledge of glaucoma pathogenesis and facilitate development of targeted therapeutic interventions.

Commercial Relationships: Kelley, None; Liu, None; Ashford, None; Aga, None; Samples, None; Acott, None.

Support: NEI grants: EY031071 (MJK), EY021800 (MJK); EY023242 (YL), EY028671 (YL), EY028671S (YL), EY031631 (YL); EY008274 (TSA), EY003279 (TSA), EY025721 (TSA), EY030238 (TSA), P30EY010572 (TSA); the Lewis Rudin Glaucoma Prize (MJK), Glaucoma Research Foundation Shaffer Award (MJK); ACED PhD Training Grant (AJA); The Glaucoma Foundation (YL), Glaucoma Research Foundation (YL), BrightFocus Foundation (YL), the Malcom M. Marquis, MD Endowed Fund for Innovation (YL), and an unrestricted grant to the Casey Eye Institute, Oregon Health & Science University from the Research to Prevent Blindness Foundation.

15. Reduced abundance of trabecular meshwork stem cells in human donor eyes with POAG

Markus H. Kuehn and Sarah Brumley

University of Iowa, Department of Ophthalmology and Visual Sciences

Purpose: Extensive data has been presented to demonstrate that the density of trabecular meshwork (TM) cells decreases with age and that it is particularly low in eyes with primary open angle glaucoma (POAG). TM cells are thought to be derived from a population of multipotent stem cells, designated trabecular meshwork stem cells (TMSC), that reside largely in an area referred to as Insert Zone, which is located anterior to Schwalbe's line. TMSC can be detected even in human eyes obtained from older donors and only sparse data exist to describe the relationship between the number of TMSC and TM cellularity during aging and POAG pathology.

Methods: Human donor eyes were obtained from the Iowa City Lions Eye Bank and fixed in 4% paraformaldehyde within 7 hours post-mortem. Groups included eyes from young donors (n=6, age: 21.3 $\pm$ 4.3 yrs), older donors without glaucoma (n=8, age: 79.5 $\pm$ 10.9 yrs), and those with a clinical diagnosis of POAG (n=7, 79.7$\pm$4.8 yrs). From the anterior segment of each eye >10 radial sections were obtained from two distinct areas. These were stained with DAPI and with antibodies directed against the stem cell markers Nestin and ABCG2. The number of Nestin/ABCG2 double-positive cells as well as the total number of nuclei was determined in insert zone, the non-filtering TM and the filtering TM by an observer blinded to the status of the sample.

Results: As expected, the number of DAPI positive cells in the TM was highest in young eyes (72.2$\pm$3.8/section), lower in old eyes (58.9$\pm$6.2/section), and lowest in POAG eyes (48.2$\pm$2.3/section). TMSC double positive for Nestin and ABCG2 were primarily located in the insert zone, but are also commonly detected in the non-filtering TM. TMSC are rare the filtering TM. Overall numbers of TMSC were highest in young eyes (6.9$\pm$0.8/section) and significantly lower in older eyes (3.1$\pm$1.1/section; $p<0.0001$). The number of TMSC was even further reduced in eyes with POAG (1.1$\pm$0.4/section, $p=0.0007$ vs age-matched old eyes). Consequently, young eyes contained 10.4$\pm$1.6 TM cells per TMSC while older, healthy eyes contained 18.8$\pm$7.8 TM cells for each TMSC ($p=0.07$). The ratio increased dramatically in POAG eyes (40.3$\pm$12.6 TM cells/TMSC, $p<0.0001$ vs. age-matched eyes).

Conclusions: Our data demonstrate that the abundance of human TMSC decreases with age and that it is significantly lower in eyes with POAG than in age-matched controls. TMSC loss in POAG eyes is more pronounced than the decline in TM cell density leading to a higher TM to TMSC ratio in POAG eyes. While not direct proof, our findings are consistent with the notion that mounting loss of TMSC stemness leads to failure to compensate for TM cell loss, and ultimately to dysfunction of the tissue.

16. Activation and Migration of Endogenous Trabecular Meshwork Stem Cells

Yiqin Du[1], Hongmin Yun[2], Enzhi Yang[1]

[1] Dept. of Ophthalmology, Morsani College of Medicine, University of South Florida, Tampa, FL
[2] Dept. of Ophthalmology, University of Pittsburgh, Pittsburgh, PA

Purpose: We have isolated and characterized stem cells from human trabecular meshwork (TM) and confirmed that exogenous TM stem cells (TMSC) can home to the TM tissue and function to replenish the TM cellularity and restore the TM function. We have reported that BrdU label retaining TMSCs in mice are mainly located in the insert region. In this study, we investigated whether endogenous TMSC can be activated and migrate into the filtering TM region for functioning.

Methods: We used thymidine analogs 5-Chloro-2′-deoxyuridine (CldU) and iodo-deoxyuridine (IdU) double labeling and chasing approach to label dividing cells and chase label-retaining stem cells. We did three sets: (**1**) CldU was periocularly injected into newborn baby mice (three days after birth) twice a day for 3 days and waited for 10 wks. After 10-wk chasing period, mice were treated with a 532 nm CW-diode laser on the TM region with a 50-μm diameter spot size. Forty hrs later, IdU was periocularly injected twice at a 4-hr interval, and then mice were sacrificed at 4-hr, 24-hr, and 1-wk after the second IdU injection. (**2**) Similar to Set (1), newborn mice were injected with CldU and waited for 22 wks before laser treatment and IdU injection. Mice were sacrificed 24 hrs after the second IdU injection. (**3**) Adult mice at 10-wk old of age were tested by CldU injection twice a day for 9 days and chasing for 10 days, then treated by laser and injected with IdU twice and sacrificed 24 hrs after the second IdU injection. Age-matched mice without laser treatment served as controls. The mouse TM tissues were stained with antibodies to CldU, IdU, and a mitotic marker phospho-histone H3 (H3) and wholemount pictures were taken under a confocal microscope. Single and double stained cells were counted. The TM tissues of adult mice in Set 3 were also digested and analyzed by flow cytometry for CldU, IdU, and H3 expression.

Results: After both 10-wk and 22-wk chasing periods, label retaining stem cells were detected mainly in the insert region. After laser, CldU labeled (+) and CldU/IdU double labeled (+/+) cells were detected in both the insert region and the TM region. The numbers of CldU+ and CldU+/IdU+ cells were significantly increased in laser treated TM tissue than those in the TM without laser treatment. Some CldU+ and most CldU+/IdU+ cells also expressed mitotic marker H3 indicating they were dividing/proliferating. Adult mouse insert region was also labeled with CldU after 9-day injection and 10-day chasing, indicating adult mouse TMSCs could intake CldU

and they were proliferating. These label retaining stem cells were dividing and migrating as indicated by increased CldU+ and CldU+/IdU+ cells in the insert region and TM region after laser treatment by both wholemount staining and flow cytometry.

Conclusions: Mouse TMSCs are located in the insert region that are label retaining and can be activated by laser treatment. The activated endogenous TMSCs are mitotic and can migrate into the filtering TM region for functioning. Further research is needed to explore if endogenous TMSCs in glaucoma models can be activated by some glaucomatous treatments.

Financial Support: This work was supported by NIH grant EY025643.

V. Animal Models

17. Freeform visible-light OCT to quantify anterior chamber volume in mice

Hao F. Zhang, Danial Kim and Raymond Fang

Dept. of Biomedical Engineering, Northwestern University, Chicago, IL

Purpose: We developed a robotic visible-light OCT (vis-OCT) to conformally acquire multiple vis-OCT volumes from different locations and orientations around the anterior segment of mouse eyes.

Methods: Using a newly developed point-cloud-based method, we registered these individual volumes and reconstructed the digital twin of the eye. We acquired eight vis-OCT volumes around the full 360 degrees with a spacing of 45 degrees. To correctly initialize the adjacent OCT volumes, we located common branch points from blood vessels visualized by vis-OCT angiography.

Results: The common points were interpolated and matched in 3D space to obtain an initial estimate of the transformations required to correctly align the adjacent volumes. To increase the accuracy of the alignment, we converted the surface points of the anterior segment into point clouds and used an iterative closest point (ICP) algorithm to obtain a final transformation for each of the OCT volumes. We segmented each OCT volume to label the regions corresponding to the anterior and posterior chambers using the Segment Anything Model by Meta AI. Applying the 3D transformations from the montaging scheme on the segmented OCT volumes lead to a complete reconstruction of the anterior segment with the anterior and posterior chamber volumes labeled. We then measured the aqueous volume of the anterior and posterior chambers of the mouse eye.

Conclusion: There is no published literature on the volume of the posterior chamber *in vivo*, so this work provides a novel montaging scheme on OCT volumes and a reference value for the volume of the posterior chamber of the mouse eye.

18. A role for the arginine transporter SLC7A1 in regulating aqueous humor outflow.

Krish Kizhatil, Graham Craft

Jackson Lab, 600 Main St, Bar Harbor, ME 04609

Purpose: The Schlemm's canal inner wall endothelial cells (SCE) are the last barrier to the outflow of aqueous humor (AQH). SCE responds to shear stress and stretch resulting from IOP elevation by upregulating nitric oxide (NO) to increase the permeability of the Schlemm's canal inner wall. In endothelial cells, NOS3-mediated formation of NO from arginine paradoxically requires extracellular arginine even with sufficient intracellular arginine ("arginine paradox"). A resolution for this paradox in endothelial cells is the preferential delivery of arginine to NOS3 by its interaction with arginine transporter SLC7A1 within caveolae. Thus, SLC7A1 is likely to play a critical role in outflow physiology; hence we have determined the role of SLC7A1 in AQH outflow regulation.

Methods: We first determined the localization of SLC7A1 in the Schelmm's canal in mice. Next, using the proximity ligation technique, we determined if NOS3 and SLC7A1 are associated with each other and in caveolae labeled with CAV1. We next determined the effect of inhibiting SLC7A1 arginine transport using lysine in wild-type and CAV1 null mouse eyes on aqueous humor outflow to determine if the transporter plays a role in outflow physiology and if caveolar sequestration of NOS3 and SLC7A1 affects efficient aqueous humor outflow.

Results: Our results show that SLC7A1 is expressed in the Schlemm's canal and that a population is associated with NOS3 (40nm proximity) and CAV1, a proxy for caveolae. The facility measured in control eyes was 3.99±0.75 nl/min/mmHg (95%CI mean: 3.55-4.4) compared to lysine-treated eyes to inhibit arginine transport, which was 3.14±0.78 nl/min/mmHg (95%CImean: 2.71-3.57) showing a 21% reduction (p=0.003). Moreover, there is a pressure-dependent reduction in aqueous humor outflow. The pressure-dependent reduction in outflow is abrogated in the CAV1 null background.

Conclusions: Together, our results suggest that SLC7A1 plays a role in regulating outflow. At a molecular level, this is likely due to the close association of NOS3 and SLC7A1 in caveolae to satisfy the paradigm to explain the "arginine paradox." We are currently determining the effect of the loss of caveolae on the association of NOS3 and SLC7A1 since this has a physiological effect on outflow. In addition, we are testing the requirement from the arginine transporter directly by knocking out SLC7A1 in the Schlemm's canal inner-wall using CRIPSR-based methods.

19. Post GWAS Approaches: From Association to Function of IOP genes

Helene Choquet[1], Kiran Gangappa[2], Nivedita Singh[3], Durairaj Duraikannu[2], Rupalatha Maddala[4], Krish Kizhatil[5], Revathi Balasubramanian[6], Simon John[6], Vasantha Rao[4], Anand Swaroop[3], Saidas Nair[2]

[1] Kaiser Permanente Northern California, Division of Research, Oakland, CA 94612
[2] Dept. of Ophthalmology, School of Medicine, University of California, San Francisco, San Francisco, CA 94143
[3] National Eye Institute, National Institute of Health, Bethesda, MD 20892
[4] Dept.of Ophthalmology, Duke University, Durham, North Carolina, 27705
[5] The Jackson Laboratory, Bar Harbor, Maine 04609
[6] Dept. of Ophthalmology, Columbia University, New York, NY 10032

Purpose: Our objective is to identify genetic factors and molecular mechanisms contributing to high intraocular pressure (IOP) and primary open-angle glaucoma (POAG). Genome-wide association studies have uncovered over 300 independent risk loci and associated variants in POAG. However, translating the GWAS data into the biological mechanisms underlying disease pathogenesis has proven to be challenging. These challenges encompass:

1) Inconsistent Link Between IOP and POAG: While elevated IOP is a causal risk factor for glaucoma, not all genetic loci associated with IOP affect the risk of developing POAG.
2) Predominance of Non-Coding Variants: Most GWAS-identified genetic variants contributing to IOP are located outside the coding regions of genes, including intergenic regions. Understanding the functional role of these non-coding genetic variants in relevant ocular tissue and cell types remains a significant hurdle.
3) Unknown Functions of Identified Genes: A substantial number of the genes identified through GWAS have unknown functions, complicating efforts to determine the cellular processes and molecular networks contributing to IOP elevation.

To address these challenges, we are employing a multifaceted approach that integrates genetic, genomic, and mouse models to pinpoint IOP loci and their associated target genes.

Methods: The methods include:

1) GWAS of ocular endophenotypes: We conducted GWAS on other ocular parameters, such as central corneal thickness (CCT), to investigate whether variations in these structural measures of the eye can explain the lack of association between some IOP loci and POAG.
2) Non-Coding Genome Annotation: We are annotating the regulatory landscape of the non-coding genome by identifying distinct chromatin features in primary human

trabecular meshwork (TM) cells. This involves determining chromatin loops between TM-enriched target gene promoters and the regulatory genome through promoter capture Hi-C, as well as identifying open-chromatin regions via transposase-accessible chromatin with sequencing (ATAC-Seq).

3) Genetic mouse models to gain insight into IOP: Using mouse models, we are characterizing the role of GLIS1, an IOP-associated gene, in maintenance of the TM.

Results: Our findings include:

1) IOP and CCT Association: We discovered that IOP loci strongly associated with CCT were not linked to POAG. This supports the idea that CCT influences IOP measurements but does not directly impact the risk of developing POAG.
2) Integration of 3D Genomic Mapping: Combining the 3D genome map derived from Hi-C and ATAC-Seq analysis with PAOG-GWAS identified potential new gene targets of the associated variants.
3) Role of GLIS1 in IOP regulation: We identified a distinct subset of TM cells expressing Glis1, a Krüppel-like zinc finger transcriptional factor, in mice. This provides insights into the Glis1-dependent regulatory network contributing to TM cell maintenance.

Conclusions: Our comprehensive approach combines various methods to identify and functionally characterize specific genetic mechanisms responsible for elevated IOP, ultimately enhancing our understanding of how increased IOP impacts the risk of glaucoma.

20. Autophagy deficiency protects against ocular hypertension and neurodegeneration in experimental and spontaneous glaucoma mouse models

Paloma B. Liton[1], Angela Dixon[1], Myoung Sup Shim[1], April Nettesheim[1], Aislyn Coyne[1], Chien-Chia Su[1], Haiyan Gong[2,3]

[1]Dept. of Ophthalmology, Duke University, Durham, NC, 27705, USA. paloma.liton@duke.edu.
[2] Dept. of Ophthalmology, Boston University Chobanian & Avedisian School of Medicine, Boston, MA, USA
[3] Dept. of Anatomy and Neurobiology, Chobanian & Avedisian Boston University School of Medicine, Boston, MA, USA

Objectives: Previous studies in our laboratory found that overactivation of autophagy in DBA/2J::GFP-LC3 mice led to higher IOP elevation, RGC death and optic nerve degeneration. We found similar findings in aging GFP-LC3 mice subjected to chronic IOP elevation. Here, we follow up on these studies and investigate the impact of autophagy deficiency on ocular hypertension and glaucoma in experimental and spontaneous mouse models.

Methods: Transgenic DBA/2J-*Atg4b*^{ko} mice were generated by deleting a ~ 8 kb region encompassing exons 4–8 in the *Atg4b* gene via CRISPR/Cas technology. Deletion of this region results in a frameshift mutation beginning in exon 9 and a premature STOP codon in exon 10 of *Atg4b*. *Atg4b*^{ko} mice were obtained from Dr. Carlos Lopez-Otin's lab at the University of Oviedo (Spain). Autophagy deficiency in *Atg4b*^{ko} and DBA/2J-*Atg4b*^{ko} mice was confirmed by evaluating protein levels of LC3 and p62 in whole tissue lysates from dissected the iridocorneal region and retina tissues. Experimental ocular hypertensive mice were generated by unilaterally injecting a recombinant lentivirus expressing constitutively active human TGFβ2 (2×10^6 TU/eyes, 2 µL bolus) via intravitreal injection. Empty lentivirus vector (L-Null) was used as control. OP was measured using a Tonolab rebound in isoflurane-anesthetized mice. A series of six measurements per eye (OS and OD), taken within one minute post anesthesia, were collected and averaged to produce a single IOP value per eye for each measurement session. Outflow facility measurements were conducted ex-vivo using the iPerfusion MK V system. Retinal ganglion cell (RGC) quantification was conducted in whore retinal flat mounts, using an anti-Brn3a antibody. Optic nerve axon count was performed in axonal cross-sections using AxioVision imaging system. Tissue morphology was evaluated in thick and ultrathin sections.

Results: Eye cups from *Atg4b*^{ko} mice developed normally. While ATG4 deficiency did not cause RGC death or ON degeneration, abnormalities in outflow pathway tissue function were note with aging. A gradual decline in IOP with aging was observed in *Atg4b*^{ko} mice starting at 16 m.o. of age. *Atg4b*^{ko} did not show increase outflow facility with aging, as observed in *Atg4b*^{wt}. Intriguingly, in contrast to DBA/2J mice,

DBA/2J-*Atg4b*^{ko} mice failed to develop glaucomatous IOP elevation. No signs or RGC loss or ON atrophy was observed in DBA/2J-*Atg4b*^{ko} mice. Atg4b deficiency also protected against glaucomatous IOP elevation in the experimental TGFβ2 chronic ocular hypertensive model and protected against TGFβ2-induced fibrosis.

Conclusions: Together, these and prior reports from our lab strongly indicate a role of autophagy in IOP homeostasis, in particular with aging, and that autophagy deficiency protects against glaucomatous IOP elevation, RGC death and ON atrophy.

21. Testing of IOP Lowering Drugs in a Mouse Model of Glaucoma

Judith A. West-Mays[1], Fatima Shirazee[1], Terete Borras[3], Heather Sheardown[1], Trevor Williams[2], Aftab Taiyab[1]

[1] McMaster University, Health Sciences Centre, 1280 Main St. W., L8S 4L8, Hamilton, ON, Canada
[2] University of Colorado, Craniofacial Biology Mail Stop 8120, RC1-S, Rm L18 12801 E. 17th Ave., Aurora, CO 80045, USA
[3] Department of Ophthalmology, Gene Therapy Center, University of North Carolina School of Medicine, 321 S. Columbia Street, Ste.1001 Bondurant Hall, CB #9500, Chapel Hill, NC 27599-9500, USA

Purpose: Glaucoma is one of the leading causes of irreversible blindness throughout the world. This disease occurs due to a rise in intraocular pressure (IOP), which can cause pressure on the optic nerve and subsequent loss of retinal ganglion cells (RGC); ultimately causing vision loss. Topical medications are commonly used for treatment. However, poor patient compliance is associated with these medications due to the need for frequent dosing. We have recently developed a partially open angle mouse model of glaucoma termed the AP-2β trabecular meshwork region knockout (AP-2β TMR KO), where the gene encoding transcription factor AP-2β, tfap2b, is conditionally deleted from the periocular mesenchyme using MgpCre recombinase. This study utilizes the AP-2β TMR KO mouse model to explore an alternative approach for drug delivery to prolong the efficacy of current medication and prevent the onset of glaucomatous effects.

Methods: The AP-2β TMR-KO or *MgpCre*$^{+/-}$*;tfap2b*$^{-/lox}$ mice, as well as control littermates, were developed by breeding male *MgpCre*$^{+/-}$*;tfap2b*$^{+/-}$ with female *tfap2b*$^{lox/lox}$ mice. Since the AP-2β TMR KOs possess a partially open iridocorneal angle, the functionality of the unconventional outflow pathway was tested by treating the eyes of these mutants and their wild-type littermates with latanoprost (LTP), a prostaglandin analogue that increases outflow through the unconventional pathway. An equal number of mutant and wildtype littermates were treated daily with 0.005% LTP (10µl in each eye) for up to 40 consecutive days. In addition, a mucoadhesive micelle-based polymer system loaded with 0.005% LTP was employed to facilitate effective, longer term drug delivery. An equal number of mutant and wildtype littermates were treated every three days with micelle-0.005% LTP (M-LTP) (10µl in each eye) for up to 40 consecutive days to compare with the LTP treatments. IOP measurements were taken before treatment and then at 20min, 1 hour, 24 hour and 5 days after treatment. For the extended treatment groups IOP was taken before treatment and then every three days up until study completion. At the end of the treatment period, the mice were euthanized, and their eyes were enucleated, fixed, sectioned, and stained for retinal ganglion cells using Brn3a.

Results: Initial baseline measurements of the AP-2β TMR-KO mice were significantly higher than controls ($P \leq 0.05$ and $P \leq 0.0001$, respectively) (Fig 1). 20 minutes after treatment with LTP there was a significant reduction in IOP for the AP-2β TMR KO mutant mice ($P \leq 0.001$). However, by one hour after treatment the mutant mice exhibited IOP levels that were similar to those observed prior to treatment. Interestingly, following extended treatment with LTP, the AP-2β TMR-KO mice showed a consistent downward pattern in their baseline IOP readings with a final, significant reduction in IOP at 35 days as compared to untreated mutants ($P < 0.0001$)(Fig. 2). Importantly, mutant mice treated every three days with micelle delivered LTP (M-LTP) when compared to ones treated daily with LTP alone exhibited a sustained reduction in IOP even after 5 days of treatment (Fig. 1). Furthermore, mutants treated over extended periods of time with the M-LTP showed a reduction in baseline IOP that occurred sooner and was significantly lower than mutants treated with LTP alone (Fig. 2). Finally, mutant mice exhibited a significant decrease in RGC cell number when compared to wildtype, and this loss was *not* rescued by treatment with LTP. However, mutants treated with M-LTP demonstrated some RGC cell protection compared to eyes of untreated mutants, as well as that of the everyday LTP treated mutants.

Conclusions: These data demonstrate that although the conventional outflow pathway is absent in the AP-2β TMR KO mice, the unconventional-uveoscleral outflow pathway appears to be functional and responsive to LTP. Additionally, our findings show that long-term LTP treatment significantly reduces the baseline IOP in our glaucoma mouse model. We further showed that the three-day micelle delivered LTP (M-LTP) was more effective than daily LTP treatment in its ability to reduce IOP in the short term, and baseline IOP levels overtime. Along with the significant reduction in IOP, the M-LTP treatment also resulted in improvement in RGC cell protection. Thus, the micelle-based drug delivery system may slow down the progression of disease and preserve remaining visual function in individuals affected by glaucoma.

Acknowledgements: NIH EY025789; CIHR 202003PJ

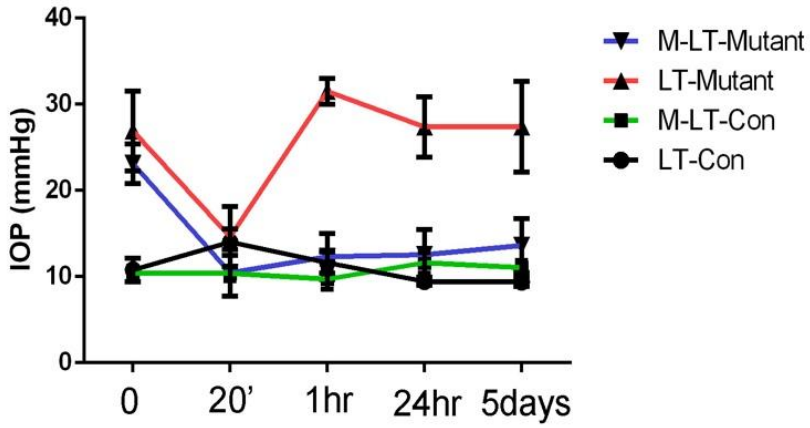

Figure 1. *Mean IOP of mutants and wild-type littermates treated with latanoprost (LT-Mutant;LT-Con) and micelle-latanoprost conjugate (M-LT-Mutant; M-LT-Con) after 20 minutes (20'), 24 hour (24h) and 5 days. p<0.01, LT-Mutant vs M-LT-Mutant.*

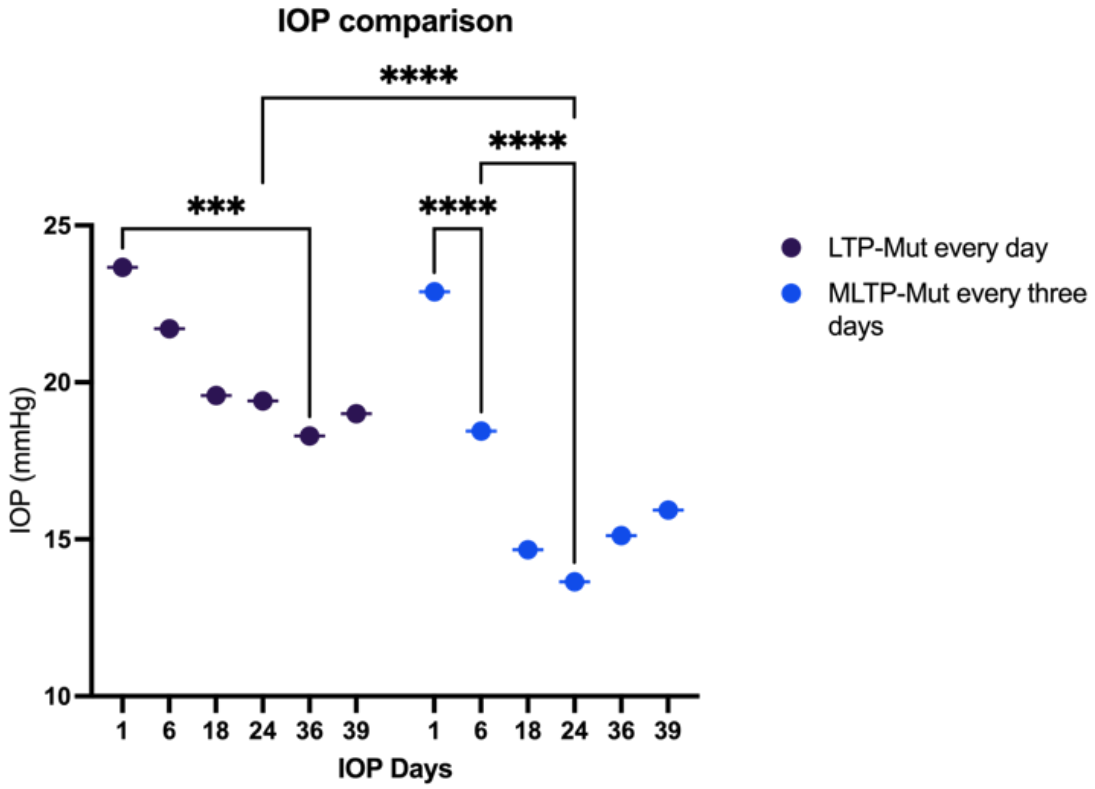

Figure 2. *IOP of mutants treated everyday with LTP vs mutants treated every 3 days with MLTP. IOP in AP-2β TMR KOs (N = 16 eyes) treated with LTP every day is significantly reduced at 36 day of treatment (***p < 0.001). Whereas the IOP in the MLTP group significantly reduced from baseline at day 6 of treatment (N = 10 eyes); ****p < 0.0001) (all error bars signify standard deviation). The IOP of the MLTP treated mutant mice continued to reduce up until day 24 of treatment (p < 0.0001). There was also a significant reduction in the IOP of MLTP mice (N = 10 eyes); p < 0.0001) when compared to IOP of mutant mice treated with daily LTP on 24 days of treatment.*

22. Effect of Thrombospondin-1 on Outflow Facility, Outflow Pattern and Morphology in Porcine Eyes

Haiyan Gong[1,2], Lucia Yang [3], David L. Swain[1,2], Sujeoung Kim[1], Abid Khan[1], Michelle Yung[1] , Hoi-Lam Li[1]

[1] Dept. of Ophthalmology, Boston University Chobanian & Avedisian School of Medicine, Boston, MA, USA
[2] Dept. of Anatomy and Neurobiology, Chobanian & Avedisian Boston University School of Medicine, Boston, MA, USA
[3] New England College of Optometry, Boston, MA, USA

Purpose: Primary open-angle glaucoma (POAG) is the major type of glaucoma, accounting for 74% of all glaucoma cases (1). Elevated intraocular pressure (IOP), due to the increased resistance in the trabecular outflow pathway, is the main risk factor for POAG (2, 3). In the trabecular outflow pathway, aqueous humor departs from the trabecular meshwork (TM), passes through Schlemm's canal (SC), collector channels (CCs), intrascleral veins (ISVs), and finally reaches the episcleral veins (ESVs). Instead of having a single SC in human eyes, porcine eyes have aqueous plexus (APs), which serves an equivalent function. Thrombospondin-1 (TSP1) was found to be upregulated after transforming growth factor-β2 (TGF-β2) and dexamethasone treatment in TM cells, which are related to the IOP elevation (4). The immunoreactivity of TSP1 was more intense in TMs of eyes with glaucoma (4). Conversely, TSP1 knockout mice demonstrated a lower IOP (5). All together, these studies suggest that TSP1 plays a role in the regulation of IOP. The aim of this study is to identify the effect of TSP1 on the outflow facility, flow pattern, and morphology in the conventional outflow of porcine eyes.

Method: Fresh porcine eyes were obtained from local abattoirs (Research 87) within 6 hours of death. Porcine eyes (N= 14 pairs) were perfused with Dulbecco's phosphate-buffered saline containing 5.5 mM of D-glucose (GPBS) at 15 mmHg for 30 minutes to establish a stable baseline outflow facility. One eye of each pair was then exchanged and perfused with TSP1 (0.8 μg/mL) for 3 hours, while the contralateral eye of each pair was exchanged and perfused with GPBS as control. Outflow facility was recorded. All eyes were then perfused with fluorescent tracer to label the outflow pattern, followed by perfusion-fixation. The fixed eyes were dissected into 16 radial segments and the images of frontal sections of the TM and APs were captured by a confocal microscope after nuclear counter-staining. The effective filtration length (PEFL = ΣFL/ΣTLx100%) along the inner wall of APs in each eye was calculated. The sections were further processed, embedded, and cut into 4-6 μm sections for light microscopy. The morphology of TM was evaluated and the cross-sectional areas of the ESV and ISV (N=4 pairs) were measured using ImageJ. The measured data was normalized following the formula where the normalized area= vein area of TSP1 treated eye/ vein area of the paired control eye, then compared between the two groups.

Results: Three hours perfusion of TSP1 significantly lowered the outflow facility in porcine eyes compared to control eyes by 0.05 ± 0.02 µl/min/ mmHg (15 ± 10%, N=14 pairs, $p < 0.0001$, Figure 1). No significant difference was observed in the PEFL along the inner wall of APs (N=7 pairs) and in the general morphology of the TM between TSP-1-treated and control groups (N=4 pairs). However, the normalized areas of ESVs (Figure 2A) and ISVs (Figure 2B) of TSP-1-perfused eyes were significantly smaller than those in the control eyes by 50 ± 7% ($p < 0.01$) and 29 ± 8% ($p < 0.05$), respectively.

Conclusion: Decreased outflow facility by TSP1 is associated with reducing the size of ESVs and ISVs. Our results highlight the potential for regulating IOP by targeting the size of ISV and ESV in the distal outflow pathway.

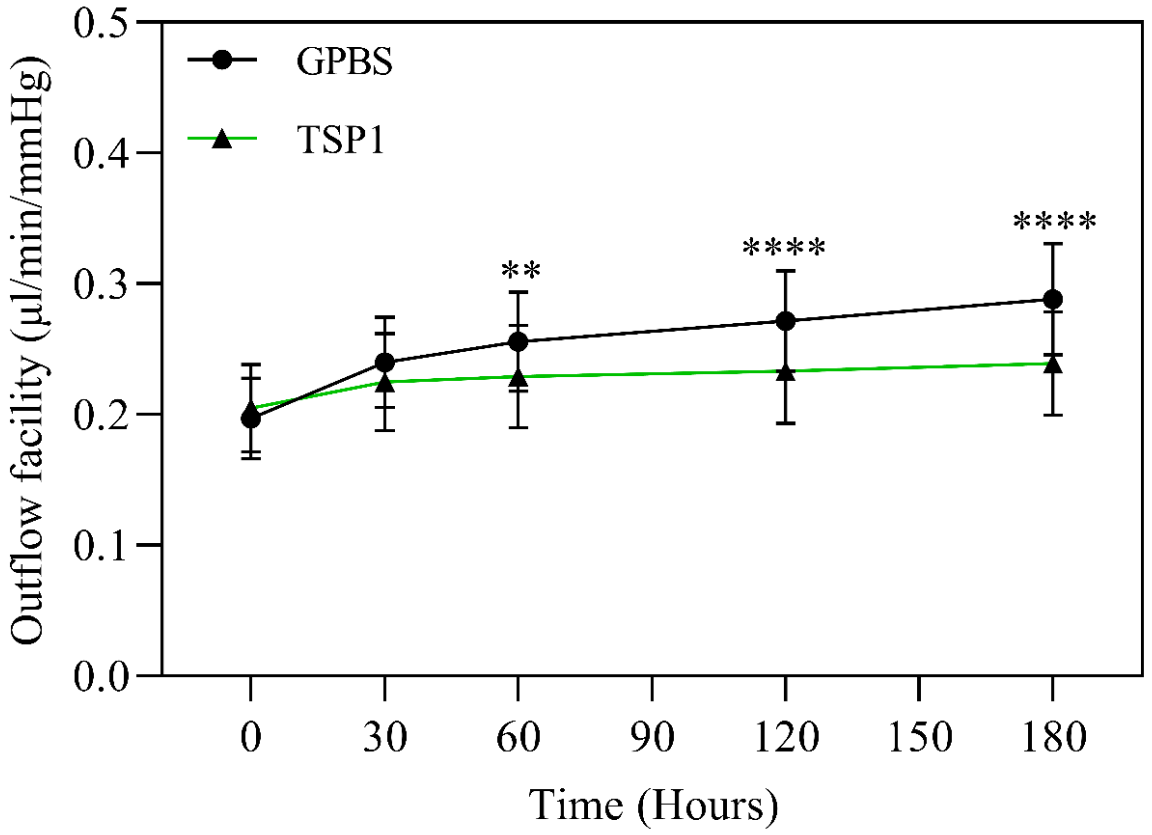

***Figure 1**: Effect of TSP1 on outflow facility in paired porcine eyes. Changes in outflow facility for 3 hours treatment of GPBS and TSP1 was presented. Effect of TSP1 on outflow facility in porcine eyes. Results were expressed as mean ± standard error of the mean (SEM). (n = 14, ** p < 0.01, **** p < 0.001, two-way repeated measures ANOVA followed by Bonferroni t-test).*

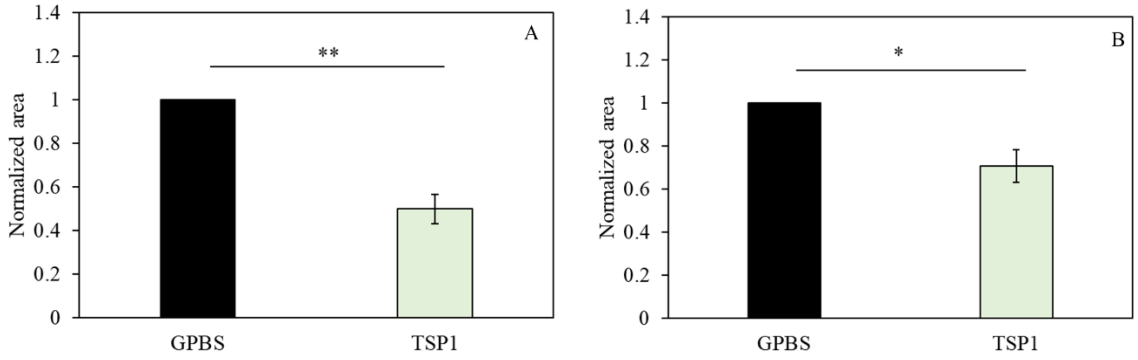

***Figure 2**: Effect of TSP1 on the area in ESV and ISV in paired porcine eyes. Normalized ESV area compared to the paired control (TSP1) eyes (A) and normalized ISV area compared to the paired control eyes (B) for 3 hours treatment of GPBS and TSP1 was presented. Results were expressed as mean ± standard error of the mean (SEM). (n = 4, * p < 0.05, ** p < 0.01, paired t-test).*

References:

1. Tham YC, Li X, Wong TY, Quigley HA, Aung T, Cheng CY. Global prevalence of glaucoma and projections of glaucoma burden through 2040: a systematic review and meta-analysis. Ophthalmology. 2014;121(11):2081-90.
2. Grant WM. Further studies on facility of flow through the trabecular meshwork. AMA archives of ophthalmology. 1958;60(4):523-33.
3. Grant WM. Experimental aqueous perfusion in enucleated human eyes. Arch Ophthalmol. 1963;69:783-801.
4. Flugel-Koch C, Ohlmann A, Fuchshofer R, Welge-Lussen U, Tamm ER. Thrombospondin-1 in the trabecular meshwork: localization in normal and glaucomatous eyes, and induction by TGF-beta1 and dexamethasone in vitro. Exp Eye Res. 2004;79(5):649-63.
5. Haddadin RI, Oh DJ, Kang MH, Villarreal G, Jr., Kang JH, Jin R, et al. Thrombospondin-1 (TSP1)-null and TSP2-null mice exhibit lower intraocular pressures. Invest Ophthalmol Vis Sci. 2012;53(10):6708-17.

VI. TM Biomechanics

23. Dynamic 3D Traction Force in Normal and Glaucomatous Human Trabecular Meshwork Cells

Alireza Karimi[1,2], Mini Aga[1], Taaha Khan[1], Siddharth Daniel D'costa[1], Sebastian Cardenas-Riumallo[1], Meadow Zelenitz[1], Mary J. Kelley[1,3], Ted S. Acott[1,4], Haiyan Gong[5,6]

[1] Dept. of Ophthalmology, Casey Eye Institute, Oregon Health & Science University (OHSU), Portland, OR, USA
[2] Dept. of Biomedical Engineering, OHSU, Portland, OR, USA
[3] Dept. Integrative Biosciences, School of Dentistry, OHSU, Portland, OR, USA
[4] Dept. Chemical Physiology & Biochemistry, School of Medicine, OHSU, Portland, OR, USA
[5] Dept. of Ophthalmology, Boston University School of Medicine, Boston, MA, USA
[6] Dept. of Anatomy and Neurobiology, Boston University School of Medicine, Boston, MA, USA

Purpose: Glaucoma, which is associated with intraocular pressure (IOP) elevation, results in trabecular meshwork (TM) cellular dysfunction, leading to increased rigidity of the extracellular matrix (ECM), larger adhesion forces between the TM cells and ECM, and higher resistance to aqueous humor drainage. TM cells sense the mechanical forces due to IOP dynamic and apply multidimensional forces on the ECM. Recognizing the importance of cellular forces in modulating various cellular activities and development, this study is aimed to develop 2D and 3D *in vitro* cell culture models to calculate the 3D, depth-dependent, dynamic traction forces, tensile/compressive/shear strain of the normal and glaucomatous human TM cells within a deformable polyacrylamide (PAM) gel substrate.

Methods: Normal and glaucomatous human TM cells were isolated, cultured, and seeded on top of the PAM gel substrate with embedded FluoSpheres, spanning elastic moduli of 1.5 to 80 kPa. For the 3D cell culture model, serial block-face scanning electron microscopy (SBF-SEM) images of the TM, juxtacanalicular tissue, and inner wall endothelial cells of the Schlemm's canal with their basement membrane were segmented, 3D volume-meshed, and 3D printed at various elastic moduli. Sixteen-hour post-seeding live confocal microscopy in an incubator was conducted to image the 3D displacement map of the FluoSpheres within the 2D and 3D cell culture models (PAM gels). Combined with the known PAM gel stiffness, we ascertained the 3D traction forces in the gel.

Results: Our results revealed meaningfully larger traction forces in the glaucomatous TM cells compared to the normal TM cells. The higher the stiffness of the gel led to a larger traction force. The traction force within the PAM gel having the stiffness of 20 kPa was analyzed at depths of 10-µm (2D) and 150-µm (3D) from the gel's surface.

In comparison to the 2D model, the traction force observed in the 3D cell culture model was ~1.72-fold larger. In the 2D setup, the highest traction force was observed at the gel's surface where direct contact between the cells and gel occurs, while in the 3D model, the peak traction force is found 150-µm deep within the gel, where cells are spread across a broader, flatter region. The 2D model depicted a steady decrease in traction force from the top to the base but the 3D model presented a more dispersed pattern of traction forces throughout the depth. When analyzing displacement vectors, a more pronounced displacement in the Z direction was evident, perpendicular to the gel's surface, in comparison to the 2D model. This can be attributed to the cell-gel interaction at the gel's wall where the cells directly interface with the flow. Stress fibers in TM cells increased with gel rigidity, but diminished when stiffness rose from 20 to 80 kPa.

Conclusions: The developed 2D and 3D cell culture models aid in understanding how altered mechanical properties in glaucoma impact TM cell behavior and aqueous humor outflow resistance.

24. The Effects Of Mechanical Stimuli On Trabecular Meshwork Extracellular Vesicles

Reynolds Ablordeppey[1], Caroline Nelson[1], Bre'Ida J. Riddick[2], W. Daniel Stamer[2], Fiona S. McDonnell[1, 3]

[1] John Moran Eye Center, University of Utah, Salt Lake City, UT, USA
[2] Duke Eye Center, Duke University, Durham, NC, USA
[3] Dept. Biomedical Engineering, University of Utah, Salt Lake City, UT, USA

Purpose: Dysregulation of extracellular matrix (ECM) homeostasis in the conventional outflow pathway results in accumulation of ECM molecules and elevated IOP. A major function of extracellular vesicles (EVs) is regulation of ECM turnover. EV release from cells is tightly regulated, and they are differentiated from other nanoparticles based on their smaller size, cell type-specific cargo, and thus function. EVs from glaucoma TM (GTM) cells show differences in their proteomic cargo of the ECM proteins fibronectin and EDIL3 compared to EVs from non-glaucomatous TM (NTM) cells. We hypothesize that mechanical stimuli applied to NTM cells will affect how EVs released from these cells regulate ECM turnover.

Methods: NTM cells were subjected to cyclical mechanical stretch (20%, 1 Hertz for 24 h) and conditioned media (CM) was collected. EVs were selectively isolated from CM using double-cushion iodixanol buoyant density gradient ultracentrifugation. Fractions were then pooled to form two distinct samples of EV populations, and assessed using nanoparticle tracking analysis (NTA) and authenticated using established marker proteins by Western blotting (WB). WB data was normalized to the concentration of the respective samples.

Results: Nanoparticle tracking analysis showed EVs were within the expected size range (0% stretch 151.8±21.49; 20% stretch 147.9±40.87) and there was no significant difference in the concentration between the samples (X vs Y). Stretched NTM cells showed decreased fibronectin expression in both EV sample populations (fold change 0.74±0.32 and 0.46±0.69, respectively) compared to unstretched controls (n=3). EDIL3 was increased in one EV population (fold change 1.58±0.72) and decreased in the other EV population (fold change 0.4±0.39, $P<0.05$).

Conclusions: Together, data indicate that cyclic mechanical stretch of TM cells (modeling a response to IOP oscillations) affects extracellular vesicles' cargo, in particular ECM proteins that are likely involved with maintenance of TM structure.

25. TRPV4 and IOP: What is going on?

Sarah N. Redmon[1], Sarah N. Redmon[1], Christopher N. Rudzitis[1], Terete Borras[2], Monika Lakk[1] and David Krizaj[1,3,4]

[1] Dept. of Ophthalmology & Visual Sciences, University of Utah School of Medicine, Salt Lake City, UT
[2] Dept. of Ophthalmology, University of North Carolina School of Medicine, Chapel Hill, NC;
[3] Dept. of Bioengineering and [4] Dept. of Neurobiology, University of Utah, Salt Lake City, UT

Purpose: Intraocular pressure (IOP) is fluctuates on multiple time scales: from seconds (blood pulse) to hours (circadian rhythmicity), while also changing in response to alterations in body positions, blinking, sneezing, eye rubbing and microgravity, trumpet playing, yoga and running yet remains stable over the lifetime on the individual. Acute and chronic changes in IOP are associated with homeostatic and pathological function of the trabecular meshwork (TM) that were suggested to involve TRPV4 (transient receptor potential vanilloid isoform 4), a polymodal nonselective cation channel. Current hypotheses reached different conclusions regarding its coupling to downstream signaling pathways and function in outflow regulation and IOP homeostasis. The purpose of this presentation is to discuss these hypotheses within the framework of our experiments.

Methods: Wild type and global *Trpv4*$^{-/-}$ mice were as in our previous reports. Conditional knockout mice lacking TRPV4 within the TM were generated by mating floxed *Trpv4* animals with a *Mgp*^{Cre} line developed in the Borras laboratory. Whole-cell patch-clamp recordings, optical imaging, pharmacology, tonometry were used to investigate TRPV4 function in cultured mouse and human trabecular meshwork cells and intact eye. High-speed pressure clamp was used to apply pressure steps to cultured cells. Ocular hypertension was induced through injection of microbeads, glucocorticoid administration, lentiviral transduction of TGFb2 or by measuring nocturnal IOP.

Results: TRPV4 -mediated calcium influx functions modulates the Rho signaling pathway, cytoskeletal dynamics and outflow studied *in vitro* and *in vivo*. Pharmacological and genetic manipulations of TRPV4 expression and function impact the amplitude of steady-state IOP, with potential differences with respect to channel participation in genetic, physiological and pathological models of ocular hypertension. Some but not all aspects of evoked OHT were suppressed by TRPV4 ablation, suggesting involvement of inflow, uveoscleral and/or Schlemm's canal mechanisms.

Conclusions: Stretch-activated TRPV4 channels dynamically participate in conventional outflow regulation and IOP homeostasis, possibly as one of the final

common mechanisms through which the biomechanical milieu (strain, compression, shear, cell volume) communicates with the cells' genes and actomyosin machinery. The channel appears to be activated by circadian and pathological signals yet is regulated by different systemic factors, indicating a hitherto unsuspected refinement in TM mechanoregulation.

Acknowledgements: Funded by the National Eye Institute, Department of Defense, Stauss-Rankin Foundation, Crandall Glaucoma Initiative and an unrestricted RPB award to the Department of Ophthalmology at the University of Utah.

VII. Keynote: A journey from … DNA Reassociation Kinetics to … Gene Therapy of Glaucoma

VIII. TM Cell Signaling and Regulation

26. Deciphering the role and origin of cross-linked actin networks in the trabecular meshwork

Weiming Mao[1], Haiyan Li[2], C. Ross Ethier[2], Taeyoon Kim[3], Steven P. Swingle[4], Todd A. Sulchek[2], Devon H. Harvey[1], Jiannong Dai[1], Sheng Liu[5], Tsai-Yu Lin[5], Jun Wan[5]

[1] Dept. of Ophthalmology, Eugene and Marilyn Glick Eye Institute, Indiana University School of Medicine
[2] Wallace H. Coulter Department of Biomedical Engineering at Georgia Institute of Technology & Emory University School of Medicine
[3] Weldon School of Biomedical Engineering, Purdue University
[4] George W. Woodruff School of Mechanical Engineering, Georgia Institute of Technology & Emory University School of Medicine
[5] Dept. of Medical and Molecular Genomics, Indiana University School of Medicine

Purpose: Cross-linked actin networks (CLANs), an enigmatic feature of trabecular meshwork (TM) cells, are associated with many aspects of ocular hypertension (OHT), yet the specific role of CLANs in OHT remains poorly understood. This is a critical knowledge gap, as understanding how CLANs cause OHT could reveal new therapeutic targets for OHT control in glaucoma. We serendipitously discovered a TM cell line, here denoted GTM3L, obtained by lentiviral transduction (lenti-CMV-LifeAct-GFP) of immortalized human glaucomatous TM cells (GTM3). GTM3L cells form fluorescently labeled CLANs (due to LifeAct-GFP expression) spontaneously, and thus are a valuable research tool. However, the formation rate of CLANs in GTM3L cells is low (~0.04%). In this study, we combined several methods to increase CLAN formation in GMT3L cells, developed a computational model to mimic and study the biomechanical properties of CLANs, and explored the role and origin of CLANs.

Methods: GTM3L cells were flow sorted based on GFP intensity. Some GTM3L cells were treated by adding 0-5% polyethylene glycol 300 (PEG300) to the media for at least 2-7 days to cause cell deswelling, followed by atomic force microscopy (AFM) measurements of cell stiffness. We selected CLAN-positive (CLAN+) GTM3L cells by exposing GTM3L cells to 0.25% trypsin for 2 mins to remove non-adherent cells, which tended to be CLAN-negative. The remaining adherent cells were then dislodged by retreatment with 0.25% trypsin for 30 seconds and were seeded on cell culture dishes/flasks for expansion. After 9 cycles of adherence-based selection as above, we further selected CLAN+ enriched GTM3L cells using a microfluidic device that uses angled constrictions to sort cells based on their stiffness. To study the effect of matrix stiffness on CLAN formation, some enriched GTM3L cells were cultured on glass or on a soft hydrogel (Elastic modulus = 2 kPa), and were treated with 2% PEG300 for either 2 or 5 days. At the end of treatment, the cells were fixed by paraformaldehyde and stained with phalloidin-Alexa-488 and DAPI to determine CLAN formation rate

(Number of CLAN+ cells/number of DAPI+ cells). We also constructed computational models using agent-based models to mimic and study the biomechanical properties of CLANs. In these models, the microstructure of CLANs with actin filaments and actin-binding proteins were explicitly simulated with or without cell membrane/nucleus. Finally, to determine CLAN origin, we used CLAN-enriched GTM3L cells, CLAN-unenriched GTM3L cells, and naïve GTM3 cells for viral copy number analysis, DNA sequencing (DNAseq) using the Integration Site Pipeline for Paired-End Reads (INSPIIRED) pipeline, and RNA sequencing (RNAseq).

Results: CLAN formation rate (CLAN incidence) could be increased from ~0.04% to ~50% in GTM3L cells by a combination of CLAN enrichment/selection strategies, namely cell-substrate adherence (based on trypsin release), cell stiffness-based sorting, and PEG300 treatment. We also observed that GTM3L cells formed more CLANs when cultured on the stiff glass substrate compared to those cultured on a soft hydrogel substrate ($p<0.0001$). Using AFM, we found that CLAN+ GTM3L cells were significantly stiffer than CLAN- GTM3L cells ($N=4$, $p<0.05$).

Using computational models, we determined how CLANs could potentially enhance cell stiffness. We found that two-dimensional CLANs surrounding a cell nucleus limited the deformability of the nucleus, and therefore overall cell stiffness measured by compressive stress/strain was increased. In addition, our model showed that three-dimensional CLANs in the cytoplasm had stronger resistance to compressive loads, leading to enhanced cell stiffness.

Viral copy number analysis showed that all GTM3L cells, regardless of their GFP expression levels, had an average of 1 viral copy in their genome per cell. We then compared the viral insertion site of GTM3L cells with CLAN enrichment (containing ~20% CLAN+ cells) vs. GTM3L cells without enrichment (containing ~0.04% CLAN+ cells) vs. naïve GTM3 cells (without lentiviral-LifeAct-GFP transduction as a technical control) using the INSPIIRED pipeline. We found that in some GTM3L cells with 0.04% CLAN+ cells (but not in 20% CLAN+ cells), the lentivirus inserted into introns of the Notch2NLC/R or Notch2 genes (all on chr 1). The lentivirus also inserted into introns of the ZNF595 and NUP214 genes (chr4 and 9, respectively) in both 0.04% and 20% CLAN+ cells. A subsequent RNAseq study using the same 3 groups of cells showed that Notch2NLC/R mRNA was 9% higher, and Notch2 mRNA was 15% higher in 0.04% CLAN+ cells vs. in 20% CLAN+ cells, suggesting that enhanced Notch2NLC/R and Notch2 expression may be protective against CLAN formation. In contrast, although both 0.04% and 20% CLAN+ cells showed insertions in ZNF595 and NUP214, the expression of these genes was 25% and 15% higher, respectively, in 20% CLAN+ cells vs. 0.04% CLAN+ cells, suggesting a CLAN-inducing role for these genes.

Conclusions: We developed and combined several strategies to greatly enhance CLAN formation rate in GTM3L cells. We showed that CLANs increase TM cell stiffness, and that a stiff substrate increases CLANs. These biomechanical processes can be simulated using computational models to give insights into CLANs. Also, we believe that the presence or absence of CLANs in GTM3L cells depends on the locus of lentiviral insertion. Further research is needed to determine the effect of CLANs on TM biomechanics and mechanobiology as well as the etiology of CLAN formation in the TM.

Financial support: This work was supported by NEI R01EY026962 (W.M.), R01EY031700 (W.M.), R01EY031700-03S1 (W.M), R21EY033929 (W.M.), BrightFocus Foundation (W.M.) G2023009S (W.M.), the Georgia Research Alliance (C.R.E.), NSF CBET 2225476 (T.S.), and a Challenge Grant from Research to Prevent Blindness (Department of Ophthalmology, Indiana University School of Medicine).

27. Opioid Receptor-Mediated Mechanisms in Maintaining IOP

Karen Russell Randall and Dorothy Crumity

Pharmacology and Toxicology, Morehouse School of Medicine, Atlanta, GA

Purpose: The physiological functions of the eye depend upon IOP, but many aspects of the processes involved in ocular fluid balance remain to be elucidated. Studies in our lab have shown that select opioid receptor (OR)-subtype agonists reduce IOP and may therefore have a role in ocular function. Specifically, we have demonstrated that kappa and mu opioid receptor activation and resulting nitric oxide (NO) and natriuretic peptide (NP) increases, are involved in reducing IOP and regulating fluid dynamics, but there is limited information about the role of delta opioid receptor (DOP) activation in the front of the eye. We therefore hypothesize that NPs and possibly NO are functionally linked to OR-mediated ocular effects. Our overall hypothesis is that opioids contribute to the regulation of IOP by mechanisms involving guanylyl cyclase-mediated systems.

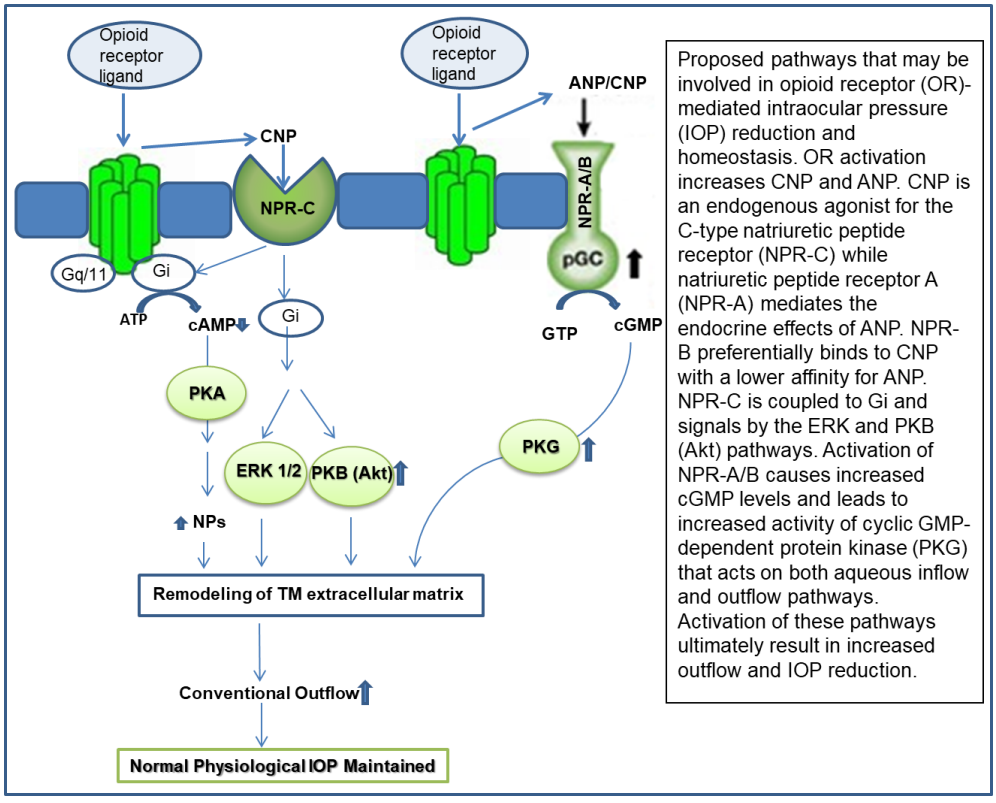

Methods: Standard immunocytochemical techniques using polyclonal antibodies directed against human kappa and delta opioid peptide receptors (KOP and DOP), natriuretic peptide receptors (NPR-A and NPR-B) or atrial natriuretic peptide (ANP) were utilized to determine the localization of these receptors to NTM-5 (normal TM) and GTM-3 (glaucomatous TM) cells. Both single protein and co-localization immunocytochemical studies were performed. Initial immunofluorescence

experiments were also performed in early passage primary human TM (HTM46) cells to compare opioid receptor localization with that of the transformed cells. To determine receptor expression, standard protocols were followed for Western blot experiments. Quantitative RT-PCR was also used to determine if there was a difference in mRNA expression of KOP & DOP in normal & glaucomatous TM cells. For NO determination, GTM-3 cells seeded in 6-well plates were grown to approximately 90% confluence before drug treatments. Experimental protocols were carried out on cells incubated at 37ºC in dye-free DMEM growth media containing protease inhibitor cocktail (Roche, Complete, Mini, EDTA-free Protease Inhibitor Cocktail Tablets) and L-arginine, which was included in the media of control and treated cells to stimulate nitric oxide production *in vitro*. For ANP & cGMP experiments, arginine was not included in the media. Enzyme immunoassay (EIA) was utilized to determine the effect of drug treatment on NO, ANP and cGMP levels. Cells were treated with SNC80, a selective DOP agonist, estradiol (positive control for the NO experiments) or sodium nitroprusside (SNP, positive control for cGMP).

Results: Our data show that DOPs and KOPs localize to cell membranes of HTM46, NTM-5 & GTM-3 cells. Immunostaining experiments with NTM-5 & GTM-3 cells also showed localization of NPR-A/B receptors and ANP to these cells. Similar experiments showed co-localization of DOP and NPR-A/B receptors to both cell types. In all co-localization studies with DOR and NPR, there appeared to be more intense fluorescence labelling in GTM-3 cells than in NTM-5 cells. Western blot analyses for the presence of KOR and DOR proteins in HTM46, NTM-5 and GTM-3 cells, show KOR and DOR bands at approximately 50 kDa and 54kDa, respectively. Our data indicate that KOPs and DOPs are differentially expressed in NTM-5 cells, with DOP being more highly expressed. qRT-PCR data also showed differences in mRNA expression of the 2 opioid receptors. Western blot confirmed the presence of the NP receptors and ANP in the cell types under investigation. ANP levels were significantly higher in NTM-5 cells than in GTM-3 cells.

Treatment with SNC80 (24 hours) caused a concentration-dependent increase in NO levels in GTM-3 cells. When compared to control, NO levels in SNC80-treated cells increased from 146.15 ± 16.23% of control (0.1 µM) to 323.50 ± 51.50% of control (100 µM). SNC80 concentrations of 10 µM and 100 µM revealed significant differences. The selective DOR antagonist naltrindole was used to confirm that the activation of DOR mediated SNC80-stimulated NO release. Pretreatment with naltrindole (100 µM; 30 minutes) resulted in significant inhibition of SNC80 (100 µM)-induced increases in NO levels. SNC80 also caused significant increases in ANP levels in NTM-5 & GTM-3 cells at concentrations of 100 µM and 10 µM, when compared to vehicle-only controls. Significant increases in cGMP levels in both cell types were also observed following treatment with SNC80 at 1, 10 and 100 µM when compared to vehicle-only controls.

Conclusions: Our data indicate that KOPs and DOPs are differentially expressed in TM cells, suggesting that they might have different effects in the anterior segment of the eye. The immunofluorescence data showed co-localization of DOP receptors with NPR A/B receptors, suggesting the possibility of interactions between the opioid

peptidergic system and natriuretic peptide pathways in the maintenance and physiological regulation of IOP, preventing the dysfunction that induces glaucoma. Our data also suggest that DOR-mediated reduction in IOP could be due to elevated NO, ANP and cGMP production in human trabecular meshwork tissue. Further work is needed to elucidate the specific involvement of the delta opioid system in regulating IOP, and to determine the signaling mechanisms involved in this regulation.

28. Estrogen Receptors, Biomechanical Factors, and Trabecular Meshwork

Jingwen Cai[1], Hannah Youngblood[1,2], Hongfang Yu[1], Patricia Schoenlein[1], Hongyan Xu[3] and Yutao Liu[1,4,5]

[1] Department of Cellular Biology and Anatomy, Augusta University, Augusta, GA
[2] Department of Chemistry, Georgia Institute of Technology, Atlanta, GA
[3] Department of Population Health Science, [4] Center for Biotechnology and Genomic Medicine and [5] James and Jean Culver Vision Discovery Institute, Augusta University, Augusta, GA.

Purpose: Our recent research and other literature have implicated the potential protective role of estrogen receptor signaling in outflow facility and intraocular pressure (IOP) regulation. Our bioinformatics research has identified networks of IOP-associated genes targeted by estrogen or its receptors. Our immunohistostaining suggested the expression of estrogen receptor 1 in human outflow tissues, including trabecular meshwork (TM) and Schlemm's canal (SC). mRNA-based expression analysis indicated the varying expression of three different estrogen receptors: estrogen receptor 1 (ESR1), estrogen receptor 2 (ESR2), and G-protein coupled estrogen receptor 1 (GPER1). Knockout mice with the loss of Esr1 led to significantly elevated IOP (1.5mmHg) in homozygous female mice compared to wild-type littermates after eight months of age. Knockout mice with the loss of Gper1 have significantly elevated IOP (2 mmHg) in heterozygous and homozygous males/females after three months of age. These data suggest the involvement of estrogen receptor signaling in IOP regulation and maintenance. It is necessary to identify what genes/pathways are targeted by estrogen receptors in TM cells.

Methods: We used validated primary human TM cells to identify the target genes of estrogen signaling. These human TM cells (n=10) were treated with 17-β estradiol (E2) (50μM), TGFβ2 (10ng/ml), TGFβ2 (10ng/ml) +E2 (50μM), and DMSO undergoing cyclic mechanical stretch (CMS 15%, 1 cycle/s, half-sine mode, 24 hrs) using a FX-6000T Tension system from FlexCell International Inc. To identify the contribution of three different estrogen receptors, we treated primary human TM cells (n=4) with PPT (agonist for ESR1, 50μM), DPN (agonist for ESR2, 50μM), and G1 (agonist for GPER1, 50μM) undergoing the similar procedure for cyclic mechanical stretch. Total RNA was extracted using the Qiagen miRNeasy kits and was profiled with Total RNA-Seq using the Zymo-Seq RiboFree Total RNA Library kit with an Illumina NovaSeq sequencer. Differential expression (DE) analysis was performed using Partek Flow, and gene ontology analysis was done using the WebGestalt software. E2 treatment alone without CMS inhibited cytoskeleton organization, polymeric cytoskeletal fiber, actin binding (FDR<0.05), up-regulated stress response to different ions, ER stress, unfolded protein response, and mineral absorption. E2 treatment alone with CMS led to increased response to induced unfolded protein response. TGFβ2 alone without

CMS inhibited cell migration, intracellular signal transduction, NADP+ activity, MAP kinase activity, lipid metabolism, increased protein phosphorylation regulation, transmembrane receptor protein serine/threonine kinase signaling pathway, and ECM synthesis. TGFβ2 alone with CMS inhibited cell migration, intracellular signal transduction, intracellular catalytic activity, oxidoreductase activity, PI-3 kinase activity, small GTPase binding, MAPK /EGFR /Rap1/ TNF signaling, increased cell adhesion, focal adhesion, ECM synthesis, and integral plasma membrane component synthesis. E2+TGFβ2 without CMS inhibited cell death, TGFβ receptor-mediated activity, actin binding, PLC activity, increased response to ER stress, ER chaperone complex, ECM component, mineral absorption, and unfolded protein response. E2+TGFβ2 under CMS inhibited cell motility/migration, Rho GTPase activation of CIT, increased ECM conferring compression resistance, cAMP response element binding protein binding, and P53 pathway. These differential expression gene expression data strongly indicate the anti-TGFβ2 effect of E2.

Results: To identify which estrogen receptor plays a significant role against the TGFβ2 effect, we treated human TM cells (n=4) with receptor-specific agonists in the presence of TGFβ2 followed by total RNA-Seq with data analysis using Partek Flow. Using a cutoff of |fold change|≥2 and FDR≤0.05, 604 genes were differentially expressed due to TGFβ2 treatment without CMS. Without CMS, PPT treatment (ESR1 activation) led to the non-significance of 537 TGFβ2-induced DE genes, DPN treatment (ESR2 activation) to the non-significance of 486 TGFβ2-induced DE genes, and G1 treatment (GPER1 activation) to the non-significance of 546 TGFβ2-induced DE genes. Under CMS, 360 genes were differentially expressed due to TGFβ2 treatment. PPT co-treatment led to the non-significance of 347 TGFβ2-induced DE genes, DPN co-treatment to the non-significance of 342 TGFβ2-induced DE genes, and G1 co-treatment to the non-significance of 334 TGFβ2-induced DE genes. These data suggest the similar contribution of ESR1, ESR2, and GPER1-based signaling pathways against TGFβ2-induced TM cellular and ECM alterations.

Conclusion: Overall, these RNA-Seq data analyses suggest the potential involvement of ESR1, ESR2, and GPER1 receptor signaling in maintaining human TM cellular function related to TGFβ signaling.

Financial Support: We appreciate all the financial support from NIH grants R01EY023242, R01EY023242-08S1, R21EY028671, R21EY028671-01S1, R01EY032960, R21EY033961, P30EY031631, The BrightFocus Foundation, the Glaucoma Research Foundation (GRF), The Glaucoma Foundation (TGF), Zymo Research Corporation, and the Medical College of Georgia at Augusta University.

Conflict of Interest: None for all the authors

29. Signaling Cytokines, Mechanochannels, and Ocular Hypertension

Christopher N. Rudzitis[1,2], Monika Lakk[1], Ayushi Singh[3], Samuel Herberg[3], and David Krizaj[1,2]

[1.] Department of Ophthalmology and Visual Sciences, John A. Moran Eye Center, University of Utah, Salt Lake City, UT
[2.] Interdepartmental Neuroscience Program, University of Utah, Salt Lake City, UT
[3.] Department of Ophthalmology and Visual Sciences, SUNY Upstate Medical University, Syracuse, NY

Purpose: Elevated levels of transforming growth factor beta 2 (TGFβ2) drive a myofibroblast-like Trabecular Meshwork TM phenotype that has been associated with fibrosis and elevated outflow resistance in primary open angle glaucoma (POAG). It is unclear whether this process involves dysregulation of TM pressure sensing and transduction, and what the molecular mechanisms that integrate biochemical (TGFβ) and biomechanical (IOP) glaucoma risk factors might be. We investigated the TGFβ2-dependence of expression of genes encoding mechanosensitive ion channels and ascertained the functional significance of TGFβ2-mechanochannel interactions for transmembrane & intracellular signaling, TM contractility and IOP homeostasis in a TGFβ2 model of ocular hypertension.

Methods: Quantitative reverse-transcription PCR (qRT-PCR), Western blot, whole cell imaging and fluorescent calcium imaging were used to profile the response of primary human and mouse trabecular meshwork cells to TGFβ2, and to assess the functionality of mechanosensitive ion channels *in-vitro*. Contractility measurements were conducted using biomimetic TM-seeded gels. Diurnal IOP measurements were used to measure ocular hypertension in a lentiviral TGFβ2 overexpression model.
Results: Exposure to TGFβ2 was associated with marked alteration of the mechanosensitive environment, as indicated by upregulation of cytoskeletal, extracellular matrix, and myofibroblast markers alongside the increased expression of a subset of mechanochannels and their membrane insertion. The potentiation of mechanosensitive channel Ca^{2+} signaling by TGFβ2 was time- and dose-dependent. Activation and inactivation were conversely associated with significant modulation of TM contractility. Finally, targeting cellular mechanotransduction interfered with TGFβ2-induced IOP elevation in living animals.

Conclusions: These experiments suggest that reactive, dynamic mechanochannel signaling integrates into the wider context of TGFβ2-induced pathology in TM cells. In-vivo, TM cells may undergo permanent differentiation due to overactive TGFβ2 signaling, but this experiment reinforces the idea that intra- and extracellular mechanical cues remain an important factor in TM health and activity. Furthermore, our in-vivo results may suggest that reducing possibly aberrant signaling by some

mechanochannels may be a viable method to reduce growth factor induced ocular hypertension.

Acknowledgements: This research has been funded by the National Eye Institute, the Stauss-Rankin Foundation, the Crandall Glaucoma Initiative and an unrestricted RPB award to the Department of Ophthalmology at the University of Utah.

30. Metabolites of Aqueous humor and deposit formation

Sanjoy K. Bhattacharya*, Anna Mueller, Anh Pham, Richard K. Lee

Bascom Palmer Eye Institute, Miami Integrative Metabolomics Research Center
University of Miami, Miami, Florida 33136

Purpose: To identify whether there are metabolite differences in pseudoexfoliation glaucoma (PEXG), primary open angle (POAG) glaucoma compared to cataract only control aqueous humor (AH). To determine if addition of selected metabolites differentially found in PEXG results in deposit formation in invitro assays (hanging drop method used for crystallization).

Methods: *Metabolomics.* The AH samples were obtained from human donors [control (n = 30), POAG (n = 30) and PEXG (n= 30)]. The AH samples were subjected to one-dimensional ^{1}H nuclear magnetic resonance (NMR) analyses on a Bruker Avance 600 MHz instrument with a 1.7 mM NMR probe. The same samples were then subjected to isotopic ratio outlier analysis (IROA) using a Q Exactive orbitrap mass spectrometer after chromatography on an Vanquish Horizon UPLC system. Clusterfinder Build 3.1.10^{TM} was used for identification and quantification based on long-term metabolite matrix standards. We also performed an untargeted metabolomics using the same system as IROA and analyzed the data using CompoundDiscoverer3.2^{TM}. In total, 278, 273 and 298 metabolites were identified in control, POAG and PEXG AH respectively. We found about 125 unique PEX, 63 unique POAG and 100 common metabolites among three types of AHs.
In vitro assays. We next used hanging drop method and control/normal AH samples (n=20 each) collected from donors age range 43-66 years, all Caucasian with equal gender distribution. We subjected the addition of 50 mg/desi liter of L-arginine, L-tyrosine 5 hydroxypentanoate and vitamin D in normal AH to evaluate deposit formation in vitro assays.

Results: About 12 significant metabolites identified when comparing PEXG to controls including L-arginine, L-lysine, L-glutamine, L-tyrosine, 2,4-diacetamido-2,4,6-trideoxy-beta-l-altrose, N(6)-acetonyl lysine, 1-aminocyclopropane-1-carboxylate, L-histidine, C6H9N4O3P, C6H13NO9, and 5 hydroxy pentanoate. The parent ion or modified version of vitamin D was identified (12th metabolite) only stratification of PEXG in field workers (n=12) who had PEXG for multi-years (>8 years). L-arginine, L-tyrosine 5 hydroxy pentanoate were consistently at 2.5-6.0-fold change (logarithmic scale) compared to others in PEXG AH compared to control or POAG. We evaluated whether the addition of 50 mg/desi liter of L-arginine, L-tyrosine 5 hydroxy pentanoate and vitamin D is sufficient to result in nucleation or fluffy deposit formation.

Conclusion: The differential metabolites found in PEXG alone are sufficient to result in formation of nucleation centers. The presence of other factors such as charged proteins, in addition to these metabolites results in larger fluffy deposit formation in in vitro experiments in normal AH.

31. Role of Dysregulated Glypicans in the Pathobiology of Ocular Hypertension

P. Vasantha Rao, Levi Lankford, and Rupalatha Maddala

Dept. of Ophthalmology, Duke University School of Medicine, Durham, NC, USA.

Purpose: This study aims to elucidate the molecular mechanisms governing the aqueous humor outflow through the trabecular meshwork in both normal and glaucomatous eyes.

Methods: We employed a range of approaches, including proteomics, ELISA, biochemical assays, immunofluorescence, gene targeting, primary cultures of human trabecular meshwork (TM) cells, analysis of aqueous humor (AH), and live mouse models. These techniques were utilized to explore the role of glypicans in regulating TM cell contractility, cell adhesion, actin cytoskeletal rearrangements, and IOP.

Results: Our findings indicate that human TM cells express cell surface heparan sulfate proteoglycans, glypican 1, 4, and 6, with the first two being the most abundant. Notably, GPC4 was consistently and significantly upregulated by dexamethasone and TGF-β2 in human TM cells. Additionally, GPC4 was detectable in both AH of human and conditioned medium of human TM cells, and its levels were significantly elevated in the AH of POAG patients compared to age and gender-matched non-glaucoma (cataract) patients. Furthermore, recombinant GPC4 induced the formation of actin stress fibers, focal adhesions, and cell-cell adhesions in TM cells, coinciding with increased levels of Wnt5A, phosphorylated JNK, myosin light chain, paxillin, and the Rho kinase substrate (MYPT1). In contrast, GPC4 deficiency in TM cells suppressed these cellular characteristics, leading to changes in cell shape. Moreover, our results also revealed that GPC4 is required for the Wnt5A-induced actin cytoskeletal reorganization in TM cells. Importantly, increased GPC4 expression in the anterior chamber of mouse eyes using lentiviral vectors raised IOP, while GPC4 deficiency lowered IOP compared to control mice.

Conclusion: In summary, our results demonstrate that AH derived from POAG patients contains elevated levels of GPC4. Moreover, recombinant GPC4 activates the Wnt5A/PCP/Rho GTPase signaling pathway, leading to increased contractility and cell adhesion in TM cells. Notably, elevated GPC4 expression results in higher IOP, suggesting that glypicans may serve as druggable targets for lowering IOP.

Financial Support: Supported by the grants (R01-EY028823, R01 EY018590 and P30EY5722) received from the National Eye Institute, NIH.

IX. White Paper Discussion #1: Consensus Recommendations for ex vivo Anterior Segment Studies of Outflow Facility and Intraocular Pressure Regulation

Consensus Recommendations for *ex vivo* Anterior Segment Studies of Outflow Facility and Intraocular Pressure Regulation

Ted S. Acott,[1,*] Michael P. Fautsch,[2] Weiming Mao,[3] C. Ross Ethier,[4] Alex S. Huang,[5] Mary J. Kelley,[1] Mini Aga,[1] Sanjoy K. Bhattacharya,[6] Terete Borras,[7] Diane Bovenkamp,[8] Uttio Roy Chowdhury,[2] Abbot F. Clark,[9] Yiqin Du,[10] Michael H. Elliott,[11] Jennifer A. Faralli,[12] Haiyan Gong,[13] Samuel Herberg,[14] Murray A. Johnstone,[15] Paul L. Kaufman,[16] Kate A. Keller,[1] David Krizaj,[17] Markus H. Kuhen,[18] Raquel Lieberman,[19] Shan C. Linn,[20] Yutao Liu,[21] Fiona McDonnell,[22] Colleen M. McDowell,[23] Gillian J. McLellan,[24] Kayarat Saidas Nair,[25] Darryl R. Overby,[26] Donna M. Peters,[12] VijayKrishna Raghunathan,[27] Ponugoti Vansantha Rao,[28] Najam A. Sharif,[29] Hongman Song,[30] Yang Sun,[31] Benjamin R. Thomson,[32] Carol B. Toris,[33] Colin E. Willoughby,[34] Hao F. Zhang,[35] Thomas F. Freddo,[36] Rudolf Fuchshofer,[37] Kamisha R. Hill,[19] Alireza Karimi,[1] Krishnakumar Kizhatil,[38] Casey C. Kopcyznski,[39] Paloma Liton,[40] Michael Peng,[3] Padmanabhan P. Pattabiraman,[41] Ganesh Prasanna,[27] Ester Reina-Torres,[26] E. Griffen Samples,[42] John R. Samples,[43] Cynthia L. Steel,[44] Clemens A. Strohmaier,[45] Preeti Subramanian,[8] Chenna Kesavulu Sugali,[3] Cydney Wong,[4] Hannah Youngblood,[19] Gulab S. Zode,[46] W. Danial Stamer[47]

[1]Department of Ophthalmology, Casey Eye Institute, Oregon Health & Science University, Portland, Oregon, United States
[2]Department of Ophthalmology, Mayo Clinic, Rochester, Minnesota, United States
[3]Departments of Ophthalmology, Biochemistry & Molecular Biology, Pharmacology & Toxicology, Eugene and Marilyn Glick Eye Institute, Indiana University School of Medicine, Indianapolis, Indiana, United States
[4]Coulter Department of Biomedical Engineering, Georgia Institute of Technology, Emory University, Atlanta, Georgia, United States
[5]Hamilton Glaucoma Center, The Viterbi Family Department of Ophthalmology, Shiley Eye Institute, University of California, San Diego, California, United States
[6]Department of Ophthalmology, Bascom Palmer Eye Institute, University of Miami, Florida, United States
[7]University of North Carolina, Chapel Hill, North Carolina, United States
[8]BrightFocus Foundation, Clarksburg, Maryland, United States
[9]North Texas Eye Research Institute, University of North Texas Health Science Center, Fort Worth, Texas, United States
[10]Morsani College of Medicine, University of South Florida, Tampa, Florida, United States
[11]Department of Ophthalmology and Physiology, University of Oklahoma Health Sciences Center, Oklahoma City, Oklahoma, United States
[12]Department of Pathology & Laboratory Medicine, University of Wisconsin-SMPH, Madison, Wisconsin, United States
[13]Department of Ophthalmology, Boston University School of Medicine, Boston, Massachusetts, United States
[14]Department of Ophthalmology & Visual Sciences, SUNY Upstate Medical University, Syracuse, New York, United States
[15]Department of Ophthalmology, University of Washington, Seattle, Washington, United States
[16]Department of Ophthalmology & Visual Sciences, University of Wisconsin-Madison, Madison, Wisconsin, United States

[17]Department of Ophthalmology & Visual Sciences, University of Utah, Salt Lake City, Utah, United States
[18]Department Ophthalmology & Visual Sciences, Iowa City VA Center for Prevention and Treatment of Visual Loss, University of Iowa, Iowa City, Iowa, United States
[19]School of Chemistry & Biochemistry, Georgia Institute of Technology, Atlanta, Georgia, United States
[20]Glaucoma Center of San Francisco, San Francisco, California, United States
[21]Department of Cellular Biology & Anatomy, Medical College of Georgia, Augusta University, Augusta, Georgia, United States
[22]John Moran Eye Center, University of Utah, Salt Lake City, Utah, United States
[23]Department Ophthalmology & Visual Sciences, University of Wisconsin-Madison, Madison, Wisconsin, United States
[24]Departments of Ophthalmology & Visual Sciences and of Surgical Sciences, School of Veterinary Medicine, University of Wisconsin-Madison, Madison, Wisconsin, United States
[25]Deptartment of Ophthalmology, University of California, San Francisco, San Francisco CA, United States
[26]Department of Bioengineering, Imperial College of London, London, England
[27]Department of Ophthalmology, Novartis Institutes for BioMedical Research, Cambridge, Massachusetts, United States
[28]Departments of Ophthalmology, Pharmacology & Cancer Biology, Duke University School of Medicine, Durham, North Carolina, United States
[29]Global Alliances and Collaborations, Ophthalmology Innovation Center, Santen Inc., Emeryville, California, United States
[30]Division of extramural Science Programs, National Eye Institute, Bethesda, Maryland, United States
[31]Department of Ophthalmology, Stanford University School of Medicine, Palo Alto, California, United States
[32]Department of Ophthalmology, Northwestern University Feinberg School of Medicine, Chicago, Illinois, United States
[33]Department of Ophthalmology & Visual Sciences, Ohio State University Wexner Medical Center, Columbus, Ohio, United States
[34]Genomic Medicine, Biomedical Sciences Research Institute, Ulster University, Coleraine, Northern Ireland, United Kingdom
[35]Department of Biomedical Engineering, Northwestern University, Evanston, Illinois, United States
[36]MCP Health Sciences University, Westport, Massachusetts, United States
[37]Institute for Human Anatomy & Embryology, University of Regensburg, Regensburg, Germany
[38]Jackson Laboratory, Bar Harbor, Maine, United States
[39]Aerie Pharmaceuticals, Inc., Durham, North Carolina, United States
[40]Department of Ophthalmology, Duke University, Durham, North Carolina, United States
[41]Department of Ophthalmology, Indiana University School of Medicine, Indianapolis, Indiana, United States
[42] Western Glaucoma Foundation, Olympia, Washington, United States
[43]Washington state college of medicine, Spokane, Washington, United States
[44]Glaukos Corporation, Aliso Viejo, CA, United States
[45]Department of Ophthalmology and Optometry, Kepler University Hospital, Johannes Kepler University, Linz, Austria
[46]Department of Ophthalmology, University of California at Irvine, Irvine, California, United States
[47]Departments of Ophthalmology and of Biomedical Engineering, Duke University, Durham, North Carolina, United States

*Correspondence: Ted S. Acott, Casey Eye Institute, Oregon Health & Science University, 3181 SW Sam Jackson Park Rd, Portland, OR 97239, USA; acott@ohsu.edu

Keywords
Intraocular pressure regulation models; perfused anterior segment organ culture; *ex vivo* aqueous humor outflow regulation models

Word count: 13,422

Funding: NIH/NEI, BrightFocus Foundation, Research to Prevent Blindness, Aerie Pharmaceuticals, Glaukos Corporation, Glaucoma Research Foundation, Western Glaucoma Fundation, Allergan by Abbvie,

Commercial relationships relative to topics of this manuscript

TSA (none), MPF (none), WM (none), CRE (none), ASH (none), MJK (none), SKB (none), DB (none), URC (none), YD (none), MHE (none), JAF (none), HG (none), SH (none), PLK (none), KAK (none), DK (none), MHK (none), RL (none), SCL (none), YL (none), FM (none), CMM (none), GJM (none), DMP (none, VKR (none), PVR (none), KSN (none), NAS (none), YS (none), BTR (none), CBT (none), CEW (none), HFZ (none), MA (none), TB (none), AFC (none), TFF (none), RF (none), KRH (none), MAJ (none), AK (none), KK (none), CCK (none), PL (none), DRO (none), MP (none), PPP (none), GP (none), ERT (none), EGS (none), JRS (none), CLS (none), CAS (none), PS (none), CKS (none), HY (none), GSZ (none), WDS (none)

Abstract

Purpose. Intraocular pressure (IOP) elevation is the primary risk factor and currently only treatable parameter for progression of glaucomatous optic nerve damage. Aside from direct clinical studies, variations in perfused anterior segment organ culture remain among the primary model systems for studying IOP regulation.

Methods. We present experimental details, protocols, considerations, advantages, and limitations for several *ex vivo* model systems for studying IOP regulation. These include: 1) perfused whole globes; 2) stationary anterior segment organ culture; 3) perfused human anterior segment organ culture; 4) perfused animal anterior segment organ culture; 5) perfused human corneal rims; and 6) perfused human anterior segment wedges.

Results and Conclusions. These methods, with due consideration paid to their strengths and limitations, comprise a set of very strong tools for extending our understanding of IOP regulation.

Introduction

Glaucoma is a family of common optic neuropathies, often progressing to blindness and affecting well over 70 million people worldwide.[1-3] Elevated intraocular pressure (IOP) is the primary risk factor for most types of glaucoma and the only currently treatable factor for all forms, including normal tension glaucoma.[1, 3, 4] A variety of drug, laser and surgical approaches are presently used to lower and control IOP with the

goal of limiting progression of retinal ganglion cell loss.[3, 5] Continued investigation to understand IOP regulation in normal and glaucomatous eyes as well as the efficacy and optimization of various therapeutic approaches to controlling IOP remains a central focus of vision research.

IOP depends jointly on aqueous humor (AH) inflow, produced by the ciliary body, and by the resistance to AH outflow.[1, 4] Although there are intricate regulatory aspects of aqueous humor production,[6] except at very high pressures aqueous humor production is fairly independent of IOP.[7, 8] The consequence of this is that regulation of the flow resistance to aqueous humor outflow is the main controller of IOP.[4, 9, 10] There are two primary aqueous outflow pathways: 1) the conventional pathway, which is through the trabecular meshwork (TM), Schlemm's canal inner wall endothelium (SCE), collector channels and the aqueous drainage vessels; and 2) the uveoscleral or unconventional pathway through the ciliary muscle bundles.[3, 4, 11] Most of the outflow in humans is through the conventional pathway, which is pressure sensitive, but several other animal species have different proportions of conventional and uveoscleral outflow.[12] Most of the conventional outflow resistance resides in the deepest part of the TM and SCE, but a significant portion is also located beyond Schlemm's canal.[4, 9, 10, 13-18]

In the early 1980's John Polansky and colleagues were successful in establishing primary cultures of TM cells while in 1998 Stamer and colleague isolated SCE cells.[19-23] This allowed for biochemical and molecular analysis of these cultured cells. While their experiments *in vitro* provided a wealth of knowledge regarding TM and SCE cell biology, the establishment of primary cells in culture often causes loss of some physiological properties. Additionally, since they are typically grown in an isolated state, these cell cultures are not easily amenable to studying flow, making it difficult to assess how modified cellular activity affects IOP. Perhaps more importantly, TM and SCE cells *in vivo* are in contact with other cells and tissue components that are not easily mimicked in cell culture. A recent manuscript containing the consensus recommendations for TM cell culture provides considerable information and strong guidance for this approach.[24]

It is also noteworthy that several *in vivo* models, including mouse, non-human primate, canine,[25, 26] and others have also been used to provide valuable insights into IOP regulation.[27-30] The advantages of *in vivo* models over the *ex vivo* models discussed herein, include the intactness of the whole outflow system. The disadvantages include the differences between humans and animals, which are significant, and the difficulty in isolating portions of the system for focused studies without confounding influences.

Caveats, pros and cons: To study aqueous humor outflow and the regulation of IOP, several models, primarily *ex vivo*, have been developed. These models are clearly reductionist in nature, only providing information about portions of IOP regulation and the aqueous humor outflow pathway. Since they are *ex vivo* models, they generally have no active uveoscleral outflow for structural reasons, the episcleral veinous pressure is approximately 0 mm Hg, and the ocular pulse is absent. Ciliary

muscle and any neural attachments to the TM are clearly lost. This has advantages, in that IOP regulation is complex and *ex vivo* models allow focused studies of the TM and SCE contributions to IOP regulation without the confounding effects of other portions of the system. However, it should be clear that the ciliary body, ciliary muscle, uveoscleral pathway, and components downstream of the SCE also make significant contributions to IOP regulation.[31-33]

Aqueous humor outflow: Steady-state aqueous humor dynamics are described by the modified Goldmann equation,[34]

$$F_{in} - F_u = C(IOP - EVP)$$

where aqueous production rate is F_{in}, unconventional or uveoscleral drainage rate is F_u, outflow facility is C, and EVP is episcleral venous pressure. In most *ex vivo* perfusions, the EVP is 0 mmHg and there is no uveoscleral outflow, so that Goldmann's equation simplifies to:

$$C = F_{in}/IOP$$

,

Such *ex vivo* studies generally measure the inflow (in nl/min or μl/min) or pressure (in mm Hg) that results from an applied perfusion pressure or inflow rate. Results are often given as outflow facility, C, in nl/min/mm Hg or μl/min/mm Hg. They can also be presented as outflow resistance, which is the numerical inverse of outflow facility. Typical measured C values for *in vivo* human eyes are often around 0.29 μl/min/mm Hg depending on the measurement method and patient age.[35]

Herein, we will discuss the several *ex vivo* approaches most commonly used to study aqueous humor outflow regulation and IOP homeostasis. This will include:

1) perfusion of enucleated whole globes
2) stationary human anterior segment organ culture
3) perfused human anterior segment organ culture
4) perfusion of anterior segments from several other species
5) perfusion of human corneal rims
6) perfusion of wedges of human anterior segments

1) Perfusion of intact enucleated eyes

Quantitative perfusion studies of enucleated human eyes were conducted in the 1880s and fluid injections were conducted in 1863.[16] More detailed studies were then reported by several investigators, including Grant and Barany.[14-16, 36-40] More recently, a number of studies using similar methods have been conducted perfusing intact human or bovine eyes.[41-44]

Typically, a small needle (e.g., 26- or 27-gauge) is inserted intracamerally through the peripheral cornea into the anterior chamber, carefully threading it through the pupil and into the posterior chamber to prevent deepening of the anterior chamber,

which can lead to artificial facility increases.[41] The insertion, initially nearly parallel to the corneal surface and then turning and going perpendicular to this surface, produces an entry that is much less prone to leakage and is referred to as paracentesis. Perfusion fluid is delivered from a reservoir suspended a defined distance above the eye or in some cases injected with controlled delivery rates. The perfusion medium, commonly phosphate-buffered saline, was usually at constant pressure with the flow rate determined gravimetrically as described by Grant.[14-16]

This method has the advantage of being relatively simple, measuring facility across short time frames (hours), and not requiring extensive instrumentation. It is generally limited to eyes obtained within a few hours postmortem (ideally < 24 hours) and they can only be perfused for hours before postmortem changes in outflow properties become apparent.[45] Traditionally and most typically, flow rates at 7-10 mm Hg perfusion head are in the range of 2.5-3 μl/min, which matches earlier studies by Brubaker. [7, 8, 46, 47] This, of course, does not include episcleral venous pressure since this is absent in enucleated eyes. Grant found normal enucleated eyes to have outflow facilities averaging 0.17 at room temperature, which was equivalent to 0.22 at body temperature, and glaucomatous eyes ranged from 0.05 – 0.47 μl/min/mm Hg.[16] Individual variation was quite high and numerous others have conducted similar studies.[48]

2) Stationary human anterior segment organ culture

To circumvent the relatively short time period that whole globes could be studied *ex vivo*, a stationary human anterior segment organ culture model was developed.[45, 48] Rohen, et. al., had earlier done similar short term stationary organ culture studies measuring glycosaminoglycan biosynthesis.[49]

Preparation and dissection: Using aseptic technique in a cleaned and unobstructed laminar flow biosafety cabinet, the globe is rinsed with sterile phosphate buffered saline (PBS) or culture medium. Sometimes the external surface of the eye is rinsed with Betadine (10% Povidone-iodine) to reduce possible contamination. The eye is then approximately bisected with an initial razor blade or scalpel cut followed by sterile small curved surgical scissors. Instruments can be gas-autoclaved or rinsed extensively in 70% alcohol. The cornea, TM and approximately 5-10 mm of sclera is used. The lens, iris and ciliary body are gently teased away using Dumont forceps without damaging the TM. (If the dissection is too rough, the TM may be compromised). The anterior segment is rinsed several times with sterile PBS or culture medium and placed in a well of a 6-well culture dish containing culture media with the anterior segment concave side up. The culture media should completely cover the anterior segment. Note that Figure 1 shows a similar dissection. Most investigators carefully remove all pigmented ciliary body remnants since co-culture of the ciliary body with the TM causes signal transduction-related changes.

Culture media and incubation: Although other variants are occasionally used, Dulbecco's modified Eagle medium (DMEM) containing 1x antibiotic-antimycotic (final concentration 100 units/ml Penicillin G, 100 mg/ml Streptomycin sulfate, 0.25 mg/ml

Fungizone (amphotericin)) all sterile and prewarmed to 25-37^{o} C, is the most common. Note that anterior segment organ culture is normally conducted serum-free, since aqueous humor contains only very low levels of serum proteins. Adding serum will cajse signaling changes and can also initiate TM cell migration off the beams, as is sometimes used to start TM cell cultures.[24] Anterior segments in these 6-well plates are incubated in a sterile CO_2 incubator at 5% CO_2, 37^{o} C and 100% humidity with media changes every 2-3 days. The TM tissue is very susceptible to damage by reduced pH, indicated by yellowing of the media, which occurs if the media is not changed often enough.[45] Other medium can be used. Since glucose levels can change some cell signaling parameters, some studies mix high glucose (4.5 mg/ml) and low glucose (1 mg/ml) 1:1, while others use only high glucose. Changing glucose levels during experiments causes significant signaling changes, so should be avoided.

Validation and characterization: To initially characterize this method, the glycosaminoglycan (GAG) biosynthetic profile and ultrastructure in transmission electron micrographs was compared at different postmortem times with or without stationary culture.[45] The ultrastructure of the outflow pathway of uncultured tissue showed deterioration with increased vacuoles and extracellular matrix disorganization at 24 hours postmortem and continued to worsen over time compared to fresh 2-12 hour postmortem tissue. However, tissue subjected to stationary culture retained good ultrastructural organization for 21 days in culture and was only modestly worsened by 28 days.[45] In addition, tissue placed in culture at 24. 48 or even 72 hours postmortem, when eyes had been stored refrigerated and humidified after enucleation, regained good ultrastructure after stationary culture for around 5 days. The GAG biosynthetic profile behaved similarly. Because of this observation, unless tissue is obtained within 12 hours, it may be advisable to “recover” it in stationary culture for 5 days before initiating most types of studies or before using it for perfusion culture as detailed in the next section.[45]

Stationary organ culture is a viable tool for many kinds of studies where flow does not need to be taken into consideration.[45, 50-53] As noted, the tissue and cells remain relatively typical and functional for 21 – 28 days.[45] This also has some advantages since tissue integrity and organization is maintained and the different cell types of the outflow tissue, up to 19 cell types have been identified using single-cell transcriptomics,[54, 55] presumably retain most of their relationships and interactions. Thus, this stationary culture approach has some significant advantages over cell culture for certain types of analyses.

3) Perfused human anterior segment organ culture

Stationary human anterior segment organ culture was modified by Johnson and separately by Erickson-Lamy to develop a perfusion organ culture method.[56, 57] This allows direct studies of outflow regulation and parameters for up to several weeks while facility is assessed continuously as impacted by various perturbations or conditions.[56, 58, 59] Here, we break down the overall perfusion culture setup and experimentation into separate steps for clarity.

A) Preparation of human donor eyes: Eyes are procured by eye banks or hospital mortuaries within 24-48 hours postmortem. All excess muscle, orbital fat and conjunctiva are removed from the external eye. Following brief sterilization by rinsing in betadine (10% Povidone-iodine) and sterile PBS, a superficial incision is made around the limbus to release vascular resistance created by episcleral veins (Figure 1). Some researchers have determined that this incision is not necessary. The whole eyes are bisected at the equator with a scalpel or single-edged razor blade, leaving enough sclera to secure to the flow cell (approximately 8-10 mm). The vitreous, retina, pars plana of the ciliary body and lens are carefully removed. The iris and pars plicata are also normally removed to minimize shedding of pigment. The anterior segment is then washed with sterile PBS. Different groups carefully remove more or less of the iris/ciliary body since pigment can obstruct outflow and the ciliary body contains factors, which affect aqueous outflow facility.

B) Perfusion culture setup: Using a modified petri dish flow cell (Figure 3), the anterior segment is secured on the central pedestal with a circular sealing ring and screws, creating a closed chamber that can be perfused with media at the chosen flow rate (Figure 2). The anterior segment is carefully centered on the pedestal and the sealing ring gently applied over it, contacting the scleral rim of the anterior segment but not damaging the cornea or underlying outflow pathway. The mounting ring screws are tightened in a sequential/cross manner starting at position 1 partially tightening, moving to position 3 and partially tightening, moving to position 2 and partially tightening and then moving to position 4 and partially tightening. This is repeated for several steps to achieve tight and uniform sealing of the tissue and avoid leaks. Occasionally after initial perfusion, additional tightening is needed. Some groups include a rubber O-ring over the sclera and beneath the clamping ring to further reduce leaks. Perfusion through the entry port is then started via a pump (Figure 4) or a pressure head as discussed later, and pressure transducer readings initiated.

The perfusion can be constant flow, where a precise syringe pump provides adjustable flow at the desired rates (typically around 2.5 μl/min for human eyes or as needed; see Figure 4) and a pressure transducer is used to obtain dynamic pressure readings. Alternatively, as detailed later, a constant perfusion head can be applied, and fluid flow measured gravimetrically as discussed later.

C) Data collection: Pressure is measured by a pressure transducer attached to the second canula port on the dish the eye is mounted on. The pressure transducer (e.g., DTX Plus, Merit Medical, Galway, Ireland) is linked to an analog-to-digital conversion unit. Software then collects voltage data at regular intervals (e.g., once per minute) and averages readings of 60 time points to provide a one-hour readout. The collected data is converted, with suitable and regular calibration of the pressure transducers, into graphs of pressures, e.g., of IOP (anterior chamber pressure) vs. Time. The

measurement time frame here is, of course, totally dependent on the type and rate of changes expected and experimental design considerations.

D) Post experiment analysis: At the end of the experiment, the effects of treatments or manipulations on the TM can be assessed by dissecting the tissue for Western or transcript analysis or cutting sections for immunohistochemistry, electron microscopy, or light microscopy to assess experimental tissue changes.

E) Post experiment validation of tissue cellularity and integrity: It is well known that a certain percentage of human eyes, particularly those from aged individuals, are compromised.[60, 61] Although the tissue often flows typically, in some cases physiological flow responses are not observed. Since there is no easy way to independently assess the condition of the outflow pathway tissue prior to or during the perfusion experiment, post-experiment assessment is absolutely required. Small radial tissue sections are always collected from different quadrants of each eye and placed in 4% paraformaldehyde or Formalin for morphology/cellularity assessment. Hematoxylin & Eosin (H&E) or Toluidine blue staining allows determination of tissue organization and cellularity, both of which can be disrupted in some eyes.[60, 61] This is a critical step, since it is not unusual for this post-analysis to show that there were few or even absolutely no TM cells in the outflow pathway or that the tissue is dramatically disrupted, sometime by earlier clinical glaucoma surgeries and sometimes just by the aging process. This happens frequently enough that all eyes need to be assessed in this manner post-experiment. Studies with these dramatic disruptions or cell loss must be thrown out as they are invalid. It is not unusual for an outflow pathway that is totally or nearly acellular on post analysis to show typical baseline outflow facilities.[60, 61] Judgement on the tissue condition requires some experience and entails comparison to normal tissue.

F) Criteria for acceptance of tissue and results: Several criteria need to be considered before accepting, using, or interpreting data from human or other species tissue. Some of these criteria are experiment-specific and some are generally necessary. Most eye bank eyes come with some basic information, i.e., age, gender, race, cause of death, time of death, time from death to enucleation, and some medical information often including some ocular disease information and medications. In general, at least some of this information is required, usually in a supplement table, to publish studies based on these eyes.

1) **Postmortem time** – Ideally, human eyes would be obtained within 12 hours postmortem and used immediately. Also quite important is time from death to enucleation and beyond 8 hours this can become problematic. In general, < 12 hours postmortem is not practical for logistical reasons and most investigators use eyes out to either 24 or 48 hours postmortem.[60] Donor eyes that can be used for clinical transplant generally upstage research usage in terms of priority and expense. We have shown that by 48 hours, some tissue changes are apparent and these become

quite pronounced by 72 hours.[45] As mentioned in the last section, stationary organ culture of human anterior segments for around 5 days restores morphology, ultrastructure and glycosaminoglycan biosynthesis profiles to approximate eyes from 2-6 hours postmortem acquisition.[45] Because of this observation, some groups normally accept eyes out to 72 hours postmortem and if they are more than 12+ hours postmortem, subject them to stationary organ culture for around 5 days to "recover" them from postmortem effects. This practice is not universally used.

2) **Confounding or unsafe conditions** – The medical information that commonly comes with eyes provides several indicators of acceptability of the eyes for the experiments planned. Research eyes are seldom tested for various diseases, so it is incumbent on the researcher and personnel using the eyes to assume that the donor had some severe infectious disease that was not listed on the eye bank paperwork. Subsequently, eye preparation should always be conducted in a BSL2 safety cabinet using gloves, lab coats and using protocols that protect the dissector from transmission of possible unidentified diseases. Caution with dissecting instruments is also always a must since contagion of bloodborne or fluid-borne diseases such as HIV/AIDS by a slip or accident must be avoided. Tissue remains should always be disinfected by soaking in 10 % bleach and then disposed of in hazard bags.

For many types of studies, glaucoma surgeries such as trabeculectomy or MIGs in the donor eyes will compromise the outcomes. This is not always listed on the eye paperwork and occasionally is not known until the eye is dissected. Many aged donor eyes have also had cataract surgery, which *per se* is not an issue. Glaucomatous eyes will also often be on one or more IOP control drugs and this can impact the outflow pathway behavior in some cases. Since most glaucoma drugs are short-acting, some of their effects may be dissipated by the time studies are conducted. Many are also focused on inflow or uveoscleral outflow and thus not primarily on the TM itself.

Depending on the type of study being conducted, other conditions such as cancer chemotherapy or other types of systemic treatments could impact interpretation of treatment efficacy or outflow facility. Sepsis, inflammation, or other types of medical situations can also impact facility or other types of studies. Although the outflow tissue is avascular and generally not highly available to the immune system, this is not absolute. Immune and vascular cells can be found in the outflow pathway.[54, 55] Generally, these types of possible outflow effectors need to be noted and deviations from normal may require that results not be included.

3) **Age** – Although using younger tissue would provide more robust study conditions, the average age of most eye bank eyes for research is around 75+ years. Younger eyes are often used for corneal transplants. To the extent possible, age-matching is important in experimental design and age as an experimental variable is very difficult to consider due to the low proportion of eyes available from people less than 50 years old. Glaucoma is also a disease of aging.

4) **Gender** – Although no clear sex differences in outflow regulation are well-established, it would not be surprising if there were some. Funding agencies now require some attention to this issue. Eye bank eye distributions are often approximately equal in this regard. However, total eye availability is quite limited such that robust gender accountability is difficult to superimpose on the basic study proposed in almost all cases.

5) Actual **outflow facilities** for donor eyes can vary considerably and some criteria for acceptance and rejection of outliers is valuable. Johnson showed that anterior segments with extremely low outflow rates, < 1 μl/min, were often morphologically and ultrastructurally compromised.[62] However, stationary cultured anterior segments were relatively normal.[62] For constant pressure perfusion at 8.8 mm Hg, anterior segments that flow much less than 1 μl/min or greater than 10 μl/min after a stabilization period (24 hours) are likely better excluded. For constant flow perfusion at 2.5 μl/min, anterior segments that have facilities less than 0.1 or more than 1 or 1.2 μl/min/mm Hg are usually not used. Limiting untreated eyes to this range, except for glaucomatous eyes, seems like a reasonable approach to eliminate extreme outliers.

6) **Glaucoma** – Criteria for designation of glaucoma eyes are not simple. Since IOP is a risk factor, not a simple cause for glaucoma and since normal-tension glaucoma is common, there are no universally accepted criteria. In addition, most anterior segment studies are focused on IOP regulation, not on glaucomatous nerve damage itself. Eye bank eye sheets frequently list glaucoma and/or glaucoma drugs or treatments and this is often taken as support for the eyes having glaucoma. Human eye bank eyes are not considered human subjects research by NIH. However, obtaining full patient records from an Ophthalmologist is a daunting task, requiring intense and ongoing human subjects compliance and approvals. IOP records would be ideal, except the patient is immediately subjected to drug or other therapies to restore IOP control so only pre-treatment values are of value. Other ophthalmic information such as OCT scans that document extent of damage provides information about glaucoma progression. Eye bank glaucomatous eyes are typically from patients that had glaucoma for 10-40 years with various treatment throughout that time. Some investigators get an ophthalmologist to grade the optic nerves of the putative glaucoma eyes they use, but this is not as simple as it might appear for tissue acquired 24-48 hours postmortem. This is also limiting, since this may have little to do with IOP regulation at the anterior chamber and will rely on the extent of damage acquired and the resilience of the individual optic nerve rather than the existence of IOP dysregulation. If clinical IOP control was in place early on, damage may be minimal and essentially undetectable in the postmortem tissue. One criterion would be to subject the anterior segment to a 2x pressure challenge, which glaucomatous eyes should fail, but this is not always used.[9, 63-65] In summary, there are no simple criteria and none of the options mentioned above are adequate. This remains an unsettled point of controversy in the field with occasional arbitrary criteria. At the least, it is important to include all available information on the eyes and comparison of facility for the glaucomatous and normal comparators in an appendix.

G) Troubleshooting

1) **Leaks** - In terms of very high flow rates, this is often an indication that the outflow pathway was damaged during the removal of the ciliary body/iris, etc. Another potential reason for high flow rates or facilities is the possibility of leaks around the anterior segment, at the tubing connections, or in the perfusion cell itself. These types of leaks are usually visible in terms of where perfusion fluid accumulates. A paper towel beneath the flow cell will make the latter types of leaks more visible. Some investigators add fluorescein to help visualize leaks. Leaks around the sealing ring can often be eliminated by additional tightening the nuts that hold the sealing ring or by reseating the anterior segment on the pedestal and reclamping it. This can only be done a few times, as the tissue becomes damaged and can no longer be clamped to create a seal. The rubber O-ring suggested earlier could also help with this issue. Cutting the anterior segment with too little sclera will also result in leakage. It requires some experience to learn how tightly to clamp the sclera to get a good seal without extensive damage or cutting the tissue with the sealing ring edges.

2) **Contamination** – Flow cells should be washed with soap and rinsed extensively after each usage. Small passages, i.e., the perfusion ports, should also be rinsed extensively. If they are made of plastics that are not vulnerable to crazing upon exposure to 70% ethanol, e.g., PVC, then the flow cells should be soaked and rinsed with 70% ethanol in the laminar flow biosafety cabinet after they have been washed with soap and rinsed thoroughly. Some groups use gas-sterilization, which also works very well. Washing the biosafety cabinet with 70% ethanol before use is always advised as well. Tubing and syringe pumps or perfusion head vessels should be cleaned similarly with soap, rinsed and then rinsed with 70% ethanol or gas sterilized. Autoclaving is also an option for components that can take the heat. If extensive rinsing afterwards is conducted, 5% bleach solutions can also be used. The same is true for the dissecting tools.

Since eye tissue is not collected under sterile conditions, rinsing extensively prior to opening the eye is always advisable. Removal of muscle and other external tissue also diminished contamination. Here, the Betadine wash can be helpful, although extended exposure to the cornea can compromise the ion pumps and cause it to swell. At any sign of contamination throughout the process, throw the eye away. It is never viable to try to clean it and all solutions and components should be cleaned and/or discarded.

Solutions should also be sterile. The CO2 incubator and biosafety cabinets also need to be extensively and completely cleaned periodically. HEPA filters in the biosafety cabinets need to be tested regularly, usually every 6 months or yearly. HEPA filters on the CO2 incubator, if available, need to be changed regularly and the culture room needs to be cleaned and dust removed occasionally. Keeping covers over all flow cells, tissue, etc. when moving between the biosafety cabinet and the incubator is critical. Keeping covers on the flow cell inside the incubator and keeping the door closed as much as possible also reduces contamination. Contamination is a much

larger issue than in cell culture, since you are starting with a non-sterile tissue and have more points of entry of contaminants. In terms of the antibiotic/antimycotic, this should be maintained as frozen aliquots and stability is only a few days at 37 degrees. The antimycotic stock is a suspension, rather than a solution, so should be mixed well before adding to medium. Repeated freeze-thaw is also not advisable.

3) **Culture room pressure** - If you are doing minimal biohazard experiments, it is advantageous to have the culture room pressure positive. This will push air out slightly and minimize incoming bacterial, fungal, yeast or viral contamination from adjacent labs or rooms. On the other hand, if you are doing serious biohazard work, like viral or such infections, etc., you should have the room at a negative pressure to avoid escape of biohazard agents to adjacent labs or rooms. This is normally a requirement of biosafety committees. Since most culture rooms are not HEPA filtered, incoming air cannot be assumed to be contaminant free.

H) Experimental design and Power calculations: To the extent possible, paired-eye studies have more power, since biological variation between individuals is almost always larger than left-right eye differences in an individual. When feasible, using an eye as its own internal control is advisable, i.e., before and after a treatment. Normally, facility is quite consistent over days to a few weeks in perfusion culture making this a viable approach.

Although the variability compared to the size of the treatment effect expected is always somewhat difficult to predict, unless numerous very similar studies have been previously conducted, power calculation to determine sample sizes is usually quite important. This is also increasingly emphasized by funding agencies. The biological variation between individuals, particularly aged human eye doners, is typically quite high. The good news is that in most cases, the biological variability is effectively “noise” and does not include the variables of interest in most studies. However, this must be considered in any power calculations.

From the observed variability in numerous studies over many years, most studies with medium sized effects require a sample size of 5-6 human eye pairs to achieve clear statistical resolution in paired-eye or pre-post internal control designs studies. Since the size of the effect expected can be quite different for different types of experiments, some adjustments to this may be essential. For very subtle differences between treatment and control, sample sizes as high as 7-10 pairs may be necessary.

A caveat to the sample size(s) mentioned above is the occasional eye or pair of eyes that, upon postmortem evaluation of H&E sections either exhibit very low cellularity or major tissue disorganization. These eyes are typically just thrown out as invalid and not included in the sample size. It is of note, however, that older eyes exhibit significant TM cell loss and this is much accentuated in aged glaucomatous eyes, i.e., the loss can be as much as 50%.[66-69] Since TM cellularity is an important component of glaucomatous outflow compromise, this must be considered carefully within the context of the experimental design.

I) Variations in perfused human anterior segment organ culture: An alternative flow cell design is shown in Figure 6. As with Johnson or Erickson-Lamy's original flow cells, this cell can be used with constant flow and pressure transducer measurement of resultant pressure generated or it can be used with constant pressure perfusion and flow rate measured gravimetrically (Figure 7).

For perfusion at constant flow, a pressure transducer is connected to one port and details are as detailed above. For perfusion at constant pressure, either a 100 ml culture bottle or a 50 ml conical centrifuge tube serve as the perfusion reservoir filled with perfusion medium and positioned such that the fluid level is the desired distance above the flow cell sealing ring (as in figure 7), which is where the perfused fluid seeps out of the episcleral veins. A perfusion head of 8 or 8.8 mm Hg (10.8761 or 11.9637 cm H_2O) is considered 1x and is equivalent to perfusion at 2.5-3 μl/min, which is typical for normal human eye excluding episcleral venous pressure.[47] Tygon tubing is attached to one perfusion nipple on the bottom of the flow cell and to a broken-off 1 ml plastic pipette inserted through a hole in a loose-fitting lid on the perfusion bottle. Alternatively, the Tygon tubing is inserted through a small hole high up in the side of the centrifuge tube with the cap loosely attached. It is preferrable to use tubing with a small inner diameter with a moderately rigid wall so that there is less "dead" space and less tubing compliance (tubing expansion or shrinking with pressure changes). Also, it is important to remove all air bubbles from the system. Using 2-way stop cocks for connections facilitates this. The other perfusion ports on the bottom of this flow cell are sealed off when not in use but can be used for drug or agent delivery without interrupting flow (described later).

Constant pressure gravimetric flow measurements can be long-term, where the tubing is clamped with a hemostat, removed from the bottle, and the bottle weighed on a balance at time intervals of greater than 15 minutes and often only a few times a day. In this case, three readings 15-minutes apart are averaged to reduce reading errors. The bottle must be handled with gloves to avoid moisture on the hands modifying the weight. Often, the changes in outflow facility are slow, as in the case of IOP homeostatic responses or other treatments, and this long-term measurement protocol is advantageous.

For shorter-term or more frequent gravimetric measurements, micro balances can be placed in the CO_2 incubator and continuous measurements passed through a USB-linkage and conversion box to be captured on a laptop in Excel files. As an example, 2 Ohaus AZ423/E Adventurer Precision balances were placed in each CO_2 incubator and continuously monitored via USB output passage through a GageMux USB 4-input gage (Advanced Systems & Designs, ADS/QMS) USB interface to a laptop as an Excel file. The GageMux can be set to read each of the 4 balances in the two incubators every 2 minutes or at longer intervals.

Gravimetric measurements can be somewhat noisy since the desired flow rate is obtained by numerically differentiating the measured weight vs. time. Vibrations and direct air currents such as created by the incubator fans should also be carefully avoided, especially if weights are taken over relatively short time intervals. With

precautions, this is generally not an issue. Of course, many alternative setups are viable. The Excel file can then be processed to produce flow (μl/min) or facility output (C=flow/pressure) as a function of time and integrating various treatments into the profile.

J) Steel Eye facility measurements: Ethier developed a "steel eye" perfusion method (Figure 10).[70] This method is relatively easy and inexpensive to set up and produces excellent data. The central idea is that flow rate is determined by measuring the pressure drop across a fixed known resistor (resistance tubing). After calibration, it is relatively easy to convert the pressure drop into a flow rate, and this approach does not suffer from the noise that can affect gravimetric methods. Complete details are provided in this manuscript.[70] Although shown perfusing a whole eye, it is easily adapted to use with the flow cells as discussed above. The reference flow resistance is provided by a length of 30-gauge tubing (0.15 mm ID and 60 cm long from Vita Needle Co). A pressure reservoir is positioned at a pressure head above the eye or flow cell (Pres). The actual pressure at the eye (IOP) is Pres minus the pressure drop across the resistance tubing, DP, which is read by the pressure transducer, DPT. The flow resistance tubing is calibrated and both pressure transducers are separately calibrated. Fluid outflow rate through the eye at a given IOP is then calculated from the DP reading and previous calibration values. A computer-controlled feedback loop can be incorporated to adjust the reservoir height such that the pressure delivered to the eye remains constant even if flow rate (and hence pressure drop across the resistance tubing) changes.

K) Flow meters: Flow meters, which measure flow in the ranges required here are another option. This approach seems plausible and should be significantly lower cost although calibration is a potential issue to be dealt with. There are commercially available microfluidics flow rate sensors that directly measure the flow rates in the range of 1-50 μl/min.

L) iPerfusion system: Overby modified this approach for use with his iPerfusion system.[71-74] This has been detailed in a previous consensus paper and will not be further detailed herein.[27] His system works well for this analysis.

M) Drug, treatment, modulators, or agent delivery: Of course, one important aspect of these model systems is to study the effects of various molecular or cellular modulators or drugs on outflow facility. Several approaches are commonly used:

1) **Push-pull syringes** - To deliver agents to the anterior chamber during an experiment without changing the pressure on the outflow pathway, two extra ports on the flow cell (Figure 6) can be attached to a pair of syringes mounted on a push-pull device. This can also be done by disconnecting and substituting connections if only two ports are available. Two syringe barrels are attached to a board or rod facing away from each other and at a distance such that one plunger is completely depressed and

the other is just barely into the syringe. The two plungers are clamped to each other such that pushing them fills one while emptying the other. One is filled with the delivery solution and then both are attached to different ports on the flow cell. Slowly ejecting fluid from the filled syringe into the flow cell simultaneously sucks an equal volume of fluid out of the flow cell. If this is done slowly, i.e., over a few minutes, the anterior chamber fluid is exchanged for the treatment fluid without changing the pressure in the anterior chamber. It is usually advisable to clamp off or close the other port or ports to avoid mixing during this process. If the syringe volume is somewhat larger than the anterior chamber volume in the flow cell, a full or even over 100% replacement of perfusion fluid can be achieved. If the treatment is to be continued, the fluid in the syringe and connecting tubing of a constant flow system or the fluid in the connecting tubing and perfusion bottle need to be changed. Several variations on this approach can be used including a two-reservoir gravity/pressure differential fluid exchange approach.

2) **In line injection** – Sometimes when small volumes are to be delivered, the agent can be injected into the delivery Tygon tubing using a small, e.g., 27-gauge, needle. This is complicated by the fact that the agent will be diluted during this process and the exact dose at the time it hits the outflow pathway is very difficult to predict. However, for some types of treatment where it is the amount of agent and not the concentration that is important, this can be suitable. New Tygon tubing will take this injection without leaking, but if it has been used several times and has become more rigid, leaks can occur interfering with facility measurements. Vacuum grease can also be applied to the hole afterwards to minimize leaks. If larger volumes are to be injected over short time periods, it will be difficult not to increase the pressure head transiently.

3) **Direct injection** – In some cases, it is possible to inject the agent directly through the central cornea and into the anterior chamber. The injection with a small needle, again 27 gauge or smaller, and using the paracenteses approach as detailed in the whole eye perfusion section above can deliver the agent close to the outflow pathway, although this relies on diffusion of the agent at rates faster than the fluid flow to avoid non-uniform delivery to different quadrants of the anterior chamber.

4) **Dismount and process** – Of course, some agents, treatments, surgeries, etc., cannot be injected but will require dismounting the anterior segment, conducting the procedure, and then remounting it on the flow cell. The sealing O-ring mentioned above is particularly helpful in this situation.

5) **Outflow Segmentation & Soaked-in vs. flowed-in** – The increased awareness of the degree of outflow segmentation, i.e., the observation that outflow is not uniform around the circumference of the eye but occurs in regions where there is high, intermediate, and low or no flow, significantly complicates agent delivery to the outflow pathway. This is true for both experimental and clinical delivery. As can be seen with perfusion of flow markers (discussed later), there are numerous regions scattered around the eye that exhibit very different levels of flow.[9, 75, 76] The high flow regions of a normal human anterior segment comprise approximately 1/3 of a human anterior segment and probably account for 70-80 % of the total flow with the

intermediate regions making up around 20-30 % of the total flow and the low flow regions accounting for almost none of the total flow. Thes highly segmental flow marker distribution after a 1-hour perfusion tells us that delivery of drugs or other agents will be similarly segmental with the low flow regions being essentially not treated at all and the high flow regions receiving nearly all of the drug or agent. Even small drugs will not diffuse sufficiently to provide even circumferential delivery. A partial remedy has been to soak the agent in with the flow stopped overnight, which results in uniform delivery to all segmental regions of the outflow pathway.[75, 77-79]

6) **Targeted delivery to low flow regions** – Ethier's group developed a method of targeting stem cells to various regions of the outflow pathway independently of outflow segmentation.[80] This involved using magnetic nanoparticles and magnet-guided delivery. This could be very useful for some types of studies alleviating the outflow segmentation patterns.

4) Other species

Fow cells designed for human anterior segments are too small for bovine anterior segments but can be used with porcine and monkey anterior chambers.[80-84] For porcine anterior chambers, the sharp sticky side of 4 small Velcro strips or an O-ring can be placed on the inside of the clamping ring to keep the sclera from slipping out. The porcine sclera is much more pliable than in humans and is thus difficult to clamp. Some investigators use SuperGlue (cyanoacrylate) to solve this problem also. Several investigators have used bovine anterior segments successfully as well with modifications of the flow cell dimensions (Figure 11).[85, 86] Perfused bovine or porcine anterior chambers typically flow at somewhat faster rates than human, i.e. around 4.5 - 6 μl/min compared to 2.5-3 μl/min for humans. Monkey anterior segments organ cultures (MOCAS) have also been used for anterior segment organ culture.[81] With proper attention to specifics, these animal anterior segments can serve good substitutes for human anterior segments and are often much more available.

Considerations – Most species, except for human and mouse, exhibit washout, a gradual decrease in the outflow resistance per volume perfused.[38, 41, 43, 86-91] This phenomenon requires special consideration when conducting perfusion studies. It can also be useful in investigating mechanisms, if handled carefully.[41, 43, 87] It is also notable that porcine corneas tend to swell during perfusion and can obstruct the outflow pathway after several days of culture. In general, 5-7 days is the upper limit that is usable without this being problematic. However, one group successfully extend this out to 21 days, although it is unclear how this was achieved.[92]

5) Corneal rims

Since corneal transplant rims are often available, they are an appealing source of human anterior segments for perfusion studies. Rims can often be cheaper, more available and include better quality tissue from younger doners. Corneal rims contain all the key components for perfusion culture: the cornea, sclera, and TM. Human corneal rims are prepared by Eye Banks using a trephine, and therefore they contain

less sclera (about a few millimeters) compared to bisected anterior segments. The amount of sclera in corneal rims is often not sufficient for using standard flow cells. If the corneal rims are clamped in the Johnson flow cell, the IOP will often be very high (sometimes over 50mmHg), which is likely due to the TM being pulled towards the dish caused by mechanical strain. As a solution to this problem, Mao developed a modified 3-D printed flow cell where the anterior segments were glued into place to achieve a seal (Figure 12).[93, 94]

Instead of clamping, a perfusion plate was designed, and the corneal rim glued on the plate using cyanoacrylate glues. These glues are easy to apply, polymerize rapidly, and provide reliable attachment and sealing between the corneal rim and the perfusion plate.[94]

A) Procedure: The corneal rim is first cleaned of residual uveal tract tissues. The scleral tissue is scored at the inner and outer surface posterior to the limbal area to prevent glue from entering the TM. After drying the edge of the corneal rim (sclera), the corneal rim is glued to the perfusion plate using the thin cyanoacrylate glue (Gluture). This step is not meant to seal the corneal rim, but to provide initial attachment for the next step. After glue polymerization, the corneal rim is securely attached to the plate. The cornea is then covered with a piece of contact lens and a bead of caulk-like cyanoacrylate glue (Gel Control Super Glue) is applied around the base of the corneal rim. The caulk-like glue provides a strong attachment and seal of the anterior chamber, after incubation in a cell culture incubator to allow the caulk-like glue to cure. Since cyanoacrylate glue is moisture cured, the incubator should be at 100% humidity, which is always essential anyway to avoid evaporation and is maintained by a pan of water as discussed earlier. The flow cell with corneal rim glued in place is then connected with the perfusion system and perfused overnight (with the contact lens still on the cornea). The next day, the contact lens is carefully removed. The corneal rim is further perfused for another day for IOP to stabilize at a baseline IOP.[94]

The materials details, 3D printing files, protocol specifics, and an instructional video are available and will not be reiterated here.[94] However, several key steps will be emphasized and explained in more detail:

B) Selection of corneal rims. The corneal rims should have relatively even and have 2-3 mm sclera tissue all round. Sometimes there are notches or unevenness at the edge of the sclera tissue. Although the sclera can be trimmed to make it even, that process will further decrease the amount of sclera available for model set up. This will cause two issues: the corneal rim becomes too small to fit onto the plate (there is a groove designed for the edge of the corneal rim); and the glue is more likely to contaminate the TM, causing high baseline IOP.

C) Drying. The glues used in this method are moisture curing glues. If the region to be glued contains water, glue will polymerize immediately and will not provide proper attachment. It is recommended to use a cotton swab to carefully dry

the region before applying glue. Also, caution should be exercised not to dry the cornea or TM to prevent cell loss.

D) Glue contamination in the TM. This is not uncommon for inexperienced users. Glue contamination in the TM will increase TM stiffness and clog the outflow pathway, causing very high IOP (usually >40mmHg). There are a few tips to minimize the chance of glue contamination. First, apply a minimum amount of glue. Second, trim the edge of the corneal rim. If the edge of the corneal rim is not even, when it is placed on the perfusion plate, the protruded region will lift the surrounding region, creating gaps/void. To fill the gap/void, more glue is needed, which increases the chance of glue contamination. Third, carefully score the sclera to create flaps. These flaps function like roof with a drip-edge, preventing glue from being siphoned into the TM or limbal region.

Although the corneal rim perfusion culture model has many advantages, it has several disadvantages:

1) **Inability to reposition during experiments**. Since the corneal rim is glued onto the perfusion plate, it cannot be repositioned.

2) **Glue contamination cannot be removed during perfusion**. Once there is suspicion of glue contamination in the TM (very high IOP), there are no good methods to remove polymerized glue from the TM without causing tissue damage. For fixed corneal rims after perfusion culture, glue can be removed by soaking in tissue clearing reagents such as xylene.

3) **Post-perfusion tissue collection**. Cyanoacrylate glue provides very strong attachment, and it is almost impossible to “tear” the tissue from the perfusion plate. Therefore, the corneal rim needs to be cut off using a sharp blade.

6) Wedge flow and pressure models

Johnstone developed a novel model where human anterior segment wedges were cut and Schlemm’s canal cannulated with a 130-150 μm outer diameter cannula and positive pressure heads applied to study the deformation of the SCE, JCT, and the TM beams (Figure 13). This was used with OCT 3D imaging at different Schlemm’s canal pressure heads, static and fluctuating, combined with inverse finite element analysis to obtain biomechanical properties of normal and glaucomatous tissue as it was distended towards the anterior chamber.[95-98] As indicated in the figure, the pressure was equal to or higher in Schlemm’s canal relative to the anterior chamber. This provides an excellent model to study the dynamics and biomechanical properties of the outflow tissue and impacts of the ocular pulse and coupling between outflow pathway components, SC and episcleral vessels.

Kelley and Aga modified this model by using higher anterior chamber pressures relative to the Schlemm’s canal pressure (Figure 14). The pressures were from the fluid level above the wedge in the Petri dish to the pressure head below this in the reservoirs at 8.8-, 17.6- or 26.5-mm Hg. This is equivalent to the physiological 1x, 2x and 3x pressure normally observed from the anterior chamber to Schlemm’s canal *in vivo*. This system, imaged with green visual OCT provides much higher resolution of

the TM. The OCT 3D images obtained from scanning systems in Figures 13 and 14 are amenable to inverse finite element analysis with modeling elastin and different collagens or other extracellular matrix regions.[99] Both approaches allow assessment of outflow pathway biomechanics using different parameters and pressures.

7) Outflow segmentation markers

Since aqueous humor outflow is very segmental, labeling regions of high, intermediate, and low flow allows molecular and cellular correlation to relative flow.[100-103] Several methods have been developed. Cationic ferritin was used earlier and at higher levels which clogged the outflow system.[76, 103] Fluorescent microspheres (FluoSpheres) with positive anionic or negative cationic charges or membrane permeant Cell Mask have been used along with numerous other markers.[100-102, 104] Comparison of marker levels defines segmental regions for relevant molecular or cellular studies. Usually, labels flow in for approximately 1 hour at the end of an experiment. As a test for marker binding rather than relative flow regions, soaking the marker in overnight without flow should provide uniform marker distribution, demonstrating that flow not binding patterns are being assessed. It is also useful to flow in one color marker at an initial time and then another color marker after a time interval to see whether the regions are dynamic or if treatments change their distributions.[104, 105] Another point of interest is that atomic force microscopy (AFM) studies are incompatible with most FluoSphere-like markers and Cell Mask is necessary for these studies.

Recently, angiography has been utilized to identify high and low flow areas in porcine and human anterior segments.[106, 107] This can be correlated with *in vivo*/clinical patterns. *Ex vivo* anterior segments are incorporated into a constant flow system (iOnly Human; iPerfusion, Imperial College London), similar to that described above. Upstream from the perfusion chamber is a 3-way stop cock that is an entry-point for the tracer. Tracers include 2% Fluorescein (Akorn Pharmaceuticals) or 0.4% ICG (Cardiogreen, Sigma). After a stable outflow facility baseline is achieved, 2 ml of the tracer is introduced into the eye via the upstream 3-way stop cock which then exits the perfusion chamber to a downstream waste reservoir placed between the eye and pressure transducer open to atmosphere. After completion of the tracer introduction, the perfusion rate is continued at the original rate.

For this setup, the camera is a clinical Spectralis HRA+OCT (Heidelberg Engineering) that can image fluorescein and ICG, but it is instead installed on a FLEX module. This means that the Spectralis camera head is detached from the manufacturer provided table and installed on a manufacturer provided boom arm to allow positioning of the camera head above and pointing down at the eye within the perfusion chamber. Typically, a 30-degree lens is used with a 25-diopter focus, although other lenses which have different working distances are available. Using the device software, images can be taken as single acquisitions or short videos for either tracer with a timer. For this study[106], after angiography the eye was dismounted and tracer rinsed out prior to subsequent experimental steps. Alternatively, residual tracer

can also be flushed from the eye using the perfusion system perfusate like the original tracer delivery method.

8) IOP homeostatic responsiveness

The most significant indicator of anterior segment health and functional integrity is the ability to mount a physiological IOP homeostatic response to a 2x pressure challenge.[9, 63, 64] Normal anterior segments respond to a 2x pressure challenge by reducing the outflow resistance over the time period of a day or so in an attempt to restore pressure to its normal level.[9, 63, 64, 108] This response is absent in glaucomatous anterior segments or in anterior segments depleted of TM cells by saponin treatment.[65, 109] It can be restored by restoration of TM cellularity.[109] This test of anterior segment functionality is relatively easy to administer, in that doubling the perfusion pressure or perfusion flow rate, which triggers a 2x pressure immediately, followed by sustaining the 2x pressure or flow rate for several days, initiates a reduction in the outflow resistance over this time period, if the anterior segment is functionally healthy.[9, 63-65, 109]

Literature Cited

1. Quigley HA. Glaucoma. *Lancet* 2011;377:1367-1377.
2. Quigley HA, Broman AT. The number of people with glaucoma worldwide in 2010 and 2020. *Br J Ophthalmol* 2006;90:262-267.
3. Weinreb RN, Leung CK, Crowston JG, et al. Primary open-angle glaucoma. *Nat Rev Dis Primers* 2016;2:16067.
4. Stamer WD, Acott TS. Current understanding of conventional outflow dysfunction in glaucoma. *Curr Opin Ophthalmol* 2012;23:135-143.
5. Weinreb RN, Aung T, Medeiros FA. The pathophysiology and treatment of glaucoma: a review. *JAMA* 2014;311:1901-1911.
6. Delamere NA. Ciliary Body and Ciliary Epithelium. *Adv Organ Biol* 2005;10:127-148.
7. Brubaker RF. The measurement of pseudofacility and true facility by constant pressure perfusion in the normal rhesus monkey eye. *Investigative Ophthalmology* 1970;9:42-52.
8. Brubaker RF. The effect of intraocular pressure on conventional outflow resistance in the enucleated human eye. *Invest Ophthalmol* 1975;14:286-292.
9. Acott TS, Vranka JA, Keller KE, Raghunathan V, Kelley MJ. Normal and glaucomatous outflow regulation. *Prog Retin Eye Res* 2021;82:100897.
10. Johnson M, Erickson K. Mechanisms and routes of aqueous humor drainage. In: Albert D, Jakobiec F (eds), *Principles and Practice of Ophthalmology.* Philadelphia: W.B. Saunders; 2000:2577-2595.
11. Weinreb RN. Uveoscleral outflow: the other outflow pathway. *J Glaucoma* 2000;9:343-345.
12. Kaufman PL. Pressure-dependent outflow. In: Ritch R, Shields MB, Krupin T (eds), *The Glaucomas.* St Louis: Mosby; 1996:307-335.
13. Johnson M. 'What controls aqueous humour outflow resistance?'. *Exp Eye Res* 2006;82:545-557.

14. Grant WM. Facility of flow through the trabecular meshwork. *Arch Ophthalmol* 1956;54:245-248.
15. Grant WM. Further studies on facility of flow through the trabecular meshwork. *Archives Ophthalmology* 1958;60:523-533.
16. Grant WM. Experimental aqueous perfusion in enucleated human eyes. *Arch Ophthalmol* 1963;69:783-801.
17. Rosenquist R, Epstein D, Melamed S, Johnson M, Grant WM. Outflow resistance of enucleated human eyes at two different perfusion pressures and different extents of trabeculotomy. *Curr Eye Res* 1989;8:1233-1240.
18. Sit AJ, McLaren JW. Measurement of episcleral venous pressure. *Exp Eye Res* 2011;93:291-298.
19. Polansky JR, Alvarado JA. Isolation and evaluation of target cells in glaucoma research: hormone receptors and drug responses. *Curr Eye Res* 1985;4:267-279.
20. Polansky JR, Weinreb R, Alvarado JA. Studies on human trabecular cells propagated in vitro. *Vision Res* 1981;21:155-160.
21. Polansky JR, Weinreb RN, Baxter JD, Alvarado J. Human trabecular cells. I. Establishment in tissue culture and growth characteristics. *Invest Ophthalmol Vis Sci* 1979;18:1043-1049.
22. Polansky JR, Wood IS, Maglio MT, Alvarado JA. Trabecular meshwork cell culture in glaucoma research: Evaluation of biological activity and structural properties of human trabecular cells in vitro. *Ophthalmol* 1984;91:580-595.
23. Stamer WD, Roberts BC, Howell DN, Epstein DL. Isolation, culture, and characterization of endothelial cells from Schlemm's canal. *Invest Ophthalmol Vis Sci* 1998;39:1804-1812.
24. Keller KE, Bhattacharya SK, Borras T, et al. Consensus recommendations for trabecular meshwork cell isolation, characterization and culture. *Exp Eye Res* 2018;171:164-173.
25. Gelatt KN, Gum GG. Inheritance of primary glaucoma in the beagle. *Am J Vet Res* 1981;42:1691-1693.
26. Gelatt KN, Gum GG, Gwin RM, Bromberg NM, Merideth RE, Samuelson DA. Primary open angle glaucoma: inherited primary open angle glaucoma in the beagle. *Am J Pathol* 1981;102:292-295.
27. McDowell CM, Kizhatil K, Elliott MH, et al. Consensus Recommendation for Mouse Models of Ocular Hypertension to Study Aqueous Humor Outflow and Its Mechanisms. *Invest Ophthalmol Vis Sci* 2022;63:12.
28. Overby DR, Clark AF. Animal models of glucocorticoid-induced glaucoma. *Exp Eye Res* 2015;141:15-22.
29. Rasmussen CA, Kaufman PL. Primate glaucoma models. *J Glaucoma* 2005;14:311-314.
30. Kuchtey J, Olson LM, Rinkoski T, et al. Mapping of the disease locus and identification of ADAMTS10 as a candidate gene in a canine model of primary open angle glaucoma. *PLoS Genet* 2011;7:e1001306.
31. Roy Chowdhury U, Fautsch MP. Isolation and Culture of Vascular Distal Outflow Pathway (VDOP) Cells From Human Donor Eyes. *Curr Protoc* 2022;2:e528.
32. Roy Chowdhury U, Hann CR, Stamer WD, Fautsch MP. Aqueous humor outflow: dynamics and disease. *Invest Ophthalmol Vis Sci* 2015;56:2993-3003.
33. McDonnell F, Dismuke WM, Overby DR, Stamer WD. Pharmacological regulation of outflow resistance distal to Schlemm's canal. *Am J Physiol Cell Physiol* 2018;315:C44-C51.
34. Goldmann H. [The aqueous veins and the Poiseuille law]. *Ophthalmologica* 1949;118:496-519.
35. Kazemi A, McLaren JW, Lin SC, et al. Comparison of Aqueous Outflow Facility Measurement by Pneumatonography and Digital Schiotz Tonography. *Invest Ophthalmol Vis Sci* 2017;58:204-210.

36. Grant W, Trotter R. Tonographic measurements in enucleated eyes. *Arch Ophthalmol* 1955;53:191-200.
37. Bárány E. In vitro studies of the resistance to flow through the angle of the anterior chamber. *Acta Soc Med Upsal* 1953;59:260-276.
38. Bárány EH, Scotchbrook S. Influence of testicular hyaluronidase on the resistance to flow through the angle of the anterior chamber. *Acta Physiol Scand* 1954;**30**:240-248.
39. Bárány EH, Woodin AM. Hyaluronic acid and hyaluronidase in the aqueous humour and the angle of the anterior chamber. *Acta Physiol Scand* 1954;33:257-290.
40. Van Buskirk EM, Brant WM. Influence of temparature and the question of involvement of cellular metabolism in aqueous outflow. *American Journal Ophthalmology* 1974;77:565-572.
41. Overby D, Gong H, Qiu G, Freddo TF, Johnson M. The mechanism of increasing outflow facility during washout in the bovine eye. *Invest Ophthalmol Vis Sci* 2002;43:3455-3464.
42. Gong H, Brown K, Johnson M, Kamm RD, Freddo TF. Hydraulic conductivity of juxtacanalicular connective tissue using quick-freeze/deep-etch. *Investigative Ophthalmology Visual Science* 1997;38 Suppl:S564.
43. Gong H, Freddo TF. The washout phenomenon in aqueous outflow--why does it matter? *Exp Eye Res* 2009;88:729-737.
44. Gong H, Yang CY. Morphological and hydrodynamic correlations with increasing outflow facility by rho-kinase inhibitor Y-27632. *J Ocul Pharmacol Ther* 2014;30:143-153.
45. Acott TS, Kingsley PD, Samples JR, Van Buskirk EM. Human trabecular meshwork organ culture: Morphology and glycosaminoglycan synthesis. *Investigative Ophthalmology Visual Science* 1988;29:90-100.
46. Brubaker R. Measurement of aqueous flow by fluorophotometry. In: Ritch R, Shields, MB, Krupin, T (ed), *The Glaucomas.* St Louis: Mosby; 1996:447-454.
47. Brubaker RF. Flow of aqueous humor in humans. *Invest Ophthalmol Vis Sci* 1991;32:3145-3166.
48. Van Buskirk EM, Pond V, Rosenquist RC, Acott TS. Argon laser trabeculoplasty. Studies of mechanism of action. *Ophthalmology* 1984;91:1005-1010.
49. Rohen JW, Schachtschabel DO, Lütjen-Drecoll E, Rohrbach M, Berghoff K (eds). *Morphological and biochemical studies on cell and tissue cultures of human trabecular meshwork*: Springer-Verlag; 1983:39-43.
50. Acott TS, Nobis CA, Van Buskirk E. Studies of human trabecular extracellular proteoglycans. *Proceedings International Society Eye Research* 1986;4 (Suppl.):184.
51. Acott TS, Samples JR, Bradley JMB, Bacon DR, Bylsma SS, Van Buskirk EM. Trabecular repopulation by anterior trabecular meshwork cells after laser trabeculoplasty. *American Journal Ophthalmology* 1989;107:1-6.
52. Acott TS, Truesdale AT, Samples JR, Van Buskirk EM. Trabecular extracellular matrix synthesis in human explant organ culture. *Investigative Ophthalmology & Visual Science* 1986;26 (Suppl.),:211.
53. Acott TS, Westcott M, Passo MS, Van Buskirk EM. Trabecular meshwork glycosaminoglycans in human and cynomolgus monkey eye. *Investigative Ophthalmology Visual Science* 1985;26:1320-1329.
54. van Zyl T, Yan W, McAdams A, et al. Cell atlas of aqueous humor outflow pathways in eyes of humans and four model species provides insight into glaucoma pathogenesis. *Proc Natl Acad Sci U S A* 2020;117:10339-10349.
55. Patel G, Fury W, Yang H, et al. Molecular taxonomy of human ocular outflow tissues defined by single-cell transcriptomics. *Proc Natl Acad Sci U S A* 2020;117:12856-12867.

56. Johnson DH, Tschumper RC. Human trabecular meshwork organ culture. *Investigative Ophthalmology & Visual Science* 1987;28:945-953.
57. Erickson-Lamy K. The perfused human ocular anterior segment as a model for aqueous outflow physiology. *Journal of Glaucoma* 1992;1:44-53.
58. Johnson DH, Tschumper RC. The effect of organ culture on human trabecular meshwork. *Experimental Eye Research* 1989;49:113-127.
59. Johnson DH, Bradley JM, Acott TS. The effect of dexamethasone on glycosaminoglycans of human trabecular meshwork in perfusion organ culture. *Invest Ophthalmol Vis Sci* 1990;31:2568-2571.
60. Acott TS. Perfusion organ culture of anterior segments: A twenty-year odyssey of practice and pitfalls., *ARVO SIG*: Invest Ophthalmol Vis Sci Supplement; 2008:#456.
61. Fautsch MP, Johnson DH. Aqueous humor outflow: what do we know? Where will it lead us? *Invest Ophthalmol Vis Sci* 2006;47:4181-4187.
62. Johnson DH. Human trabecular meshwork cell survival is dependent on perfusion rate. *Invest Ophthalmol Vis Sci* 1996;37:1204-1208.
63. Acott TS, Kelley MJ, Keller KE, et al. Intraocular pressure homeostasis: maintaining balance in a high-pressure environment. *J Ocul Pharmacol Ther* 2014;30:94-101.
64. Acott TS, Kelley MJ, Keller KE, et al. IOP Homeostasis - Why most people do not ever develop glaucoma. In: Knepper PA, Samples JR (eds), *Glaucoma Research and Clinical Advances 2016-2018.* Amsterdam, The Netherlands: Kugler Publications; 2016:87-98.
65. Raghunathan VK, Benoit J, Kasetti R, et al. Glaucomatous cell derived matrices differentially modulate non-glaucomatous trabecular meshwork cellular behavior. *Acta Biomater* 2018;71:444-459.
66. Alvarado J, Murphy C, Juster R. Trabecular meshwork cellularity in primary open-angle glaucoma and nonglaucomatous normals. *Ophthalmology* 1984;91:564-579.
67. Alvarado J, Murphy C, Polansky J, Juster R. Age-related changes in trabecular meshwork cellularity. *Invest Ophthalmol Vis Sci* 1981;21:714-727.
68. Grierson I, Calthorpe CM. Characteristics of meshwork cells and age changes in the outflow system of the eye: Their relevance to primary open-angle glaucoma. In: Mills KB (ed), *Glaucoma Proceedings of the Fourth Iinternational Symposium of the Northern Eye Institute.* Oxford: Pergamon Press; 1989:12-31.
69. Grierson I, Howes RC. Age-related depletion of the cell population in the human trabecular meshwork. *Eye* 1987;1 (Pt 2):204-210.
70. Ethier CR, Ajersch P, Pirog R. An improved ocular perfusion system. *Current Eye Research* 1993;12:765-770.
71. Sherwood JM, Boazak EM, Feola AJ, Parker K, Ethier CR, Overby DR. Measurement of Ocular Compliance Using iPerfusion. *Front Bioeng Biotechnol* 2019;7:276.
72. Sherwood JM, Reina-Torres E, Bertrand JA, Rowe B, Overby DR. Measurement of Outflow Facility Using iPerfusion. *PLoS One* 2016;11:e0150694.
73. Madekurozwa M, Reina-Torres E, Overby DR, Sherwood JM. Direct measurement of pressure-independent aqueous humour flow using iPerfusion. *Exp Eye Res* 2017;162:129-138.
74. Madekurozwa M, Reina-Torres E, Overby DR, van Batenburg-Sherwood J. Measurement of postmortem outflow facility using iPerfusion. *Exp Eye Res* 2022;220:109103.
75. Keller KE, Bradley JM, Vranka JA, Acott TS. Segmental versican expression in the trabecular meshwork and involvement in outflow facility. *Invest Ophthalmol Vis Sci* 2011;52:5049-5057.
76. de Kater AW, Melamed S, Epstein DL. Patterns of aqueous humor outflow in glaucomatous and nonglaucomatous human eyes. A tracer study using cationized ferritin. *Arch Ophthalmol* 1989;107:572-576.

77. Hann CR, Bahler CK, Johnson DH. Cationic ferritin and segmental flow through the trabecular meshwork. *Invest Ophthalmol Vis Sci* 2005;46:1-7.
78. Swaminathan SS, Oh DJ, Kang MH, et al. Secreted protein acidic and rich in cysteine (SPARC)-null mice exhibit more uniform outflow. *Invest Ophthalmol Vis Sci* 2013;54:2035-2047.
79. Swaminathan SS, Oh DJ, Kang MH, Rhee DJ. Aqueous outflow: segmental and distal flow. *J Cataract Refract Surg* 2014;40:1263-1272.
80. Snider EJ, Kubelick KP, Tweed K, et al. Improving Stem Cell Delivery to the Trabecular Meshwork Using Magnetic Nanoparticles. *Sci Rep* 2018;8:12251.
81. Hu Y, Gabelt BT, Kaufman PL. Monkey organ-cultured anterior segments: technique and response to H-7. *Exp Eye Res* 2006;82:1100-1108.
82. Quinn RF, Tingey DP. Effects of cytoskeleton-reactive agents on aqueous outflow facility in a porcine ocular anterior segment preparation. *Can J Ophthalmol* 1995;30:4-10.
83. Goldwich A, Ethier CR, Tamm ER. Perfusion With the Olfactomedin Domain of Myocilin Does Not Show Major Effects on Outflow Facility in Anterior Eye Segment Organ Cultures. *Invest Ophthalmol Vis Sci* 2002;43:#1036.
84. Snider EJ, Hardie BA, Li Y, et al. A Porcine Organ-Culture Glaucoma Model Mimicking Trabecular Meshwork Damage Using Oxidative Stress. *Invest Ophthalmol Vis Sci* 2021;62:18.
85. Mao W, Tovar-Vidales T, Yorio T, Wordinger RJ, Clark AF. Perfusion-cultured bovine anterior segments as an ex vivo model for studying glucocorticoid-induced ocular hypertension and glaucoma. *Invest Ophthalmol Vis Sci* 2011;52:8068-8075.
86. Erickson-Lamy K, Rohen JW, Grant WM. Outflow facility studies in the perfused bovine aqueous outflow pathways. *Current Eye Research* 1988;7:799-807.
87. Kelly RA, McDonnell FS, De Ieso ML, Overby DR, Stamer WD. Pressure Clamping During Ocular Perfusions Drives Nitric Oxide-Mediated Washout. *Invest Ophthalmol Vis Sci* 2023;64:36.
88. Erickson-Lamy K, Schroeder AM, Bassett-Chu S, Epstein DL. Absence of time-dependent facility increase ("washout") in the perfused enucleated human eye. *Investigative Ophthalmology Visual Science* 1990;31:2384-2388.
89. Kaufman PL, True-Gabelt B, Erickson-Lamy KA. Time-dependence of perfusion outflow facility in the cynomolgus monkey. *Curr Eye Res* 1988;7:721-726.
90. Ramos RF, Stamer WD. Effects of cyclic intraocular pressure on conventional outflow facility. *Invest Ophthalmol Vis Sci* 2008;49:275-281.
91. Lei Y, Overby DR, Boussommier-Calleja A, Stamer WD, Ethier CR. Outflow physiology of the mouse eye: pressure dependence and washout. *Invest Ophthalmol Vis Sci* 2011;52:1865-1871.
92. Loewen RT, Roy P, Park DB, et al. A Porcine Anterior Segment Perfusion and Transduction Model With Direct Visualization of the Trabecular Meshwork. *Invest Ophthalmol Vis Sci* 2016;57:1338-1344.
93. Peng M, Curry SM, Liu Y, Lohawala H, Sharma G, Sharma TP. The ex vivo human translaminar autonomous system to study spaceflight associated neuro-ocular syndrome pathogenesis. *NPJ Microgravity* 2022;8:44.
94. Peng M, Margetts TJ, Sugali CK, et al. An ex vivo model of human corneal rim perfusion organ culture. *Exp Eye Res* 2022;214:108891.
95. Johnstone M, Xin C, Acott T, et al. Valve-Like Outflow System Behavior With Motion Slowing in Glaucoma Eyes: Findings Using a Minimally Invasive Glaucoma Surgery-MIGS-Like Platform and Optical Coherence Tomography Imaging. *Front Med (Lausanne)* 2022;9:815866.
96. Wang K, Johnstone MA, Xin C, et al. Estimating Human Trabecular Meshwork Stiffness by Numerical Modeling and Advanced OCT Imaging. *Invest Ophthalmol Vis Sci* 2017;58:4809-4817.

97. Karimi A, Razaghi R, Rahmati SM, et al. Modeling the biomechanics of the conventional aqueous outflow pathway microstructure in the human eye. *Comput Methods Programs Biomed* 2022;221:106922.
98. Karimi A, Rahmati SM, Razaghi R, et al. Biomechanics of human trabecular meshwork in healthy and glaucoma eyes via dynamic Schlemm's canal pressurization. *Comput Methods Programs Biomed* 2022;221:106921.
99. Karimi A, Khan S, Razaghi R, et al. Developing an experimental-computational workflow to study the biomechanics of the human conventional aqueous outflow pathway. *Acta Biomater* 2023.
100. Vranka JA, Acott TS. Molecular differences in segmental regions of the trabecular meshwork. In: Knepper PA, Samples JR (eds), *Glaucoma Research and Clinical Advances 2016-2018.* Amsterdam, The Netherlands: Kugler Publications; 2016:115-120.
101. Vranka JA, Bradley JM, Yang YF, Keller KE, Acott TS. Mapping molecular differences and extracellular matrix gene expression in segmental outflow pathways of the human ocular trabecular meshwork. *PLoS One* 2015;10:e0122483.
102. Vranka JA, Staverosky JA, Reddy AP, et al. Biomechanical Rigidity and Quantitative Proteomics Analysis of Segmental Regions of the Trabecular Meshwork at Physiologic and Elevated Pressures. *Invest Ophthalmol Vis Sci* 2018;59:246-259.
103. Ethier CR, Chan D-H. Cationic ferritin changes outflow facility in human eyes whereas anionic ferritin does not. *Invest Ophthalmol Vis Sci* 2001;42:1795-1802.
104. Vranka JA, Staverosky JA, Raghunathan V, Acott TS. Elevated pressure influences relative distribution of segmental regions of the trabecular meshwork. *Exp Eye Res* 2020;190:107888.
105. Reina-Torres E, Baptiste TMG, Overby DR. Segmental outflow dynamics in the trabecular meshwork of living mice. *Exp Eye Res* 2022;225:109285.
106. Strohmaier CA, McDonnell FS, Zhang X, et al. Differences in Outflow Facility Between Angiographically Identified High- Versus Low-Flow Regions of the Conventional Outflow Pathways in Porcine Eyes. *Invest Ophthalmol Vis Sci* 2023;64:29.
107. Saraswathy S, Bogarin T, Barron E, et al. Segmental differences found in aqueous angiographic-determined high - and low-flow regions of human trabecular meshwork. *Exp Eye Res* 2020;196:108064.
108. Bradley JMB, Kelley MJ, Zhu XH, Anderssohn AM, Alexander JP, Acott TS. Effects of mechanical stretching on trabecular matrix metalloproteinases. *Invest Ophthalmol Vis Sci* 2001;42:1505-1513.
109. Abu-Hassan DW, Li X, Ryan EI, Acott TS, Kelley MJ. Induced pluripotent stem cells restore function in a human cell loss model of open-angle glaucoma. *Stem Cells* 2015;33:751-761.

FIGURES AND CAPTIONS

Figure 1. Dissection and preparation of human anterior segments for stationary or perfusion culture. Most investigators now carefully remove all the dark material seen covering the outflow pathway in the lower right panel.

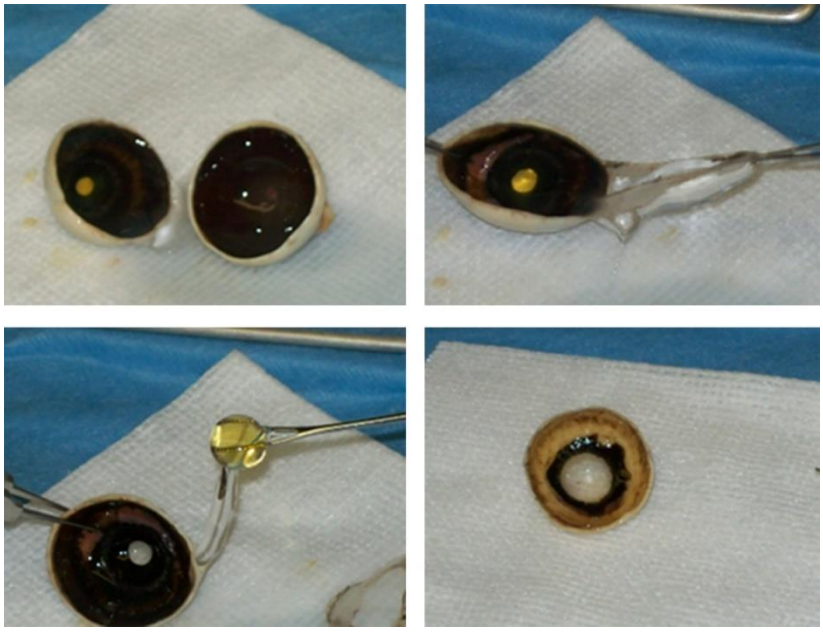

Figure 2. Setup mounting eye on flow cell.

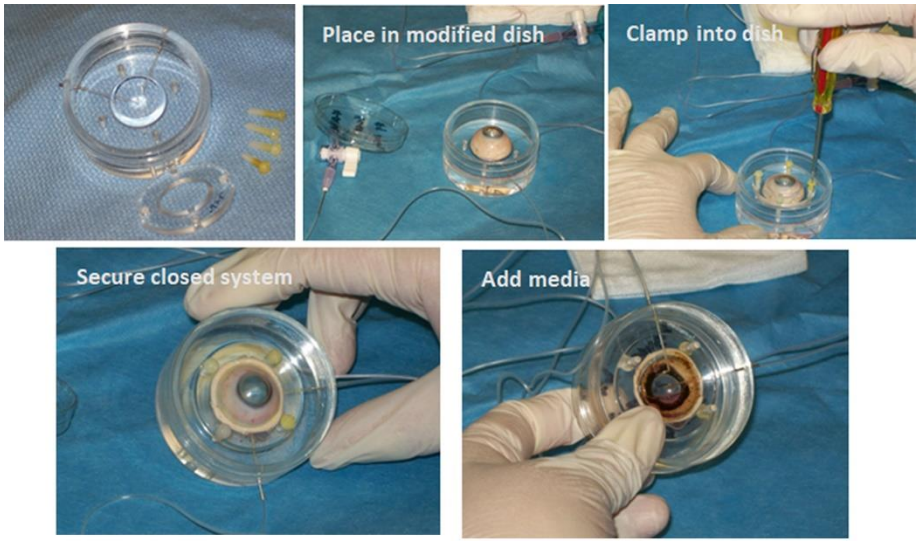

Figure 3. Perfusion cell with eye mounted. Top view of a flow cell with human anterior segment mounted. A cross sectional diagram showing fluid routes and anterior segment placement and clamping. This is the Johnson flow cell design based on a machined modified petri dish.[56]

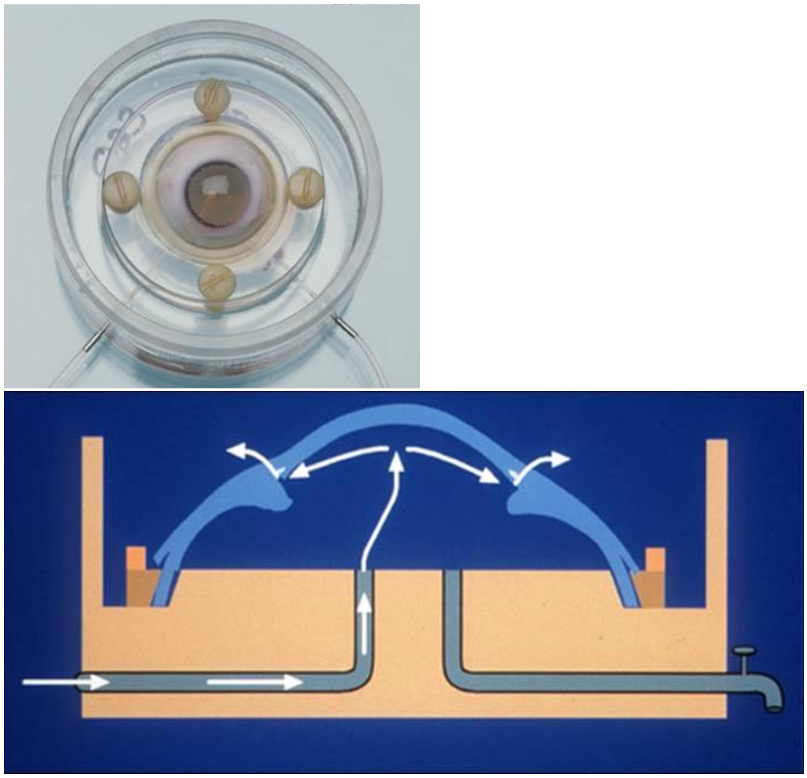

Figure 4. Constant flow syringe pump setup. An adjustable precision syringe pump can be used to produce low constant-volume perfusion. The flow rate can be adjusted as desired for the experimental design. Note that all syringe pumps have some misalignment of the lead screws, so that even a “constant flow” perfusion has some unsteadiness in the flow waveform due to the misalignment-induced oscillation of the pusher plate that contacts the syringe plunger(s). It is prudent to characterize the extent of pressure oscillation for each pump, for example by perfusing a fixed resistance such as a filter and measuring the resultant pressure waveform, which will be proportional to the flow waveform produced by the pump.

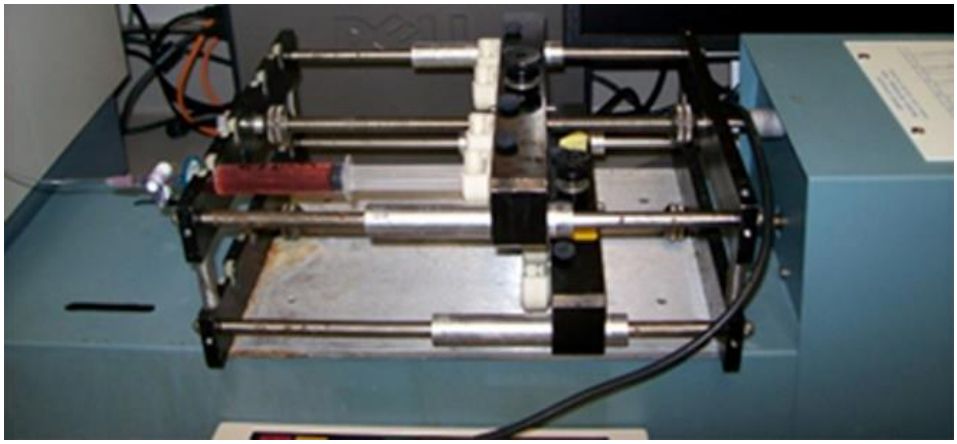

Figure 5. Perfusion system in Fautsch lab at Mayo Clinic, Rochester, MN. Humidified, 37 Degree C, 5% CO_2 incubator with PE60 tubing connecting the flow chambers to the syringe pump (blue box) and to pressure transducer (on the right outside the chamber). It is notable that a tray/pan of water with antibacterial such as Lysol placed in the bottom of each incubator and changed regularly is essential to maintain 100% humidity and to avoid evaporation errors. The monitor indicates pressure transducer readings.

Figure 6. Exploded view of a modification of the Johnson and the Erickson-Lamy flow cells. There are four ports and flow channels through the pedestal with tubing nipples on the bottom. Unused ports can be filled with the included small plastic bolts, taking

them out of play. This flow cell is machined from PVC, which is relatively resistant to solvent and heat exposure, and glued together or bonded by dissolving the two surfaces to be joined with a solvent such as butyl methacrylate or by acrylic cement. This flow cell is available through Apex Industries, Inc., Tigard, OR (www/apexind.com; Phone: 503 235, 8324) as A-008309 Rev B01, Square Eye Cell Assay – clear PVC. Recently for convenience this cell has been used flipped over and placed cornea side down on a small water glass for perfusion instead of cornea side up as is the traditional method. When used right-side-up as in the diagram, a sterile aluminum foil top is used to avoid contamination.

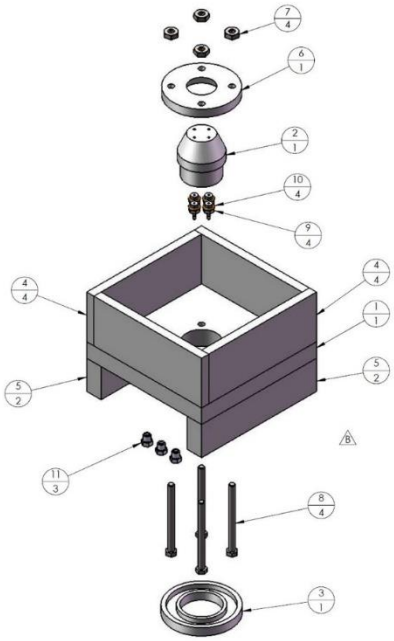

Apex	APEX INDUSTRIES, INC. TIGARD OREGON		
	TITLE: ASSY, SQUARE EYE CELL		
PROPRIETARY AND CONFIDENTIAL THE INFORMATION CONTAINED IN THIS DRAWING IS THE SOLE PROPERTY OF APEX INDUSTRIES. ANY REPRODUCTION IN PART OR AS A WHOLE WITHOUT THE WRITTEN PERMISSION OF APEX INDUSTRIES IS PROHIBITED.	SIZE B	DWG. NO. A-008309	REV AW ORKI
	DO NOT SCALE DRAWING		SHEET 3 OF 3

Figure 7. Two approaches to determining outflow facility, i.e., constant flow and constant pressure perfusion. Two initial methods used either constant perfusion rates measuring the resultant pressure with a pressure transducer or constant pressure measuring flow rate, usually gravimetrically. Both methods have advantages.

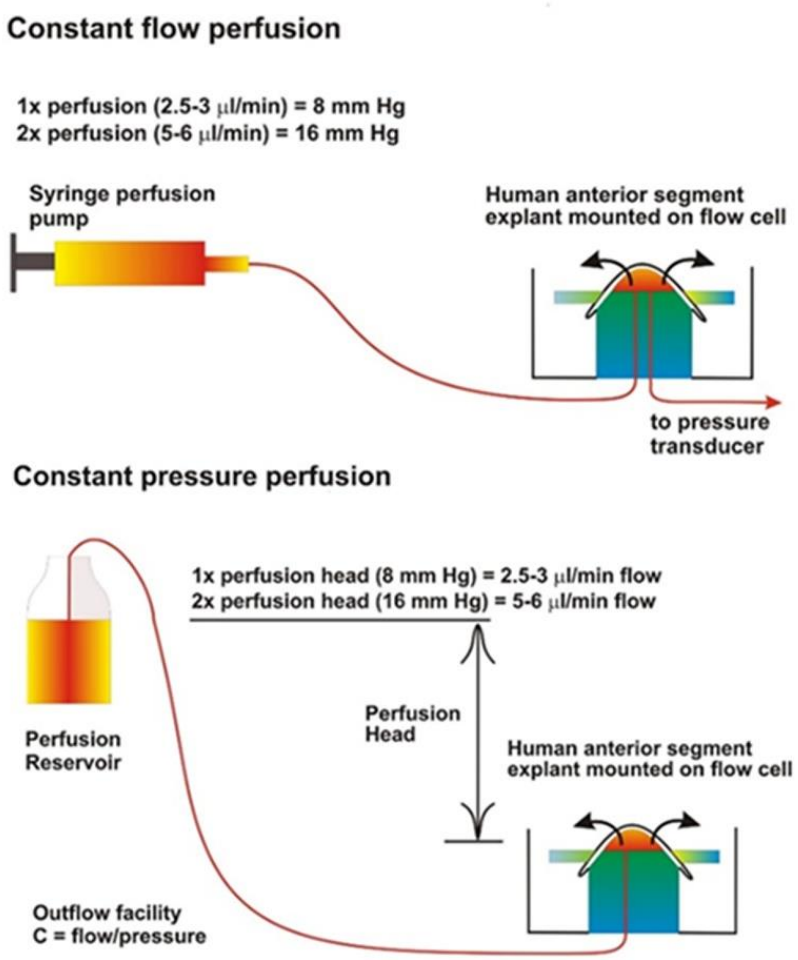

Figure 8. Balances and flow cells for continuous gravimetric assessment of flow in constant pressure perfusion approach. Two balances weighing fluid in 50 ml conical centrifuge tubes with flow cells inverted on a water glass in the lower left. Left is at 2x and right is at 1x pressure. Balances are constantly read at 2-minute intervals and data inserted into an Excel file.

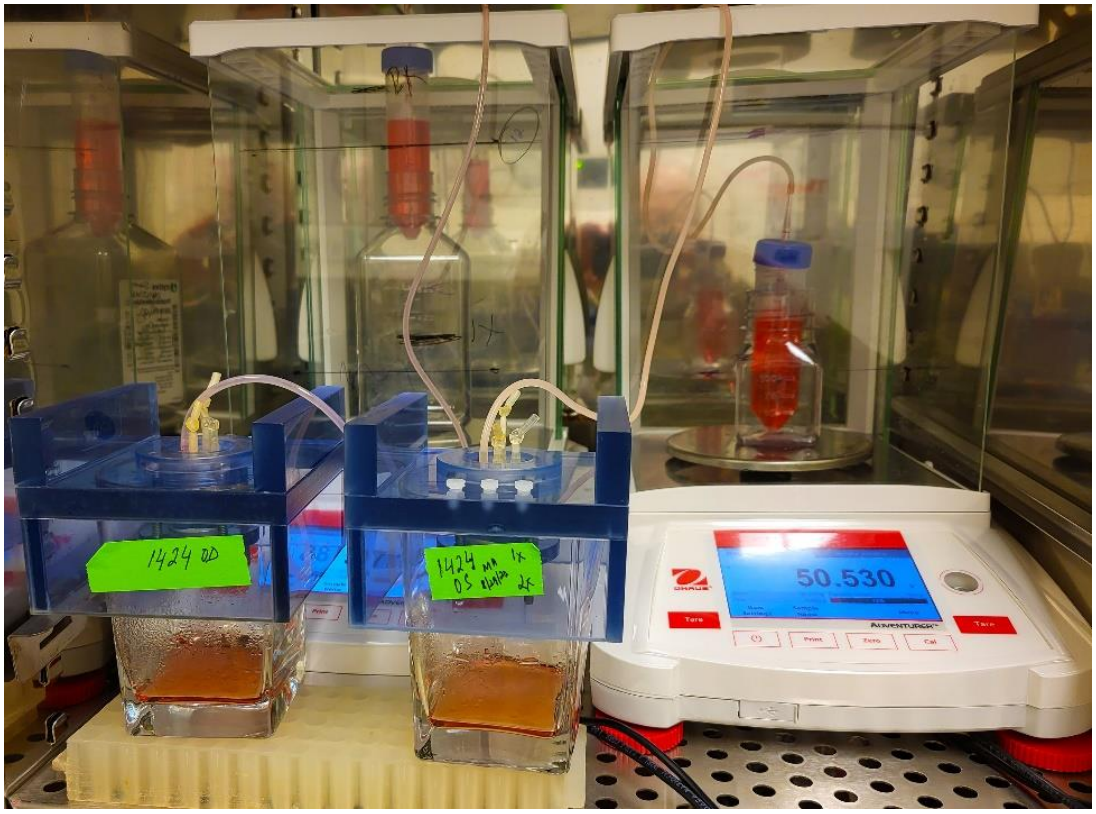

Figure 9. GageMux USB with foot pedal to trigger readings and 4 USB connections to read the 4 balances. Data are dumped into and Excel file on a connected laptop.

Figure 10. Improved outflow measurement device developed by Ethier.[70] The reservoir is mounted on a screw drive to adjust the head. BT is a bubble trap and PP are bubble purge ports. DPT is the pressure transducer that reads pressure across the steel tube and GPT is a pressure transducer that reads equivalent to the IOP at the eye. Arrows show the direction of flow during a measurement.

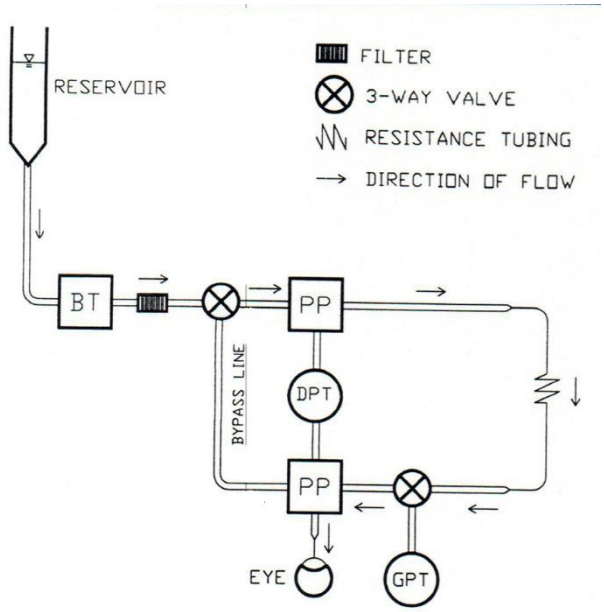

Figure 11. The bovine anterior segment perfusion culture model.[85] A) Diagram of the perfusion cell with syringe pump to control flow and pressure transducer to sense resultant pressure. Arrows indicate the direction of fluid flow and arrowheads indicate the position of the TM. B) Photograph of the flow cell with a bovine eye mounted on it.[85, 86]

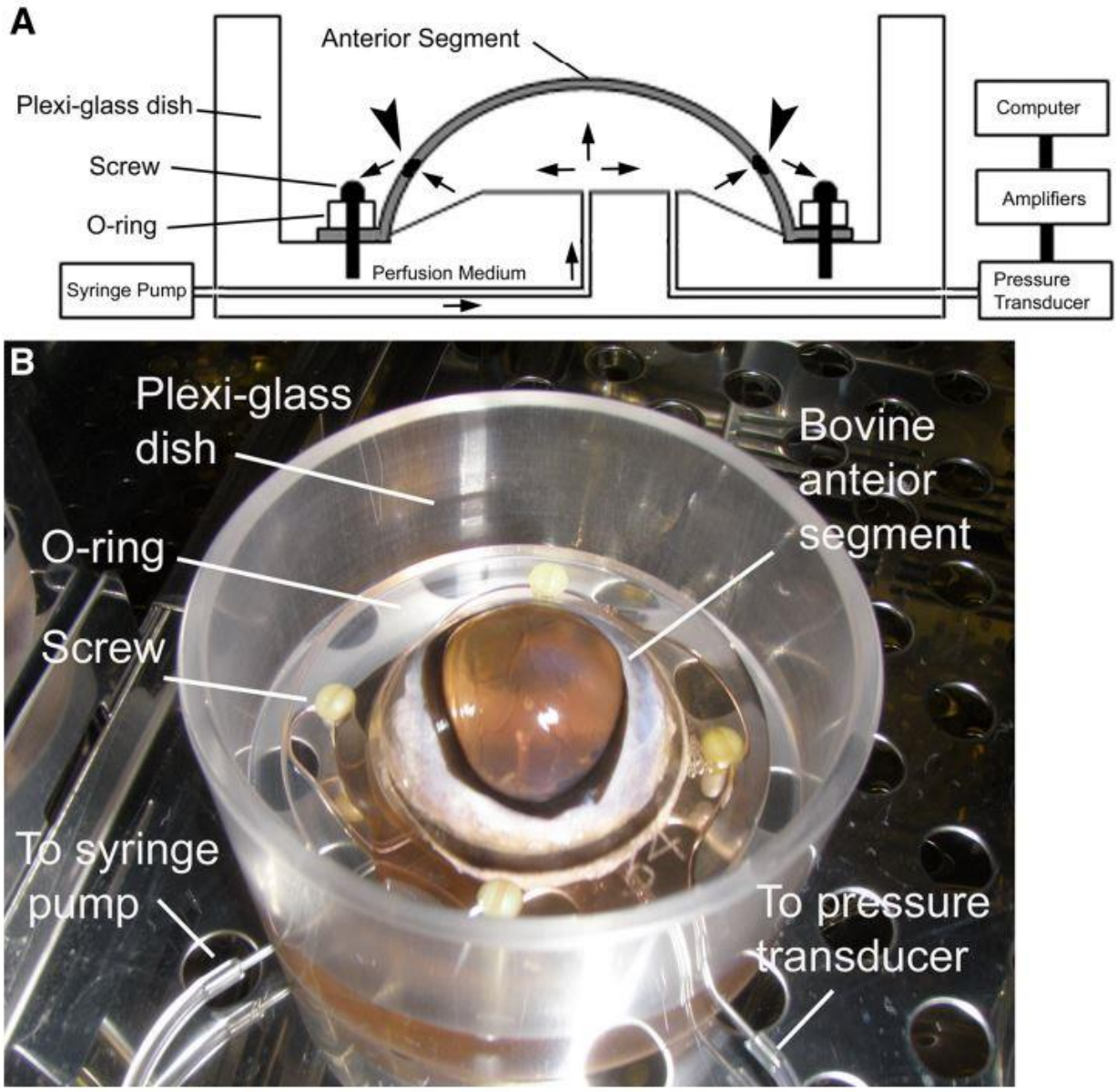

Figure 12. Corneal rim perfusion culture model.[94] A) and B) the perfusion plate. C) the perfusion plate and the holder. D) The corneal rim glued onto the plate. E): Sideview of the corneal rim after being glued onto the plate. F and G) perfusion system setup. H) Experimental timeline.

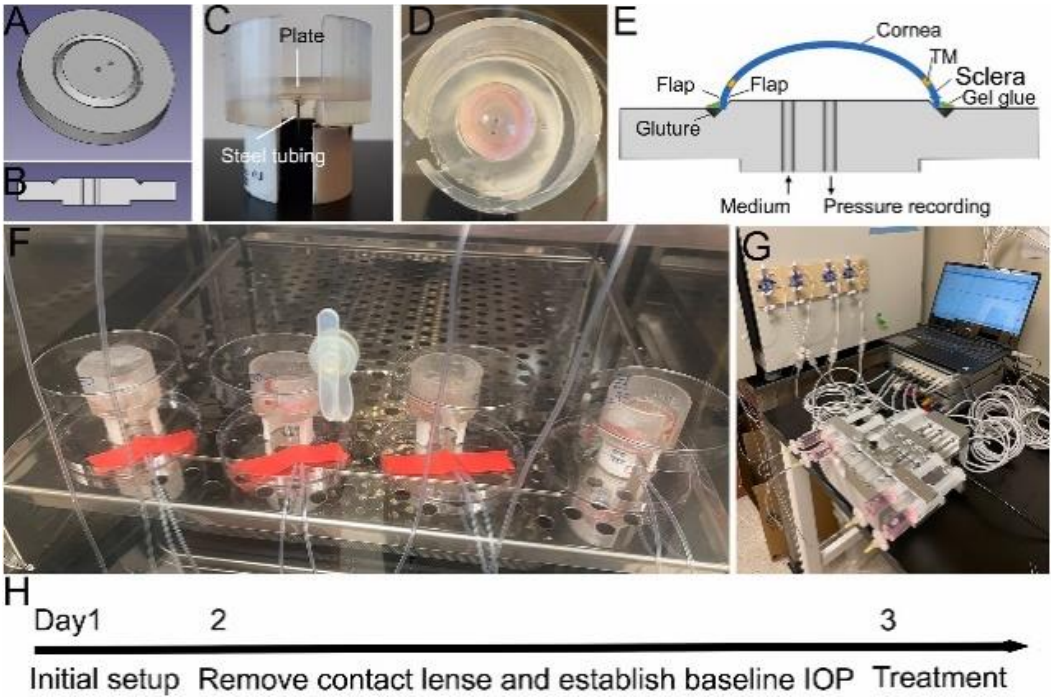

Figure 13. Glue contamination increased TM stiffness in perfusion cultured human corneal rims.[94] The stiffness (elastic modulus) of three corneal rims with no (Naïve), mild/non-visible (Glue-B), and severe (Glue-A) glue contamination.

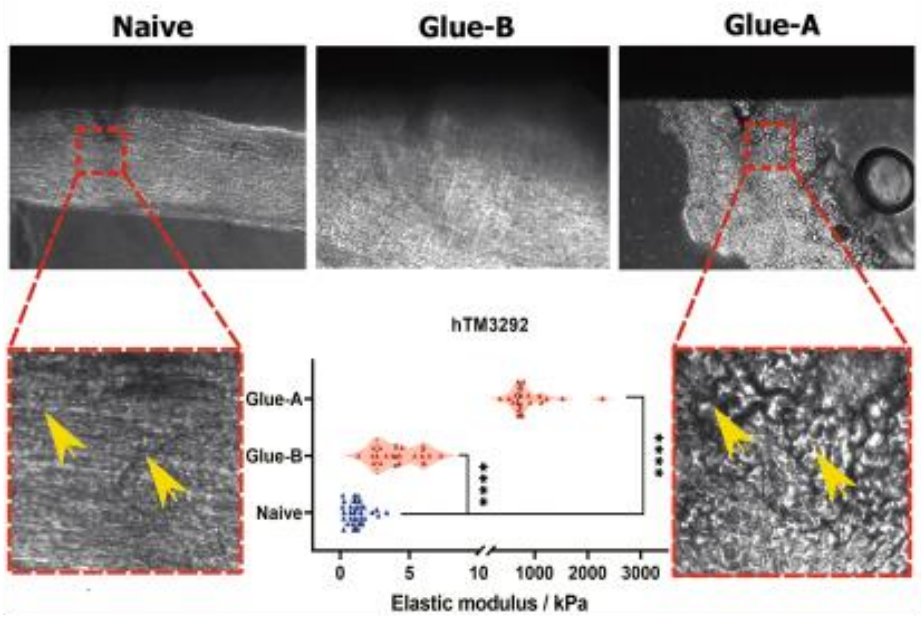

Figure 13. A) The Johnstone model of anterior segment wedge with cannula in Schlemm's canal.[95] The positive pressure in Schlemm's canal is determined by level of the pressure reservoir (0- or 30-mm Hg) relative to the fluid level in the dish. B) OCT image at 0 mm Hg pressure head and C) at 30 mm Hg positive pressure head. Scale is shown by 200 mm white bar. The pressure head can be varied rapidly to achieve dynamic responses.

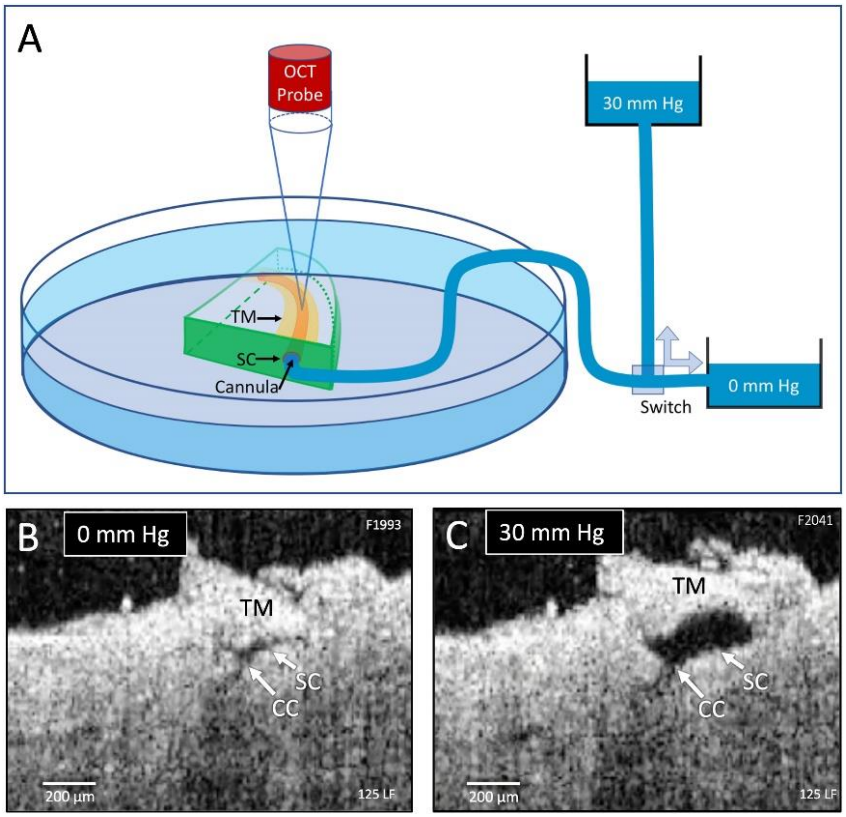

Figure 14. Wedge flow for negative Schlemm's canal pressure studies. The pressure head is from the surface of the fluid in the Petri dish to the surface of the fluid in the perfusion reservoir (i.e., 0, 8.8 (1x) or 17.6 (2x) mm Hg), i.e., the anterior chamber pressure is higher than the Schlemm's canal pressure as in the normal eye.

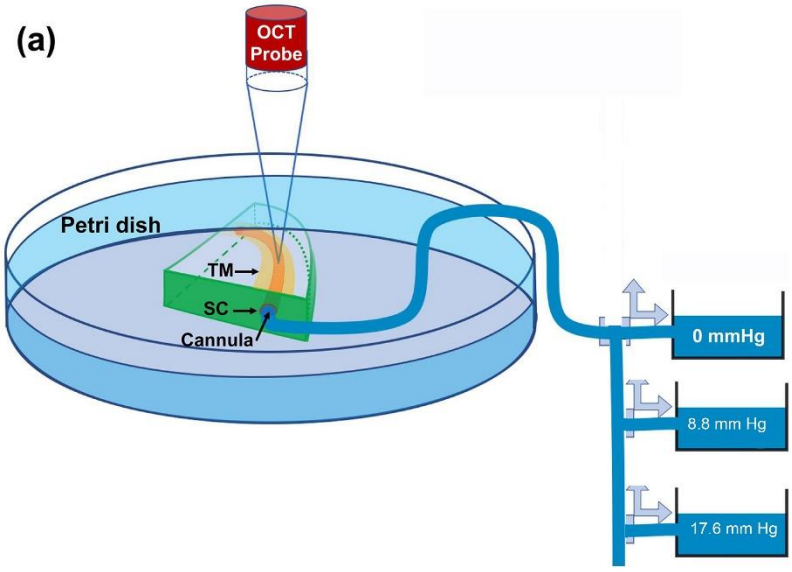

X. Clinical

32. Targeted degradation of mutant myocilin with tailored antibodies

Lieberman, Raquel L.[1], Maynard, Jennifer A.[2], Ma, Minh Thu[1], Qerqez, A. N.[2], Azouz, L. R.[2], Hill, K. R.[1], Hill, S. E.[1], Ku, Y[1]

[1] School of Chemistry & Biochemistry, Georgia Institute of Technology, 901 Atlantic Drive NW Atlanta, GA 30332 USA Raquel.lieberman@chemistry.gatech.edu
[2] Dept. of Chemical Engineering, and [3]Department of Molecular Biosciences University of Texas at Austin, Austin, TX 78712 USA maynard@che.utexas.edu

Purpose: A promising treatment for protein misfolding associated with neurodegenerative diseases is the use of antibodies, which enable degradation of the aberrant protein. Inspired by these efforts, we developed antibodies that target the aggregation-prone myocilin olfactomedin (OLF) domain.

Methods: Our antibody discovery campaign yielded two recombinant antibodies, anti-OLF1 and anti-OLF2. These antibodies were subjected to extensive validation and biochemical characterization. Following this, cellular assays were used to assess the fate of mutant myocilin in the presence of these antibodies as well as the mechanism of action.

Results: Anti-OLF1 and anti-OLF2 engage different epitopes on OLF. As such, they influence distinct steps in the protein folding/misfolding pathway, yet both promote degradation of mutant myocilin.

Conclusions: This work demonstrates the potential for therapeutic antibodies to disrupt endoplasmic-reticulum-localized myocilin aggregates by altering the fate of folding intermediates. More generally, the study supports combating proteostasis decline in anterior eye tissues associated with intraocular pressure elevation, the causal risk factor for glaucoma.

Financial Support: This work was supported by the BrightFocus Foundation [G2016027 to RLL], the National Institutes of Health National Eye Institute [R01EY021205 to RLL, T32007092 to MTM, and R21EY031093 to RLL and JAM], the Welch foundation [F-1767 to JAM] and an NSF GRFP Fellowship [ANQ]. MTM, ANQ, LRA, SEH, JAM, and RLL are co-inventors of International Publication WO 2021/237213 A1

33. Transgene expression of Stanniocalcin-1 for sustained IOP reduction

Gavin W. Roddy[1], Kjersten J. Anderson[1], Tommy A. Rinkoski[1], and Michael P. Fautsch[1]

[1] Dept. of Ophthalmology, Mayo Clinic, Rochester, Minnesota, 55905

Purpose: Less than half of patients with glaucoma take topical medications as prescribed. Medical treatment of glaucoma is limited by side effects of current medications, treatment non-response, and fluctuation in intraocular pressure (IOP) which leads to continued progression. Novel therapies with diminished side effect profiles and reduced dosing requirements are needed to improve compliance and reduce rates of progression. To combat these issues, various strategies for sustained IOP reduction are currently being explored; however, current approaches require the use of a scaffold to elute an IOP-lowering drug. In studying the mechanism of latanoprost, we identified a downstream effector molecule, Stanniocalcin-1 (STC-1), a secreted protein that lowers IOP, as a candidate molecule that could be expressed with a vector system for sustained IOP reduction. We recently demonstrated that adenoassociated virus (AAV) delivery of STC-1 (AAV-STC-1) reduced IOP for up to 6 months with a single injection into the anterior chamber of mice. Here we assess the IOP-lowering ability of subconjunctival AAV-STC-1 in normotensive and ocular hypertensive mice and compare ocular surface inflammation and IOP reduction with daily topical latanoprost.

Methods: Following baseline IOP measurements with a Tonolab tonometer, C57BL/6J normotensive wild-type mice (n=8), DBA/2J ocular hypertensive mice (n=14), or steroid-induced ocular hypertensive mice (n=8) were injected subconjunctivally in one eye with AAV-STC-1 (2 µL; 3 x 10^{12} VG/mL) and the same volume and concentration of AAV-GFP in the fellow eye. IOP was assessed twice weekly. To compare ocular IOP reduction and ocular surface inflammation, wild-type mice were treated with either once daily topical latanoprost (0.005%; 5 µL, n=5) or a single subconjunctival injection of AAV-STC-1 (2 µL; 3 x 10^{12} VG/mL, n=5). Conjunctiva were collected and assayed for TNF-α by ELISA one month after initiation of treatment.

Results: Subconjunctivally delivered AAV-STC-1 lowered IOP in normotensive mice (14.9 vs 17.3 mmHg, P<0.001) at one week. Significant IOP reduction persisted through week 10. Additionally, subconjunctivally delivered AAV-STC-1 lowered IOP in DBA/2J (16.6%, 17.2mmHg vs 14.3mmHg, P<0.001) and steroid-induced (19.9%, 18.9 vs 15.2mmHg, P<0.001) models of ocular hypertension throughout the treatment period. In normotensive mice, daily topical latanoprost and subconjunctival AAV-STC-

1 showed equivalent IOP reduction, but AAV-STC-1 showed a 42% decrease in TNFα in conjunctiva ($P<0.01$) compared to topical latanoprost.

Conclusion: Administration of AAV-STC-1 by subconjunctival injection represents a novel therapeutic approach that provides sustained IOP reduction with diminished ocular surface inflammation. Additional pre-clinical studies are warranted to determine whether this may be an effective treatment for patients unable to be treated medically for glaucoma due to ocular surface side effects or inability to instill drops daily.

34. Preliminary Evaluation of NOX4 Inhibition to Prevent FibROSis in the Trabecular Meshwork

Breedge Callaghan†, Chelsey Doyle†, Declan McKenna, Sarah D. Atkinson, Colin E. Willoughby.

Genomic Medicine, Biomedical Sciences Research Institute, Ulster University, Coleraine BT52 1SA, Northern Ireland, United Kingdom.

† Breedge Callaghan and Chelsey Doyle contributed equally and should be considered as joint first authors.

Purpose: Accumulating evidence supports the concept that NADPH oxidase 4 (NOX4) is an important effector in mediating TGF-β-induced fibrosis and ROS in the heart, lungs and kidneys, as well as, in the trabecular meshwork (TM) and Tenon's fibroblasts. NOX4-medicated redox imbalance drives TGF-β induced fibrosis and there is evidence that NOX4-dependent redox signaling may in turn regulate TGF-β/Smad signaling in a feed-forward manner. NOX4 driven ROS can convert latent TGF-β to its active form, which is one of the most important mechanisms that regulate activation of the TGF-β signaling. **Therapeutics which target NOX4 may abrogate the pathological effects of mediating TGF-β-induced fibrosis and oxidative stress in glaucoma.** No specific NOX4 chemical inhibitors exist. **The aim of this study was to evaluate two approaches to inhibit NOX4 activity in TM cells *in vitro*: (1) novel chemical inhibitors (in collaboration with Atomwise, USA) and (2) microRNA (miRNA) mimics targeting NOX4.**

Methods:

(1) Chemical Inhibitor Design. Atomwise performed a virtual screen of millions of commercially available chemical compounds using its deep learning-based computational drug discovery platform (AtomNet®). This virtual screen predicted chemical compounds that are most likely to bind to the FAD binding pocket in the NOX4 homology model: 72 compounds were identified for physical screening.

(2) MiRNA Mimics Targeting NOX4. To identify potential candidate miRNAs, a panel of experimentally validated and predicted NOX4-targeting miRNAs was generated using bioinformatics tools. A review of the literature was then conducted to investigate miRNAs that target NOX4 based on previous studies. An additional literature review was performed to identify whether any of these miRNA candidates have been detected in the TM and/or AH. Five miRNAs were selected for further study and their expression in primary human TM cells treated with TGF-β1 and -β2 (5ng/mL for 24 hrs) checked by RT-qPCR.

(3) Amplex Red Assay. Given that commercial antibodies targeting NOX4 are non-specific an amplex red assay was used to measure NOX4 activity. NOX4 is the major source of H_20_2 in cells and this can be measured using an amplex red assay. Primary human TM cells were pretreated with chemical inhibitors or transfected with miRNA mimics and NOX4 activity measured using an amplex red assay.

Results: 72 chemical compounds were screened using the amplex red assay and compared to N-acetylcysteine and NOX4 siRNA (as positive controls). 25 compounds showed a statistically significant decrease in NOX4 activity compared to the control. 3 miRNA mimics inhibited NOX4 activity in response to TGF-β1 at 6 and 24 hrs and were equivalent to a NOX4 siRNA. TGF-β2 induced NOX4 activity at 6 and 24 hrs was inhibited with miRNA mimics to a lesser degree. Two miRNA mimics showed an inhibition of NOX4 activity induced by either TGF-β1 or -β2 at 48 hours equivalent to NOX4 siRNA.

Conclusions: NOX4 activity induced by TGF-β1 or -β2 was inhibited using novel chemical inhibitors and miRNA mimics. Further work is required to assess anti-fibrotic effects and specificity, dose kinetics and delivery. Therapeutics which target NOX4 may abrogate the pathological effects of mediating TGF-β-induced fibrosis and oxidative stress in glaucoma.

Financial Support: This research was funded by Glaucoma UK (formerly the International Glaucoma Association), UK and Eire Glaucoma Society (UKEGS) and Mason Medical Research Foundation.

Graphical Abstract

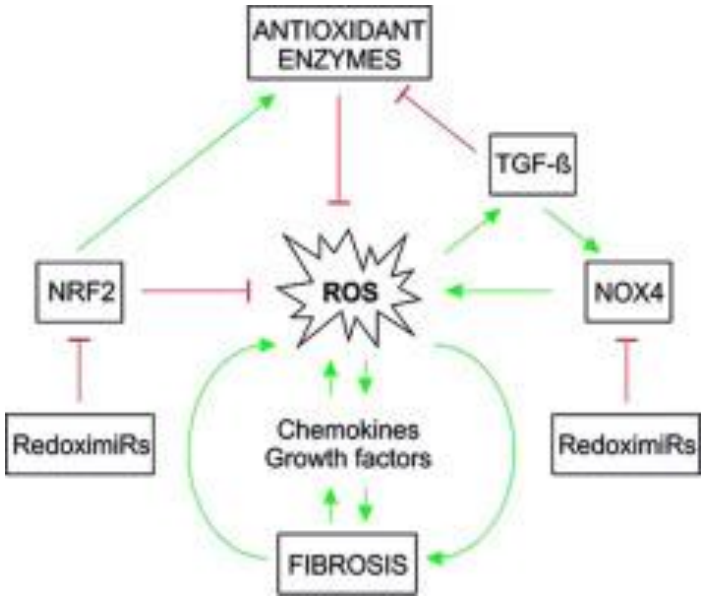

From: Richter et al. Redox Biol. 2015 Dec; 6:344-352.

35. Successes and failures of novel glaucoma drainage devices Preclinical studies of outflow facility

Carol B. Toris, PhD

The Ohio State University, Department of Ophthalmology and Visual Sciences, Columbus, Ohio, ctoris@unmc.edu

Purpose: Alternatives to pharmaceuticals are attractive options for the treatment of ocular hypertension as they reduce or eliminate patient compliance issues. Numerous glaucoma drainage devices have been designed to improve flow through the trabecular meshwork (TM) or bypass it altogether to improve outflow facility (C) and lower intraocular pressure (IOP). These devices/procedures currently are hot areas of study. Here we describe successes and failures of some of these unique devices or procedures that we have studied.

Methods: For some devices, a multilevel constant pressure perfusion technique was used to measure C in human globes. Paired globes were measured simultaneously, one was the experimental eye, and the fellow eye was the control. Baseline C was measured followed by C after the experimental or sham procedure. The experimental eye C was compared to baseline and to the control eye. One study compared devices of different lengths inserted into Schlemm's canal (SC) (iStent, iStent Inject, Hydrus). One device (Forge) was placed on the surface of the TM facing the anterior chamber. One study compared dual wall canalotomy with single-wall goniotomy to determine the improvement in C by directly accessing the downstream pathway. In one study (Camras Shunt), a tube with variable resistance was inserted between the anterior chamber and ocular surface in live monkeys and IOP was measured by tonometry.

Results: All three devices that were placed in Schlemm's canal improved C ($p<0.05$). Dual wall canalotomy improved C more than single-wall goniotomy ($p=0.05$). The FORGE improved C more than baseline and to a degree similar to the Schlemm's canal devices. The Camras Shunt lowererd IOP over a period of 3 months but failed thereafter because of inflammation and clogging. Device/procedure failures included difficult placement, dislocation, clogging, or no improvement in IOP or C.

Conclusion: Devices considered worthy of further development were those that improved C by more than 75% and could be placed within a few seconds. For the three Schlemm's canal devices, the one with greater length and dilation of the SC (Hydrus) provided the greater improvement in C. Incision into the inner and outer wall of SC (dual wall canalotomy) improved C more than incision into the inner wall only (single-wall goniotomy) suggesting direct communication to the downstream pathway. The device that attached to the TM (Forge) was placed quickly and could improve C to a level similar to the Hydrus. Drainage to the ocular surface (Camras shunt) did not reach milestones and was not developed further.

Funding Sources. Ivantis, Research to Prevent Blindness, RightFlow Medical, LLC, NEI grant, Iantrek, CamrasVision, Alievio, NIH SBIR Fast-Track 1R44EY027244 (Lucinda Camras), NSF SBIR Phase II/IIB 1555923 (Lucinda Camras).

Acknowledgements: Many investigators and technical staff at the University of Nebraska Medical Center and Case Western Reserve University contributed to this work. The key investigators were Douglas Rhee, Padmanaban Pattabiraman, Shan Fan, Vikas Gulati, Faruk Orge, George Tye, Thomas Samuelson, Iqbal Ahmed, Cassie Hays, PhD, Fan Yuan, PhD, Andrew Schieber, Gautam Kamthan, MD, Ravi D Pamnani, PhD, Tsontcho Ianchulev, MD, MPH, Lucinda Camras, PhD

XI. Clinical Laboratory

39. The role of tissue plasminogen activator in regulating outflow

John Danias[1], Arturo Barron Arambide[1]

[1]Department of Ophthalmology, University of New York (SUNY), Downstate Medical Center, Brooklyn, New York

Purpose: Determine the mechanism of tPA's effect on outflow facility and harness tPA to treat glaucoma

Methods: MMP9 KO mice and C57BL/6 mice were used. MMP9 KO mice were treated with triamcinolone acetonide (TA) periocularly. Some animals received tPA intraocularly five days post TA treatment. Outflow facility was determined using a constant pressure method 48h later and compared between eyes receiving TA only, TA+tPA and naïve ones. To harness the ability of tPA to improve outflow, C57BL/6 mice were injected intracamerally with an scAAV carrying a PLAT variant or an scAAV encoding for green fluorescent protein (GFP) while receiving weekly dexamethasone periocular injections. IOP was measured weekly. Three weeks post administration of the scAAV, animals were sacrificed and outflow facility was determined using a constant pressure method

Results: TA failed to decrease outflow facility in MMP9-KO mouse eyes. tPA did not improve outflow facility in MMP9 KO eyes treated with TA ($p>0.05$, ANOVA). C57BL/6 mouse eyes treated with dexamethasone developed elevated IOP (from 14.8 ± 0.5 mmHg to 20.2 ± 0.7 mmHg $p<0.05$). In eyes treated with scAAV-PLATvar, IOP decreased at the time of sacrifice to 15.3 ± 1.4 mmHg ($p<0.05$ from IOP in GFP treated eyes). Outflow facility was significantly different between scAAV-PLATvar and scAAV-GFP treated eyes ($p<0.05$, Kruskal Wallis)

Conclusions: MMP9 absence abrogates the effect of steroids on outflow facility. MMP9 also likely mediates at least in part the effect of PLAT on outflow facility. Upregulation of a non-enzymatically active PLAT variant in the outflow tissues can decrease IOP and improve outflow facility in steroid induced mouse model of glaucoma

XII. White Paper Discussion #2: Consensus recommendations for tonography methods to assess outflow facility

Consensus recommendations for tonography methods to assess outflow facility

Target journal: IOVS

Authors (in no particular order): Carol Toris, Alyson Kishi, Alessandra Derick, Zoltan Namenyi, Vikas Gulati, Shan Fan, Arthur Sit, Arash Kazemi, David Reed, Sayoko Moroi, Katy Liu, Joanne Wen, Pratap Challa, Paul Kaufman, Sheng Lim, TM Society members, and others

Institutions:
Tables:
Figures:
Boxes:
References:

List of Abbreviations:
IOP Intraocular pressure

Author Contact List:

Abstract

Introduction
Tonography is a technique to assess the facility of outflow through the eye in a noninvasive way. Outflow facility is an important component of aqueous humor dynamics as it is usually the reason for the intraocular pressure (IOP) elevation in glaucoma. Aqueous humor dynamics is defined by the modified Goldmann Equation and is composed of flows, pressures and facilities that, combined, determine the IOP. Facilities of outflow include those through the trabecular and uveoscleral pathways. Most of the outflow facility is in the trabecular pathway but facility in the uveoscleral pathway is not zero and does change at low pressures (Toris, Bill refs). Tonography measures total facility in humans and animals with eyes of similar size to humans including rabbits, cats, dogs, and monkeys. Formula adjustments are needed for each species. Data collection sounds simple but is challenging especially since movements from the eye or the operator can create numerous and significant artifacts. This paper describes standard procedures for tonography with a pneumatonometer (pneumatonography) and methods of tonography interpretation. This set of standard practices will increase the scientific rigor when using pneumatonography and will better enable researchers to replicate and build upon previous findings.

History
Some of the earliest observations of aqueous humor dynamics were made in the 19th century. Schwalbe used dyes and fine particles to trace the outflow of aqueous

humor to the episcleral venous system (Schwalbe 1870, Grant 1978). Not longer after, Leber identified a region of aqueous humor outflow resistance adjacent to Schlemm's canal and quantitatively perfused excised eyes to make a measurement of ex vivo aqueous humor outflow (Leber 1873, Grant 1978). Later findings from Kneis (1875), Seidel (1921), Ascher (1942) and other authors eventually established the primary route of aqueous humor outflow from the eye (Johnson 2017). Ascher and Goldmann observed aqueous humor outflow in the aqueous veins of patients (Ascher 1942, Goldmann 1950). The latter used measurements of the rate of change of fluorescein in the bloodstream and anterior chamber to estimate the facility through which aqueous humor exits the eye, known as aqueous humor outflow facility (Goldmann 1950). This fluorescein method of estimating aqueous humor outflow facility established an equation relating aqueous humor outflow facility, aqueous humor formation, episcleral venous pressure, and IOP (Goldmann 1950). This relationship was instrumental in understanding aqueous humor dynamics; however, the fluorescein method was not suitable for widespread clinical use in patients (Grant 1978).

In 1905, the Schiotz tonometer, a type of indentation tonometer, was invented (Albert 2020). It was known that the prolonged application of an external force on the eye resulted in a decrease in IOP (Weber 1867, Albert 2020). In 1913, Ballantyne reported that a fall in IOP (as shown by a decrease in scale reading) occurred upon application of the Schiotz tonometer to the eye and suggested that this phenomenon could be explained by a loss of fluid volume through normal outflow channels (Ballantyne 1913, Grant 1978). Thus, the idea of studying the capacity of the aqueous outflow channels using the Schiotz tonometer was introduced. Several authors used the Schiotz tonometer to make comparisons between eyes under different circumstances and make postulations about aqueous outflow (Seidel 1928, Kronfeld 1934, Kronfeld 1944, Grant 1978). However, these authors did not go so far as to attempt to use the Schiotz tonometer to make a quantitative measurement of aqueous humor outflow facility (Grant 1978). Tonometer data interpretation was likely hindered by a lack of understanding of the relationship between IOP and ocular volume (Mansheim 1953). Friedenwald clarified this relationship with a table relating the volume of corneal indentation and the IOP corresponding to different scale readings and loads of the Schiotz tonometer (Friedenwald 1937, Friedenwald 1948, Friedenwald 1957). He also developed the electronic Schiotz tonometer, allowing for simultaneous and continuous scale readings (Mansheim 1953).

In 1950, Grant described a new application of the electronic Schiotz tonometer to obtain an actual measure of aqueous humor outflow facility in living patients (Grant 1950). This technique of measuring the change in intraocular pressure when the external weight of the tonometer is continuously applied to the eye would be coined tonography (Grant 1950). Formulas derived from tonography would allow for calculation of aqueous humor outflow facility and a steady-state rate of aqueous flow

(Grant 1950). Unlike Goldmann's fluorescein method, tonography was non-invasive, simple to perform, and allowed for both clinical and investigative purposes in living patients (Grant 1951). In the 1970s, Langham would demonstrate that another tonometric device, the pneumatonometer, also could be used to perform tonography and evaluate outflow facility (Langham 1976). Langham developed tables for tonography with a pneumatonometer similar to Friedenwald's tables to relate pressure and volume for calculation of aqueous outflow facility (Langham 1976) in the human eye.

Tonography initially was purported to be a tool to diagnose glaucoma (McBain 1954). Early studies using tonography had demonstrated a clear distinction between outflow facility values in patients with glaucoma and subjects with normal IOPs (Grant 1951). However, subsequent studies showed that there was a broad area of overlap in outflow facility values between the two populations (Kronfeld 1952, Becker 1956). Several authors also investigated the use of tonography in predicting the risk for glaucoma development and assessing glaucoma prognosis. However, most of the results were not very predictive or equivocal (Roberts 1977, DeRoetth 1965, Armaly 1969, Fisher 1972, Wilensky 1974, Kass 1976).

Although tonography has limited clinical use as a diagnostic tool, it continues to play an important role in research studying the dynamics of aqueous humor flow. Group sizes of 15-20 animals can detect significant experimental changes using robust statistical analyses (Fourman 1989, Toris 2000, Zhao 2010). Tonography has been used in studies in humans and various research animals to elucidate the effects of therapeutic agents (Toris 1993, Lim 2008, Johnson 2010, Kazemi 2019, Kazemi 2018, Sit 2021), surgical procedures (Yablonski 1985, Keightley 1987, Kee 2000, Gulati 2017, Alaghband 2020, Tanito 2022, Lyons 2023), and other factors (Toris 1999, Liu 2011, Fan 2011, Fan 2014, Gulati 2012) on intraocular pressure and outflow facility. These findings have facilitated an improved understanding of the pathogenesis of glaucoma and related disorders.

Schiotz tonometer vs Pneumatonometer

Two instruments commonly used for tonography are the Schiotz tonometer and pneumatonometer. For most of the 20th century, the Schiotz tonometer was the most widely used tonometer worldwide until Goldmann applanation tonometry became the gold standard for IOP measurement (Albert 2020). The Schiotz tonometer consists of a foot plate with a 15 mm radius of curvature to match the average human corneal curvature (Albert 2020, Chan/Toris). The foot plate is connected to a plunger, whose weight can be altered using a series of known, standard weights (5.5, 7.5, 10, or 15 g) (Chan/Toris). The weighted plunger and foot plate is applied to the cornea while the patient is in the supine position, and a reading scale records the amount of indentation of the cornea, which is directly related to IOP (Chan/Toris). Friedenwald later made modifications to develop an

electronic Schiotz tonometer (Albert 2020), which uses an electronic amplifier and recording galvanometer instead of the reading scale to continuously record measurements on a paper strip, thus allowing for tonography measurements to be made (Chan/Toris). Outflow facility is calculated using Friedenwald's tables (Friedenwald 1937, Friedenwald 1948, Friedenwald 1957).

The pneumatonometer was first developed by Durham and later modified by Langham in the 1960s (Langham/McCarthy 1968). It consists of a cylindrical probe with a plastic sensor tip covered with a thin silicone membrane. Controlled air flows through a valve into the apparatus and through the silicone membrane to create an air bearing and near frictionless applanation surface. When the probe tip contacts the cornea, air flow is impeded through the membrane, causing air pressure within the apparatus to rise. Once the internal IOP and air pressure within the apparatus are in equilibrium, an electronic signal output is converted into a measurement of IOP (Chan/Toris). Outflow facility is calculated using Langham's tables with the tonography data (Langham 1976). The pneumatonometer allows for IOP measurement in both the seated and supine positions and has an optional program to calculate outflow facility (Chan/Toris). The calculation of outflow facility is discussed further in a later section.

Both the Schiotz tonometer and pneumatonometer have been thought to produce similar outflow facility values (Wheeler 1998, Feghali 1986, Lim 2008), despite the pneumatonometer having higher inter-subject and inter-observer measurement variability (Wheeler 1998, Feghali 1986). The higher variability with the pneumatonometer is largely explained by greater probe movement during tonography with the pneumatonometer compared to the Schiotz tonometer (Wheeler 1998, Feghali 1986). The flat diameter tip of the pneumatonometer is more mobile than the large concave diameter of the Schiotz tonometer probe (Wheeler 1998, Feghali 1986). A recent study (Kazemi 2017) comparing outflow facility values from the two instruments found that although the outflow facility values being well correlated between the two instruments, the Schiotz tonometer produced values 10-20% higher than the pneumatonometer (Kazemi 2017). Discrepancies in outflow facility between the two instruments may be explained by differences in tonometer probe characteristics, method of IOP measurement, and calibration tables (Kazemi 2017).

The focus of the following tonography procedures will be on the pneumatonometer which is the only instrument commercially available. The electronic Schiotz tonometer is not commercially available and used ones are difficult to find. Following are detailed step-by-step procedures on making the measurement in human subjects.

Performing tonography

List of equipment and supplies

1. Equipment: pneumatonometer (Model 30, Reichert, Depew, NY). with Tonography Kit, P/N 16033 Details of the pneumatonometer with tonography mode are found on the Reichert website. https://www.reichert.com/en/products/model-30
    1. ten-gram weight
    2. probe tip and membrane
    3. calibration test column
2. Supplies
    1. Artificial tears
    2. Proparacaine
    3. Soft facial tissue.

Sanitizing the probe

Prior to obtaining any measurements, the pneumatonometer probe should be carefully sanitized using a 70% isopropyl alcohol (Zhou 2020). Afterwards, care should be taken to remove the disinfectant from the patient contact surface of the probe tip as these agents can cause corneal epithelial damage (Zhou 2020). This can be done using a saline solution rinse. The probe tip should be allowed to air dry before use.

Setting up the fixation target

A fixation target is projected or placed on the ceiling directly above the head of the supine subject. A bright red laser pointer light works well for this purpose. The supine patient must fixate on this light with the uninvolved eye to keep the eye being tested as still as possible during the measurement. The patient is instructed to focus on the fixation target and is reminded throughout the measurement to maintain fixation. Any eye movement adds noise to the data.

Use of proparacaine and artificial tears

Proparacaine 0.5% eye drops are used to anesthetize the corneal surface during contact with the pneumatonometer probe tip. Prior to the measurement, 1-2 drops should be instilled in the eyes. The onset of action of proparacaine is about 10-20 seconds, with subsequent dosing allowed every 5-10 minutes as needed for a maximum total of 5-7 doses (Lexicomp). Artificial tears are used for lubrication to prevent irritation during the timed tonography measurement.

Holding the probe

The pneumatonometer uses a hand piece with a handle, shaft and tip. During a measurement air flow through the hand piece pushes the shaft out of the handpiece. The probe tip must be placed on the eye and the shaft pushed in so that the the red and black positional lines on the shaft remain visible. Proper handling of the probe requires four conditions for the entirety of the measurement:

1. The probe shaft should remain between the red and black positional lines.
2. The probe should be applied perpendicular to the cornea.
3. The probe tip should maintain contact with the center of the cornea.
4. The operator's hand is steady and maintains solid, firm contact with the patient's cheek to eliminate any potential movement. It is also helpful to grasp the pneumatonometer probe near the middle of the handle to prevent obscuration of the positional lines during the measurement.

Seated IOPs and Supine IOPs

Prior to pneumatonography, tonometry in the seated and supine positions must be obtained using the pneumatonometer. For seated IOP measurement, the patient is seated in an exam chair that can recline. A fixation target is placed in front of the patient's line of sight. A drop of proparacaine is instilled in each eye. The pneumatonometer probe tip is placed perpendicularly on the center of the patient's cornea so that the probe shaft remains between the red and black positional lines. Next, the patient is reclined into the supine position. Wait 5 minutes before making the supine measurement. The operator sits on the same side as the eye being measured. Once again, the probe tip is applied to the patient's eye. If it is necessary to hold the patient's lids open during the measurements, external pressure should not be placed on the globe with the finger holding the lid open to avoid a falsely elevated IOP.

Tonography test

There are options for a two- or four-minute test. Our experience is that the 2-minute test yields results similar to the 4-minute test and is better tolerated. After tonometry has been performed in the seated and supine positions, the patient will continue to lie in the supine position for the pneumatonography measurement. The tonography mode is chosen, a two or four minute test is selected and seated and supine IOP values are entered. A 10 g weight is attached to the shaft of the probe where it sits on the white collar of the shaft. The eyes are lubricated with artificial tears and proparacaine is added for topical anesthetic. The pneumatonometer probe is applied to the central corneal surface of the eye. The operator rests his/her hand on the forehead and/or cheek of the subject while the patient fixates on the ceiling target with the uninvolved eye. While minor adjustments (e.g. pushing the probe tip down a millimeter, etc.) can be made during the 2 minute measurement, major adjustments

(e.g. hand position, lid adjustments, moving the probe tip across the cornea, etc.) should not be attempted. The operator should not move his/her eyes from the probe and should check the alignment lines on the shaft at all times. After pneumatonography is complete, remove the probe tip from the patient's cornea and instill another lubricating eye drop into both eyes. The second eye is measured as the first.

Saving the data digitally

Older versions of the pneumatonometer recorded tonography data on a strip-chart printer. A new software upgrade now saves the data digitally. This allows export of the raw data for purposes of storage, and calculation. After opening the application and entering the subject's information, the operator selects "Acquire IOP" or "Acquire Tonography" to start the measurement. As the pneumatonometer probe is applied to the patient's eye, the software will immediately start collecting and plotting the data on the screen. Once the measurement is complete, the operator can click the "Save" button or click "Cancel" to repeat the measurement as necessary.

Repeating the Tonography Measurement

Sometimes, a tonography trace is poor and cannot be used, or a study design requires two tonography traces in a single day. If a repeat tonography needs to be done, the question arises as to how long to allow the eye to recover before the second measurement. A pilot study in rabbit eyes demonstrated that pneumatonography causes significant changes in the shape of the anterior chamber over time on ultrasound biomicroscopy under physiological conditions (Chan 2018). Studies in humans have shown that _____ in tonometry (cite), but none of these studies address the specific effects of tonography. Additionally, there appears to be no consensus on the minimum amount of time required to wait between repeated tonography measurements, with the literature values ranging from _____ (cite). Preliminary data from the Anterion (a Swept Source Anterior Optical Coherence Tomography device) on ocular biometrics and refraction after tonography found that the eye returned to baseline condition within 10 minutes in young emmetropic eyes. Myopic eyes and eyes of older subjects may take longer to recover. It should be safe to repeat tonography after a one-hour rest period. Subjects with dry eyes need numerous drops of artificial tears immediately after each measurement to prevent cornea abrasion and discomfort. Needs more work…

Grading of Tonography Traces

Subjective grading: Grade graphs on a scale of 1 to 10
Summarize Arthur Sit's manuscript
Method for objective grading of tonography traces.

Calculating Outflow Facility – *Alessandra and Zoltan*

Meaning of terms

Formulas
Grant and Langham references, Friedenwald tables, Langham tables
Use of Excel spreadsheets, R, MatLab
Cite Tian, 2006

Intra and inter-investigator variability in making the measurement

Summarize Vikas Gilati's rabbit study

Differences in measurement techniques between humans and animals

Tonography has been used in live animal models to explore basic physiologic, biochemical, and genetic issues related to aqueous humor dynamics and to establish proof of principle for potential glaucoma therapies prior to testing in humans (Toris 2008). Tonographic measurements have been reported in studies including cats (Wang/Toris 1999, Toris/Yablonski 2006), dogs (Gelatt 1977, Toris/Lane 2006), rabbits (Serle 1984, Fourman 1989, Goh 1989, Mittag 1993, Zhan 1998, Melena 1999 Zhao 2010), and monkeys (Serle 1984, Toris/Zhan 2000, Woodward 2009), who have eyes of similar size to humans. Tonography in animals is similar to that in humans in that it involves applying a weighted tonometer probe on the anesthetized cornea of a recumbent animal for 2 or 4 minutes (Toris 2008). Nevertheless, there are a few documented differences in the measurement techniques used in animals (Toris 2008). Certain animals, such as rabbits, can be fully conscious during tonography (Goh 1989, Zhao 2010), but most animals are sedated or anesthetized prior to testing (Serle 1984, Fourman 1989, Wang 1999, Toris 2000, Woodward 2009). Some authors have used specially designed chairs to aid with animal positioning during measurements (Toris 2000, Woodward 2009). It is also to note that the Schiotz tonometer and pneumatonometer reference standardized tables developed for human eyes, and thus many of the inherent assumptions of tonography may not be valid in research animals (Toris 2008).

Assumptions and Weaknesses

Tonography is based on the principle that at different intraocular pressures, aqueous humor is filtered out of the anterior chamber at a constant rate (Kaufman's papers, Chan/Toris). When the weight of the tonometer is applied on the eye, it results in a change in IOP and a certain amount of aqueous humor being displaced over a set amount of time (Weber 1867, Ballantyne 1913, Chan/Toris). Aqueous humor outflow facility is derived from the change in IOP, the change in ocular volume, and the time of the tonography measurement (Chan/Toris). This calculation is dependent on the reference tables relating volume and pressure created from experimental data (Friedenwald, Langham 1976, Grant), as well as several other assumptions regarding aqueous humor dynamics (Chan/Toris, Drews 1971):

1. Aqueous humor outflow is continuous.

2. Aqueous humor production is constant and does not change with variations in IOP. The change in ocular volume, which is equal to the production of aqueous humor minus the loss of aqueous humor, is therefore estimated to be due to aqueous humor outflow only.
3. Changes in IOP do not affect how easily aqueous humor flows out of the eye.
4. The uveal intravascular volume remains constant during tonography.
5. Tonography measures outflow facility through the trabecular meshwork, Schlemm's canal, and scleral venous network.
6. Prior to tonography, the eye maintains a steady state IOP without any ongoing fluctuations.
7. Ocular rigidity affects tonography, although it is assumed that it adds only a small correction factor to outflow facility values. Ocular rigidity includes scleral rigidity and corneal hysteresis. The outflow facility calculation uses an average standardized value of ocular rigidity, which Friedenwald, Grant, and Langham have incorporated into their tables (cite).

Real-life data has disputed some of these assumptions. First, the rate of aqueous humor production is affected by IOP. Aqueous humor production decreases with an increase in IOP, which has been termed pseudofacility (Toris 1999). Additionally, ocular rigidity has a significant impact on the tonography measurement (Moses 1958). Outflow facility calculations from tonography use an average standardized value of ocular rigidity, but ocular rigidity is inversely related to ocular volume and directly proportional to IOP (Chan/Toris, cite). For calculated outflow facility values based on this value, higher ocular rigidity is associated with a lower actual outflow facility and vice versa (Chan/Toris, Silver 2000). Ocular rigidity can also vary by anatomic eye region, subject age, and disease state (Chan/Toris).

As a result of these assumptions, tonography has several limitations and sources of error. Accurate measurements depend on proper tonometer calibration and tonography set up. Corneal properties, including surface irregularities (edema, scarring, etc.) and variations in corneal curvature, can affect tonometry and therefore tonography (cite). Additionally, tonography is highly affected by voluntary or involuntary behavior by the operator or subject. Tonometer probe tip movement can change the area being measured or the amount of applied pressure. Behaviors such as coughing, eye movement, eyelid squeezing, or the Valsalva maneuver can disturb the measurement.

Future Applications and Research

Despite tonography having limited clinical use in predicting glaucoma susceptibility or prognosis, it serves as an important tool in elucidating the dynamics of aqueous humor flow. __expand on this__. When tonography is combined with other methods to isolate outflow resistance in other _____, definitive mapping of aqueous humor flow dynamics may be possible.

Tonography also has a role in determining the mechanism of action and effects of new therapeutic agents and procedures in the treatment of glaucoma (Zhou). __discuss rise of MIGS/explosion of new glaucoma sxs?___.

Conclusion

XIII. Kaufman Lab – On the Horizon

1. Gene Therapy --
   - Technology: Special purpose catheters for viral vector delivery to Schlemm's canal in non-human primates
   - Background, Delivery techniques, Playing Chess with Mother Nature, Bigger is better, What does the board look like at present?

2. Schlemm's canal and beyond in real time --
   - How does the system deal with changing IOP?

2023 TM Literature Review

2023 Literature Review

1. Aboobakar IF, Collantes ERA, Hauser MA, Stamer WD, Wiggs JL. Rare protective variants and glaucoma-relevant cell stressors modulate Angiopoietin-like 7 expression. *Hum Mol Genet* 2023; **32**(15): 2523-31.
2. Adulla A, Patel U, Ashok A, et al. alpha-Synuclein modulates fibronectin expression in the trabecular meshwork independent of TGFbeta2. *Exp Eye Res* 2023; **226**: 109351.
3. Ai S, Zhang Y, Shi G, et al. Acoustic radiation force optical coherence elastography: A preliminary study on biomechanical properties of trabecular meshwork. *J Biophotonics* 2023; **16**(5): e202200317.
4. Amankwa CE, Young O, DebNath B, et al. Modulation of Mitochondrial Metabolic Parameters and Antioxidant Enzymes in Healthy and Glaucomatous Trabecular Meshwork Cells with Hybrid Small Molecule SA-2. *Int J Mol Sci* 2023; **24**(14).
5. Aoshima K, Inagaki S, Takagi Y, Nakamura S, Hara H, Shimazawa M. ALK5 inhibitor acts on trabecular meshwork cell and reduces intraocular pressure. *Exp Eye Res* 2023; **227**: 109382.
6. Arjmand P, Yu CW, Popovic MM, Jhaveri A, Mandelcorn ED. Prophylactic intraocular pressure lowering measures in anti-vascular endothelial growth factor therapy: A systematic review and meta-analysis. *Surv Ophthalmol* 2023; **68**(3): 425-45.
7. Armin A, Arfaee F, Ozmaie S, Asghari A. The evaluation of the effect of tafluprost on the intraocular pressure of healthy male guinea pigs under different light-and-darkness regimes. *Vet Med Sci* 2023; **9**(3): 1172-8.
8. Bahrani Fard MR, Chan J, Sanchez Rodriguez G, et al. Improved magnetic delivery of cells to the trabecular meshwork in mice. *Exp Eye Res* 2023; **234**: 109602.
9. Balasubramanian R, Kizhatil K, Li T, et al. Transcriptomic profiling of Schlemm's canal cells reveals a lymphatic-biased identity and three major cell states. *bioRxiv* 2023.
10. Batchelor W, Arcuri J, Bhattacharya SK, Ziebarth NM. Characterization of Trabecular Meshwork Mechanical Property Modulation After Application of Lipids. *Methods Mol Biol* 2023; **2625**: 347-51.
11. Bikuna-Izagirre M, Aldazabal J, Extramiana L, Moreno-Montanes J, Carnero E, Paredes J. Nanofibrous PCL-Based Human Trabecular Meshwork for Aqueous Humor Outflow Studies. *ACS Biomater Sci Eng* 2023.
12. Bolo K, Apolo Aroca G, Pardeshi AA, et al. Automated expert-level scleral spur detection and quantitative biometric analysis on the ANTERION anterior segment OCT system. *Br J Ophthalmol* 2023.
13. Buffault J, Brignole-Baudouin F, Labbe A, Baudouin C. An Overview of Current Glaucomatous Trabecular Meshwork Models. *Curr Eye Res* 2023: 1-11.
14. Cairoli A, Spenlehauer A, Overby DR, Lee CF. Model of inverse bleb growth explains giant vacuole dynamics during cell mechanoadaptation. *PNAS Nexus* 2023; **2**(2): pgac304.

15. Callaghan B, Vallabh NA, Willoughby CE. Deuterated polyunsaturated fatty acids provided protection against oxidative stress in ocular fibroblasts derived from glaucoma patients. *Mech Ageing Dev* 2023; **211**: 111778.
16. Campigotto A, Campbell RJ, Lai Y. Correlation between corneal and contact lens deformation with changes in intraocular pressure for wearable monitoring systems. *Eye (Lond)* 2023; **37**(10): 2055-60.
17. Carmichael-Martins A, Gast TJ, King BJ, Walker BR, Sobczak M, Burns SA. Imaging fine structures of the human trabecular meshwork in vivo using a custom design goniolens and OCT gonioscopy. *Biomed Opt Express* 2023; **14**(10): 5267-81.
18. Chakraborthy M, Rao A. A Feedback Loop between TGF-beta1 and ATG5 Mediated by miR-122-5p Regulates Fibrosis and EMT in Human Trabecular Meshwork Cells. *Curr Issues Mol Biol* 2023; **45**(3): 2381-92.
19. Chang YF, Cheng YH, Ko YC, Chiou SH, Liu CJ. Anti-apoptotic and autophagic effect: Using conditioned medium from human bone marrow mesenchymal stem cells to treat human trabecular meshwork cells. *Regen Ther* 2023; **22**: 50-8.
20. Cho WJ, Kim Y, Kim JD, et al. Association of trabecular meshwork height with steroid-induced ocular hypertension. *Sci Rep* 2023; **13**(1): 9143.
21. Chowdhury U, Pervan-Steel CL, Sheeler R, et al. Preclinical Pharmacokinetic Profile of Topical Ophthalmic and Intravenous Delivery of QLS-101, a Novel ATP-Sensitive Potassium Channel Opening Ocular Hypotensive Agent. *J Ocul Pharmacol Ther* 2023; **39**(5): 332-46.
22. Coan LJ, Williams BM, Krishna Adithya V, et al. Automatic detection of glaucoma via fundus imaging and artificial intelligence: A review. *Surv Ophthalmol* 2023; **68**(1): 17-41.
23. Crouch DJ, Sheridan CM, Behnsen JG, D'Sa RA, Bosworth LA. Cryo-Electrospinning Generates Highly Porous Fiber Scaffolds Which Improves Trabecular Meshwork Cell Infiltration. *J Funct Biomater* 2023; **14**(10).
24. Dada T, Bukke AN, Huang AS, Sharma N, Verma S. Recruitment of Temporal Aqueous Outflow Channels After Bent Needle Ab-Interno Goniectomy Demonstrated by Aqueous Angiography. *J Glaucoma* 2023; **32**(2): e15-e8.
25. Daniel E, Gao J, Maguire MG, et al. Prevalence and factors associated with optic disc grey crescent in the Primary Open-Angle African Ancestry Glaucoma Genetics (POAAGG) Study. *BMJ Open Ophthalmol* 2023; **8**(1).
26. De Ieso ML, Kelly R, Mzyk P, Stamer WD. Development and testing of a metabolic chamber for effluent collection during whole eye perfusions. *Exp Eye Res* 2023; **236**: 109652.
27. Deleu L, Bremer F. Two cases of acute intraocular pressure elevation with dabigatran use in glaucoma patients. *J Fr Ophtalmol* 2023; **46**(4): e114-e6.
28. Dillinger AE, Kuespert S, Seleem AA, Neuendorf J, Schneider M, Fuchshofer R. CCN2/CTGF tip the balance of growth factors towards TGF-beta2 in primary open-angle glaucoma. *Front Mol Biosci* 2023; **10**: 1045411.

29. Ding X, Huang L, Peng C, et al. Correction: Evaluation of Schlemm's canal with swept-source optical coherence tomography in primary angle-closure disease. *BMC Ophthalmol* 2023; **23**(1): 308.
30. Ding X, Huang L, Peng C, et al. Evaluation of Schlemm's canal with swept-source optical coherence tomography in primary angle-closure disease. *BMC Ophthalmol* 2023; **23**(1): 256.
31. Dixon A, Shim MS, Nettesheim A, et al. Autophagy deficiency protects against ocular hypertension and neurodegeneration in experimental and spontanous glaucoma mouse models. *Cell Death Dis* 2023; **14**(8): 554.
32. Dolatyar B, Zeynali B, Shabani I, Parvaneh Tafreshi A. High-efficient serum-free differentiation of trabecular meshwork mesenchymal stem cells into Schwann-like cells on polylactide electrospun nanofibrous scaffolds. *Neurosci Lett* 2023; **813**: 137417.
33. Fea AM, Ricardi F, Novarese C, Cimorosi F, Vallino V, Boscia G. Precision Medicine in Glaucoma: Artificial Intelligence, Biomarkers, Genetics and Redox State. *Int J Mol Sci* 2023; **24**(3).
34. Filla MS, Faralli JA, Dunn CR, Khan H, Peters DM. NFATc1 Regulation of Dexamethasone-Induced TGFB2 Expression Is Cell Cycle Dependent in Trabecular Meshwork Cells. *Cells* 2023; **12**(3).
35. Fowler S, Wang T, Munro D, et al. Genome-wide association study finds multiple loci associated with intraocular pressure in HS rats. *Front Genet* 2022; **13**: 1029058.
36. Fox AR, Fingert JH. Familial normal tension glaucoma genetics. *Prog Retin Eye Res* 2023; **96**: 101191.
37. Fujimoto T, Inoue-Mochita M, Inoue T. A ROCK inhibitor suppresses the transforming growth factor-beta-2-induced endothelial-mesenchymal transition in Schlemm's canal endothelial cells. *Sci Rep* 2023; **13**(1): 9655.
38. Gaboriau T, Dubois R, Foucque B, Malet F, Schweitzer C. 24-Hour Monitoring of Intraocular Pressure Fluctuations Using a Contact Lens Sensor: Diagnostic Performance for Glaucoma Progression. *Invest Ophthalmol Vis Sci* 2023; **64**(3): 3.
39. Gao XR, Chiariglione M, Choquet H, Arch AJ. 10 Years of GWAS in intraocular pressure. *Front Genet* 2023; **14**: 1130106.
40. Gassel CJ, Dzhelebov DN, Voykov B. Detailed intraocular pressure curve by telemetric tonometry with an implanted pressure sensor before and after PreserFlo((R)) MicroShunt implantation: a case report. *Ther Adv Ophthalmol* 2023; **15**: 25158414221149927.
41. Gharahkhani P, He W, Diaz Torres S, et al. Study profile: the Genetics of Glaucoma Study. *BMJ Open* 2023; **13**(8): e068811.
42. Giglio R, Inferrera L, De Giacinto C, et al. Changes in Anterior Segment Morphology and Intraocular Pressure after Cataract Surgery in Non-glaucomatous Eyes. *Klin Monbl Augenheilkd* 2023; **240**(4): 449-55.
43. Grant A, Roy-Gagnon MH, Bastasic J, et al. Alcohol Consumption, Genetic Risk, and Intraocular Pressure and Glaucoma: The Canadian Longitudinal Study on Aging. *Invest Ophthalmol Vis Sci* 2023; **64**(10): 3.

44. Hassan MDS, Razali N, Abu Bakar AS, Abu Hanipah NF, Agarwal R. Connective tissue growth factor: Role in trabecular meshwork remodeling and intraocular pressure lowering. *Exp Biol Med (Maywood)* 2023: 15353702231199466.
45. Hodrea J, Tran MN, Besztercei B, et al. Sigma-1 Receptor Agonist Fluvoxamine Ameliorates Fibrotic Response of Trabecular Meshwork Cells. *Int J Mol Sci* 2023; **24**(14).
46. Hsu FL, Shih PJ, Wang IJ. Development and validation of an intuitive biomechanics-based method for intraocular pressure measurement: a modal analysis approach. *BMC Ophthalmol* 2023; **23**(1): 124.
47. Ing E, Lozano DC, Cepurna WO, et al. A method describing the microdissection of trabecular meshwork tissue from Brown Norway rat eyes. *Exp Eye Res* 2023; **228**: 109367.
48. Jalilian I, Muppala S, Ali M, et al. Cell derived matrices from bovine corneal endothelial cells as a model to study cellular dysfunction. *Exp Eye Res* 2023; **226**: 109303.
49. Jia X, Wu J, Chen X, et al. Cell atlas of trabecular meshwork in glaucomatous non-human primates and DEGs related to tissue contract based on single-cell transcriptomics. *iScience* 2023; **26**(11): 108024.
50. Johnstone M, Xin C, Martin E, Wang R. Trabecular Meshwork Movement Controls Distal Valves and Chambers: New Glaucoma Medical and Surgical Targets. *J Clin Med* 2023; **12**(20).
51. Kaplan TM, Hammer JD, Kohli D, et al. Efficacy of Selective Laser Trabeculoplasty in Patients on Systemic Immunosuppressive Therapy. *J Glaucoma* 2023; **32**(9): 762-8.
52. Kapuganti RS, Alone DP. Current understanding of genetics and epigenetics in pseudoexfoliation syndrome and glaucoma. *Mol Aspects Med* 2023; **94**: 101214.
53. Karimi A, Crouch DJ, Razaghi R, et al. Morphological and biomechanical analyses of the human healthy and glaucomatous aqueous outflow pathway: Imaging-to-modeling. *Comput Methods Programs Biomed* 2023; **236**: 107485.
54. Karimi A, Khan S, Razaghi R, et al. Segmental Biomechanics of the Normal and Glaucomatous Human Aqueous Outflow Pathway. *Acta Biomater* 2023.
55. Karimi A, Khan S, Razaghi R, et al. Developing an experimental-computational workflow to study the biomechanics of the human conventional aqueous outflow pathway. *Acta Biomater* 2023; **164**: 346-62.
56. Karimi A, Razaghi R, D"costa SD, et al. Implementing New Computational Methods for the STudy of JCT and SC Inner Wall Basement Membrane Biomechanics and Hydrodynamics. *Computer Methods and Programs in Biomedicine* 2023.
57. Karimi A, Razaghi R, Kelley MJ, Acott TS, Gong H. Biomechanics of the JCT and SC Inner Wall Endothelial Cells with Their Basement Membrane Using 3D Serial Block-Face Scanning Electron Microscopy. *Bioengineering (Basel)* 2023; **10**(9).
58. Kelly RA, McDonnell FS, De Ieso ML, Overby DR, Stamer WD. Pressure Clamping During Ocular Perfusions Drives Nitric Oxide-Mediated Washout. *Invest Ophthalmol Vis Sci* 2023; **64**(7): 36.

59. Keyvanfard G, Cheraghi H, Aryaei Tabar H. Effect of vincristine on intraocular pressure and tear fluid oxidative stress biomarkers in canine transmissible venereal tumor. *Vet Ophthalmol* 2023.
60. Kiland JA, Terhaar HM, Walleck HE, Chen N, McDaniel K, McLellan GJ. Comparison of the TONOVET Plus(R), TonoVet(R), and Tono-Pen Vet tonometers in normal cats and cats with glaucoma. *Vet Ophthalmol* 2023; **26**(5): 414-21.
61. Kim SH, Ku YA, Yoo C, Kim YH, Kim DH. Comparison of RCI001 and corticosteroid on the effects on intraocular pressure in mice. *Front Med (Lausanne)* 2023; **10**: 1256569.
62. Kizhatil K, Clark G, Sunderland D, et al. FYN regulates aqueous humor outflow and IOP through the phosphorylation of VE-cadherin. *bioRxiv* 2023.
63. Kobashi H, Kobayashi M. 3D-printed eye model: Simulation of intraocular pressure. *PLoS One* 2023; **18**(3): e0282911.
64. Kumon M, Fuwa M, Shimazaki A, et al. Downregulation of COL12A1 and COL13A1 by a selective EP2 receptor agonist, omidenepag, in human trabecular meshwork cells. *PLoS One* 2023; **18**(1): e0280331.
65. Lee JH, Kwon YJ, Lee HS, Han JH, Joung B, Kim SJ. Inverse Relationship between Serum 25-Hydroxyvitamin D and Elevated Intraocular Pressure. *Nutrients* 2023; **15**(2).
66. Li H, Cui H, Ren J, et al. Elevated Angiotensin-II Levels Contribute to the Pathogenesis of Open-Angle Glaucoma Via Inducing the Expression of Fibrosis-Related Genes in Trabecular Meshwork Cells Through a ROS/NOX4/SMAD3 Axis. *Cell Transplant* 2023; **32**: 9636897231162526.
67. Li H, Kuhn M, Kelly RA, et al. Targeting YAP mechanosignaling to ameliorate stiffness-induced Schlemm's canal cell pathobiology. *bioRxiv* 2023.
68. Li H, Ren J, Cui H, et al. Dexamethasone Induces Senescence-Associated Changes in Trabecular Meshwork Cells by Increasing ROS Levels Via the TGFbeta/Smad3-NOX4 Axis. *Cell Transplant* 2023; **32**: 9636897231177356.
69. Li L, Liu Q, Shi L, et al. Baicalin prevents fibrosis of human trabecular meshwork cells via inhibiting the MyD88/NF-kappaB pathway. *Eur J Pharmacol* 2023; **938**: 175425.
70. Lin Y, Jiang B, Cai Y, et al. The causal relationship between COVID-19 and increased intraocular pressure: A bidirectional two-sample Mendelian randomization study. *Front Public Health* 2023; **11**: 1039290.
71. Liton PB, Boesze-Battaglia K, Boulton ME, et al. Autophagy in the Eye: From Physiology to Pathophysiology. *Autophagy Rep* 2023; **2**(1).
72. Liu L, Yang X, Zhang J, et al. Long non-coding RNA SNHG11 regulates the Wnt/beta-catenin signaling pathway through rho/ROCK in trabecular meshwork cells. *FASEB J* 2023; **37**(4): e22873.
73. Liu M, Honjo M, Yamagishi R, Aihara M. Effects of Brimonidine, Omidenepag Isopropyl, and Ripasudil Ophthalmic Solutions to Protect against H(2)O(2)-Induced Oxidative Stress in Human Trabecular Meshwork Cells. *Curr Eye Res* 2023; **48**(11): 1014-25.

74. Machiele R, Motlagh M, Patel BC. Intraocular Pressure. StatPearls. Treasure Island (FL) ineligible companies. Disclosure: Mahsaw Motlagh declares no relevant financial relationships with ineligible companies. Disclosure: Bhupendra Patel declares no relevant financial relationships with ineligible companies.; 2023.
75. Madadi Y, Monavarfeshani A, Chen H, Stamer WD, Williams RW, Yousefi S. Artificial Intelligence Models for Cell Type and Subtype Identification Based on Single-Cell RNA Sequencing Data in Vision Science. *IEEE/ACM Trans Comput Biol Bioinform* 2023; **20**(5): 2837-52.
76. Maddala R, Eldawy C, Bachman W, Soderblom EJ, Rao PV. Glypican-4 regulated actin cytoskeletal reorganization in glucocorticoid treated trabecular meshwork cells and involvement of Wnt/PCP signaling. *J Cell Physiol* 2023; **238**(3): 631-46.
77. Mamidipaka A, Di Rosa I, Lee R, et al. Factors Associated with Large Cup-to-Disc Ratio and Blindness in the Primary Open-Angle African American Glaucoma Genetics (POAAGG) Study. *Genes (Basel)* 2023; **14**(9).
78. Mazo SEM, Pena FY, Ramirez JVO. Intraocular pressure changes under an atmospheric pressure spectrum in a multiplace hyperbaric chamber. *Arq Bras Oftalmol* 2023.
79. Minnelli C, Piva F, Cecati M, et al. Meldonium Inhibits Cell Motility and Wound-Healing in Trabecular Meshwork Cells and Scleral Fibroblasts: Possible Applications in Glaucoma. *Pharmaceuticals (Basel)* 2023; **16**(4).
80. Mohamed Y, Passaglia CL. A portable feedback-controlled pump for monitoring eye outflow facility in conscious rats. *PLoS One* 2023; **18**(1): e0280332.
81. Mohammadi P, Nadri S, Abdanipour A, Mortazavi Y. Microchip encapsulation and microRNA-7 overexpression of trabecular meshwork mesenchymal stem/stromal cells improve motor function after spinal cord injury. *J Biomed Mater Res A* 2023; **111**(9): 1482-94.
82. Mudalegundi S, Ross RD, Larbelee J, et al. Long-Term Decrease in Intraocular Pressure in Survivors of Ebola Virus Disease in the Partnership for Research on Vaccines and Infectious Diseases in Liberia (PREVAIL) III Study. *Ophthalmol Sci* 2023; **3**(2): 100238.
83. Murgoitio-Esandi J, Xu BY, Song BJ, Zhou Q, Oberai AA. A Mechanistic Model of Aqueous Humor Flow to Study Effects of Angle Closure on Intraocular Pressure. *Transl Vis Sci Technol* 2023; **12**(1): 16.
84. Nemoto H, Honjo M, Arai S, Miyazaki T, Aihara M. Apoptosis inhibitor of macrophages/CD5L enhances phagocytosis in the trabecular meshwork cells and regulates ocular hypertension. *J Cell Physiol* 2023; **238**(10): 2451-67.
85. Niemczyk M, Iskander DR. Measuring intraocular pressure with OCT: the first approach. *Biomed Opt Express* 2023; **14**(9): 4531-41.
86. Oikawa K, Torne O, Sun D, et al. Aqueous Humor TGF-beta2 and Its Association With Intraocular Pressure in a Naturally Occurring Large Animal Model of Glaucoma. *Invest Ophthalmol Vis Sci* 2023; **64**(10): 18.
87. Okuda-Arai M, Mori S, Takano F, et al. Impact of glaucoma medications on subsequent Schlemm's canal surgery outcome: Cox proportional hazard model and propensity score-matched analysis. *Acta Ophthalmol* 2023.

88. Pandino I, Giammaria S, Zingale GA, et al. Ubiquitin proteasome system and glaucoma: A survey of genetics and molecular biology studies supporting a link with pathogenic and therapeutic relevance. *Mol Aspects Med* 2023; **94**: 101226.
89. Pillunat KR, Kocket GA, Herber R, Jasper CS, Lenk J, Pillunat LE. Efficacy of selective laser trabeculoplasty on lowering intraocular pressure fluctuations and nocturnal peak intraocular pressure in treated primary open-angle glaucoma patients. *Graefes Arch Clin Exp Ophthalmol* 2023; **261**(7): 1979-85.
90. Pimentel RL, Alves Junior RR, Lima W, Dantas LOR, Costa VP. Selective laser trabeculoplasty versus micropulse laser trabeculoplasty for intraocular pressure control in patients with primary open angle glaucoma: a 12-month retrospective comparative study. *Lasers Med Sci* 2023; **38**(1): 102.
91. Qin M, Yu-Wai-Man C. Glaucoma: Novel antifibrotic therapeutics for the trabecular meshwork. *Eur J Pharmacol* 2023; **954**: 175882.
92. Raghunathan V, Nartey A, Dhamodaran K, et al. Characterization of extracellular matrix deposited by segmental trabecular meshwork cells. *Exp Eye Res* 2023; **234**: 109605.
93. Raveendran R, Prabakaran L, Senthil R, et al. Current Innovations in Intraocular Pressure Monitoring Biosensors for Diagnosis and Treatment of Glaucoma-Novel Strategies and Future Perspectives. *Biosensors (Basel)* 2023; **13**(6).
94. Ren R, Humphrey AA, Kopczynski C, Gong H. Rho Kinase Inhibitor AR-12286 Reverses Steroid-Induced Changes in Intraocular Pressure, Effective Filtration Areas, and Morphology in Mouse Eyes. *Invest Ophthalmol Vis Sci* 2023; **64**(2): 7.
95. Ren X, Zhou Y, Lu F, et al. Contact Lens Sensor with Anti-jamming Capability and High Sensitivity for Intraocular Pressure Monitoring. *ACS Sens* 2023; **8**(7): 2691-701.
96. Robin AZ, Syar P, Darwish D, et al. Comparison of success rate and intraocular pressure spikes between selective laser trabeculoplasty and micropulse laser trabeculoplasty in African American and Hispanic patients. *Int J Ophthalmol* 2023; **16**(1): 75-80.
97. Saccuzzo EG, Youngblood HA, Lieberman RL. Myocilin misfolding and glaucoma: A 20-year update. *Prog Retin Eye Res* 2023; **95**: 101188.
98. Safa BN, Guzman NSF, Li G, Stamer WD, Feola AJ, Ethier CR. A Histomorphometric and Computational Investigation of the Stabilizing Role of Pectinate Ligaments in the Aqueous Outflow Pathway. *bioRxiv* 2023.
99. Scelsi HF, Hill KR, Barlow BM, Martin MD, Lieberman RL. Quantitative differentiation of benign and misfolded glaucoma-causing myocilin variants on the basis of protein thermal stability. *Dis Model Mech* 2023; **16**(1).
100. Schmitt HM, Hake KM, Perkumas KM, et al. Lysyl oxidase-like 1-antisense 1 (LOXL1-AS1) lncRNA differentially regulates gene and protein expression, signaling and morphology of human ocular cells. *Hum Mol Genet* 2023; **32**(21): 3053-62.
101. Sharif NA. Elevated Intraocular Pressure and Glaucomatous Optic Neuropathy: Genes to Disease Mechanisms, Therapeutic Drugs, and Gene Therapies. *Pharmaceuticals (Basel)* 2023; **16**(6).

102. Sharif NA, Odani-Kawabata N, Lu F, Pinchuk L. FP and EP2 prostanoid receptor agonist drugs and aqueous humor outflow devices for treating ocular hypertension and glaucoma. *Exp Eye Res* 2023; **229**: 109415.

103. Sharma R, Sharma A. Population stratification strategies in artificial intelligence-based glaucoma monitoring, "corneal anthropology" to bridge gap between genetics and clinics? *Indian J Ophthalmol* 2023; **71**(5): 2304-6.

104. Sheng Q, Sun Y, Zhai R, et al. Murine cytomegalovirus localization and uveitic cell infiltration might both contribute to trabecular meshwork impairment in Posner-Schlossman syndrome: Evidence from an open-angle rat model. *Exp Eye Res* 2023; **231**: 109477.

105. Shi Y, Zhang Y, Sun W, et al. 24-Hour efficacy of single primary selective laser trabeculoplasty versus latanoprost eye drops for Naive primary open-angle glaucoma and ocular hypertension patients. *Sci Rep* 2023; **13**(1): 12179.

106. Shim MS, Dixon A, Nettesheim A, et al. Shear stress induces autophagy in Schlemm's canal cells via primary cilia-mediated SMAD2/3 signaling pathway. *Autophagy Rep* 2023; **2**(1).

107. Spini A, Giometto S, Donnini S, et al. Risk of Intraocular Pressure Increase With Intravitreal Injections of Vascular Endothelial Growth Factor Inhibitors: A Cohort Study. *Am J Ophthalmol* 2023; **248**: 45-50.

108. Stamer WD, Perkumas KM, Kang MH, Dibas M, Robinson MR, Rhee DJ. Proposed Mechanism of Long-Term Intraocular Pressure Lowering With the Bimatoprost Implant. *Invest Ophthalmol Vis Sci* 2023; **64**(3): 15.

109. Strohmaier CA, McDonnell FS, Zhang X, et al. Differences in Outflow Facility Between Angiographically Identified High- Versus Low-Flow Regions of the Conventional Outflow Pathways in Porcine Eyes. *Invest Ophthalmol Vis Sci* 2023; **64**(3): 29.

110. Strohmaier CA, Wanderer D, Zhang X, et al. Greater Outflow Facility Increase After Targeted Trabecular Bypass in Angiographically Determined Low-flow Regions. *Ophthalmol Glaucoma* 2023.

111. Strohmaier CA, Wanderer D, Zhang X, et al. Lack of Correlation Between Segmental Trabecular Meshwork Pigmentation and Angiographically Determined Outflow in Ex-Vivo Human Eyes. *J Glaucoma* 2023.

112. Stubbs EB, Jr. Isoprenylation of Monomeric GTPases in Human Trabecular Meshwork Cells. *Methods Mol Biol* 2023; **2625**: 217-30.

113. Sturdivant J, Williams SS, Ina M, et al. Discovery and Preclinical Development of Novel Intraocular Pressure-Lowering Rho Kinase Inhibitor: Corticosteroid Conjugates. *J Ocul Pharmacol Ther* 2023; **39**(2): 117-27.

114. Suarez MF, Schmitt HM, Kuhn MS, et al. Genetic background determines severity of Loxl1-mediated systemic and ocular elastosis in mice. *Dis Model Mech* 2023.

115. Sung MS, Kim SY, Eom GH, Park SW. High VEGF Concentrations Accelerate Human Trabecular Meshwork Fibrosis in a TAZ-Dependent Manner. *Int J Mol Sci* 2023; **24**(11).

116. Szurman P, Gillmann K, Seuthe AM, et al. EYEMATE-SC Trial: Twelve-Month Safety, Performance, and Accuracy of a Suprachoroidal Sensor for Telemetric Measurement of Intraocular Pressure. *Ophthalmology* 2023; **130**(3): 304-12.

117. Tan JK, Xiao Y, Liu G, et al. Evaluation of trabecular meshwork-specific promoters in vitro and in vivo using scAAV2 vectors expressing C3 transferase. *Int J Ophthalmol* 2023; **16**(8): 1196-209.

118. Tran MN, Medveczki T, Besztercei B, et al. Sigma-1 Receptor Activation Is Protective against TGFbeta2-Induced Extracellular Matrix Changes in Human Trabecular Meshwork Cells. *Life (Basel)* 2023; **13**(7).

119. Ujiie N, Norden PR, Fang R, et al. Differential roles of FOXC2 in the trabecular meshwork and Schlemm's canal in glaucomatous pathology. *Life Sci Alliance* 2023; **6**(9).

120. Uner B, Ozdemir S, Nur Pilevne S, Cenk Celebi AR. Timolol-loaded ethosomes for ophthalmic delivery: Reduction of high intraocular pressure in vivo. *Int J Pharm* 2023; **640**: 123021.

121. Wagner IV, Ang B, Checo L, Simsek D, Draper C, Dorairaj S. Spotlight on Schlemm's Canal MicroStent Injection in Patients with Glaucoma. *Clin Ophthalmol* 2023; **17**: 1557-64.

122. Wang J, Li J, Shi Y, et al. Effects of antivascular endothelial growth factor drug treatment on changes in vitreomacular interface, intraocular pressure and visual acuity of patients with age-related macular degeneration. *Minerva Med* 2023; **114**(4): 529-30.

123. Wang J, Rong Y, Liu Y, et al. The effect of ET1-CTGF mediated pathway on the accumulation of extracellular matrix in the trabecular meshwork and its contribution to the increase in IOP. *Int Ophthalmol* 2023; **43**(9): 3297-307.

124. Wang R, Wang Y, Qin Y, Wei H. Antioxidative effects of ghrelin on human trabecular meshwork cells. *J Fr Ophtalmol* 2023.

125. Wang T, Pattabiraman PP. Analysis of Lipid Contents in Human Trabecular Meshwork Cells by Multiple Reaction Monitoring (MRM) Profiling Lipidomics. *Methods Mol Biol* 2023; **2625**: 291-8.

126. Wang T, Soundararajan A, Rabinowitz J, Jaiswal A, Osborne T, Pattabiraman PP. Identification of the novel role of sterol regulatory element binding proteins (SREBPs) in mechanotransduction and intraocular pressure regulation. *FASEB J* 2023; **37**(11): e23248.

127. Wang W, Wang H. Understanding the complex genetics and molecular mechanisms underlying glaucoma. *Mol Aspects Med* 2023; **94**: 101220.

128. Wang X, Tan S, Yang S, Liu X, Lei J, Li H. Activation of Sonic Hedgehog Signaling Pathway Regulates Human Trabecular Meshwork Cell Function. *J Ocul Pharmacol Ther* 2023; **39**(7): 430-8.

129. Watanabe M, Sato T, Tsugeno Y, Higashide M, Furuhashi M, Ohguro H. TGF-beta-3 Induces Different Effects from TGF-beta-1 and -2 on Cellular Metabolism and the Spatial Properties of the Human Trabecular Meshwork Cells. *Int J Mol Sci* 2023; **24**(4).

130. Wiggins SV, Schreiner R, Ferreira J, Marmorstein AD, Levin LR, Buck J. Carbonic Anhydrase Inhibitor Modulation of Intraocular Pressure Is Independent of Soluble Adenylyl Cyclase. *J Ocul Pharmacol Ther* 2023; **39**(5): 317-23.

131. Xu L, Zhang X, Zhao Y, et al. Metformin protects trabecular meshwork against oxidative injury via activating integrin/ROCK signals. *Elife* 2023; **12**.

132. Yadav M, Bhardwaj A, Yadav A, Dada R, Tanwar M. Molecular genetics of primary open-angle glaucoma. *Indian J Ophthalmol* 2023; **71**(5): 1739-56.

133. Yang Y, Shi M, Li G, Shen L, Chen L. Novel discovery of a lymphatic bridge connecting Schlemm's canal to limbal and conjunctival lymphatic pathway. *Ocul Surf* 2023; **29**: 272-8.

134. Yang Z, Zhang Z, Zhu Y, Yuan G, Yang J, Yu W. Mendelian Randomization and Transcriptome-Wide Association Analysis Identified Genes That Were Pleiotropically Associated with Intraocular Pressure. *Genes (Basel)* 2023; **14**(5).

135. Yoo H, Singh A, Li H, et al. Simvastatin Attenuates Glucocorticoid-Induced Human Trabecular Meshwork Cell Dysfunction via YAP/TAZ Inactivation. *Curr Eye Res* 2023; **48**(8): 736-49.

136. Yu PK, Tay E, An D, Cringle SJ, Morgan WH, Yu DY. Topographic distribution and phenotypic heterogeneity of Schlemm's canal endothelium in human donor eyes. *Exp Eye Res* 2023; **226**: 109309.

137. Zhang C, Tannous E, Thomas A, Jung N, Ma E, Zheng JJ. Dexamethasone Modulates the Dynamics of Wnt Signaling in Human Trabecular Meshwork Cells. *Vision (Basel)* 2023; **7**(2).

138. Zhao S, Fang L, Yan C, et al. MicroRNA-210-3p mediates trabecular meshwork extracellular matrix accumulation and ocular hypertension - Implication for novel glaucoma therapy. *Exp Eye Res* 2023; **227**: 109350.

139. Zhu W, Zhang X, Wu S, Wang N, Kuehn MH. iPSCs-Based Therapy for Trabecular Meshwork. *Handb Exp Pharmacol* 2023.

2023 Participants

2023 Participants

Ted Acott, PhD Professor of Ophthalmology and Biochemistry & Molecular Biology Oregon Health & Science University Portland, OR 97239	acott@ohsu.edu
Simon Bakker, MSc Managing Director Kugler Publications/SPB Academic Publishing Nieuwe Hemweg 7, Hal P Bedrijvenpark Hempoint Westpoortnummer 2551 1013 BG Amsterdam, The Netherlands *Mailing address* P.O. Box 20538 1001 NM Amsterdam, The Netherlands	simonbakker@kuglerpublications.com Tel: +31 20 68 45 700, office Tel: +31 61 48 11 488, mobile Tel: +31 20 68 47 788, fax www.kuglerpublications.com
Revathi Balasubramanian, PhD Asst. Professor, Dept. of Ophthalmology Columbia University Irving Medical Center 701 W 168th Street Floor 2, 201E New York NY 10032	rb3132@cumc.columbia.edu Tel: 212-342-3516, office Tel: 585-775-7342, mobile
Sanjoy K. Bhattacharya, M. Tech., Ph. D., FARVO Professor of Ophthalmology Graduate Program Director (MVSIO and Translational Focus of medical school PhD Programs) Founding Director, Miami Integrative Metabolomics Research Center Speaker, Medical School Faculty Council Bascom Palmer Eye Institute (McKnight Bldg.) 1638 NW 10th Avenue, Suite 707A University of Miami Miami, FL, 33136	sbhattacharya@med.miami.edu Tel: 305-482-4103, Office Tel: 305-482-4109, Lab Tel: 305-482-4987, Mass spec lab Fax: 305-326-6547

Robert V Brown, Ph.D. Principal Scientist II, Pharma Strategic Ideation Alcon Vision 4301 Emperor Blvd, Suite 400 Durham, NC 27703	robert-2.brown@alcon.com www.alcon.com
Terete Borras, PhD Emeritus Professor University of North Carolina at Chapel Hill	tborras@med.unc.edu
Diane Bovenkamp, PhD Vice President Scientific Affairs BrightFocus Foundation 22512 Gateway Center Drive Clarksburg, MD 20871	dbovenkamp@brighfocus.org Tel: 800-437-2423, office Tel: 240-712-3067, mobile www.brightfocus.org www.brightfocus.org/research
John Danias, MD, PhD Chair of Ophthal/SUNY Downstate Medical Center Director of Research Professor of Ophthalmology and Cell Biology	john.danias@downstate.edu
Mohammed Dibas, PhD Executive Director, Glaucoma Research Ophthalmology Discovery 2525 Dupont Drive Irvine, CA 92612	mohammed.dibas@abbvie.com Tel: 714-246-4583, office Tel: 951-382-2729, mobile www.abbvie.com
Yiqin Du, MD, PhD Professor, Department of Ophthalmology Morsani College of Medicine, University of South Florida 12901 Bruce B. Downs Blvd., MDC 2041 Tampa, FL 33612	yiqindu@usf.edu Tel: 412-482-0615, mobile
Michael H. Elliott, PhD, FARVO Presbyterian Health Fdn. Presidential Professor Professor of Ophthalmology, College of Medicine Professor of Physiology, College of Medicine Member, Harold Hamm Diabetes Center U. of Oklahoma Health Sciences Center Dean A. McGee Eye Institute 608 Stanton L. Young Blvd. DMEI PA-405 Oklahoma City, OK 73104	michael-elliott@ouhsc.edu Tel: 405-271-4019 Fax: 405-271-8128

C. Ross Ethier, PhD Lawrence L. Gellerstedt, Jr. and Mary Duckworth Gellerstedt Chair in Bioengineering Georgia Research Alliance Eminent Scholar in Biomechanics and Mechanobiology Professor of Biomedical Engineering Wallace H. Coulter Department of Biomedical Engineering at Georgia Institute of Technology & Emory University School of Medicine IBB, 315 Ferst Drive, Room 2306 Atlanta, GA 30332-0363	ross.ethier@bme.gatech.edu Tel: 404.385.0100 Fax: 404.385.1397 www.bme.gatech.edu/bme/faculty/C.%20Ross-Ethier
Raymond Fang, MD/PhD candidate Northwestern University Biomedical Engineering 2145 Sheridan Rd, Tech E310 Evanston, IL 60208	raymond.fang@northwestern.edu Tel: 713-259-9731
Ronald Fellman, MD Glaucoma Associates of Texas 10740 N Central Expy #300, Dallas, TX 75231	rfellman@aol.com
Haiyan Gong, MD, PhD Professor of Ophthalmology, Anatomy and Neurobiology Boston University Chobanian & Avedisian School of Medicine 72 East Concord St., Rm L905 Boston, MA 02118	haiyan.gong@gmail.com Tel: 617-358-2213
Samuel Herberg, PhD Assistant Professor Dept. of Ophthalmology and Visual Sciences SUNY Upstate Medical University Center for Vision Research 505 Irving Ave., NRB 4609 Syracuse, NY 13210	herbergs@upstate.edu Tel: 315-464-7773 www.upstate.edu/cvr/investigators/ twitter.com/sherberg128
Alireza Karimi, PhD Assistant Professor Department of Ophthalmology Casey Eye Institute Oregon Health and Science University 3215 SW Pavilion Loop Portland, OR, 97239	karimi@ohsu.edu Tel: 503-494-8455, office Tel: 402-810-1305, mobile

Paul Kaufman, MD Ernst H. Barany Professor of Ocular Pharmacology Dept. of Ophthalmology & Visual Sciences School of Medicine & Public Health University of Wisconsin-Madison 600 Highland Ave., CSC K4/430 Madison, WI 53792-4673	kaufmanp@mhub.ophth.wisc.edu Tel: 608-263-6074 Fax: 608-263-0543
Kate Keller, PhD Prof. of Ophthalmology School of Medicine Graduate Faculty Program in Molecular and Cellular Biosciences Oregon Health & Science University Portland, OR 97239	gregorka@ohsu.edu Tel: 503-494-2366
Mary Kelley, PhD Casey Eye Institute Oregon Health & Science University 3181 SW Sam Jackson Park Rd. Portland, OR 97239	kelleyma@ohsu.edu Tel: 503-494-3594, office Tel: 503-312-5753, mobile
Ruth A. Kelly, PhD Postdoctoral Research Associate Stamer Lab, Duke Eye Center	ruth.kelly@duke.edu Tel: 919-681-1517, lab
Krish Kizhatil, PhD The Jackson Lab 600 Main St. Bar Harbor, ME 04609	Krish.kizhatil@jax.org Tel: 207-288-6000 https://www.jax.org/research-and-faculty/faculty/research-scientists/krish-kizhatil
Casey Kopczynski, PhD Senior Scientific Advisor 4301 Emperor Boulevard Suite 400 Durham, NC, 27703	casey.kopczynski@alcon.com Tel: 919-237-5341, office Tel: 919-593-6575, Mobile www.alcon.com
David Krizaj, PhD John Frederick Carter Endowed Professor in Ophthalmology University of Utah 65 Mario Capecchi Dr. Salt Lake City, UT 84132	david.krizaj@hsc.utah.edu Tel: 801-213-2777, office Tel: 801-213-2775, lab Fax:801-587-8314 www.krizajlab.vision.utah.edu

Markus H. Kuehn, PhD Prof, Dept. Ophthalmology and Visual Sciences Assoc. Director, Iowa City VA Center for Prevention and Treatment of Visual Loss The University of Iowa 3135 MERF 375 Newton Rd. Iowa City, IA 52242	markus-kuehn@uiowa.edu Tel: 319-335-9565, office Tel: 319-335-7537, lab Fax: 319-335-6641 https://myweb.uiowa.edu/kuehnm
Hoi-Lam Li, PhD Postdoctoral Associate Ophthalmology, Boston University Chobanian & Avedisian School of Medicine, Boston, MA, USA 72 East Concord Street Room L-905 Boston, MA 02118, USA	hli3@bu.edu Tel: 857-204-0943 Whatsapp: 852-5162-2556
Raquel Lieberman, PhD Professor SEPCIC-PFIEL Endowed Chair Georgia Institute of Technology Office: IBB 1308 901 Atlantic Drive NW Atlanta, GA 30332	raquel.lieberman@chemistry.gatech.edu Tel: 404-385-3663 Fax: 404-894-2295 https://lieberman.chemistry.gatech.edu/ https://chemistry.gatech.edu/people/raquel-lieberman
Raymond John Lim, PhD Senior Scientist II Abbvie Ophthalmology Discovery Research 2525 Dupont Dr. RD3-2D Irvine, CA 92612	raymond.lim@abbvie.com Tel: 714-246-4185 www.abbvie.com
Shan Lin, MD Glaucoma Center of San Francisco 55 Stevenson Street San Francisco, CA 94105	sl@glaucomasf.com
Paloma Liton, PhD Associate Professor Dept. of Ophthalmology Duke University 2352 Erwin Rd. Durham, NC 27705	paloma.liton@duke.edu

Yutao Liu, PhD, FARVO Professor Dept. of Cellular Biology and Anatomy Medical College of Georgia at Augusta University Augusta, GA 30912	yutliu@augusta.edu Tel: 706-721-2015
Rupalatha Maddala PhD Assistant Professor Dept of Ophthalmology 4028, AERI Building 2351 Erwin Rd. Duke University Medical Center Durham, NC 27710	madda001@mc.duke.edu Tel: 919-684-0557
Weiming Mao, PhD Associate Professor Jay C. and Lucile L. Kahn Scholar in Glaucoma Research and Education, Showalter Scholar Eugene and Marilyn Glick Eye Institute Dept. of Ophthalmology Dept. of Biochemistry & Molecular Biology Dept. of Pharmacology and Toxicology Indiana University School of Medicine RM305V, 1160 W. Michigan St, Indianapolis, IN, 46202	weimmao@iu.edu Tel: 317-278-0801
Gillian McClellan, PhD Dept. of Surgical Sciences and Dept. of Ophthalmology and Visual Sciences University of Wisconsin-Madison Madison, WI, 53706, USA	gillian.mclellan@wisc.edu
Fiona McDonnell, PhD Assistant Professor John A. Moran Eye Center Room S6871 University of Utah Salt Lake City, UT 84132	fiona.mcdonnell@utah.edu Tel: 801-585-7934 www.fionasmcdonnell.com

Colleen McDowell, PhD Assistant Professor William and Phyllis Huffman Research Professor Dept. of Ophthalmology and Visual Sciences University of Wisconsin-Madison 3375A Medical Sciences Center 1300 University Ave Madison, WI 53706	cmmcdowell@wisc.edu Tel: 608-265-3996
Philip Mzyk, PhD Senior Research Associate Stamer Lab Duke Eye Center Duke Ophthalmology 2351 Erwin Road Box 3802 Durham, NC, 27705	philip.mzyk@duke.edu Tel: 919-681-0234, Lab
Sai Nair, PhD Associate Professor Department of Ophthalmology School of Medicine University of California, San Francisco 10 Koret Way San Francisco, CA 94143	saidas.nair@ucsf.edu Tel: 415-476-0461
Donna M. Peters, PhD Professor Department of Pathology & Laboratory Medicine U. of Wisconsin School of Public Health & Medicine Madison, WI	dmpeter2@wisc.edu Tel: 608-262-4626
Vansanth Rao, PhD Richard and Kit Barkhouser Distinguished Professor Professor in Pharmacology and Cancer Biology, and Ophthalmology and Visual Sciences (OVS) Box 3802 Medical Center Durham, NC 27710	p.rao@duke.edu Tel: 919-681-5883 https://dukeeyecenter.duke.edu/research/laboratory-research/laboratory-leaders/rao-laboratory
Ester Reina-Torres, PhD Dept. of Bioengineering Imperial College London, UK	e.reina-torres12@imperial.ac.uk

Gavin W. Roddy, MD, PhD Assistant Professor of Ophthalmology Glaucoma Service Mayo Clinic, Rochester, MN	roddy.gavin@mayo.edu Tel: 817-613-6206, mobile
Chris N. Rudzitis, PhD candidate Graduate Research Assistant Krizaj Lab John A. Moran Eye Center University of Utah 65 Mario Capecchi Drive Salt Lake City, UT 84132	u1205245@utah.edu
John Samples, MD Western Glaucoma Foundation 1910 4th Ave., E., PMB 264 Olympia, WA 98506-4632	glaucoma@gmail.com Tel: 303-505-0776, mobile
Myounsup Sim, PhD Senior Research Associate Duke University Liton Lab Durham, NC	myoungsup.sim@duke.edu
Ayushi Singh, MS, PhD candidate Department of Ophthalmology and Visual Sciences SUNY Upstate Medical University Center for Vision Research 505 Irving Avenue, NRB 4631 Syracuse, NY 13210	SinghAy@upstate.edu Tel: 407-371-7293
W. Daniel Stamer, PhD, FARVO Joseph A. C. Wadsworth Professor of Ophthalmology Professor of Biomedical Engineering Duke University *Courier Deliveries Only*: AERI Room 4000 2351 Erwin Rd Durham, NC 27705	dan.stamer@duke.edu Tel: 919-684-3745, office Tel: 919-681-1566, lab

Cynthia Steel, PhD, MBA Director of Global Medical Affairs Glaukos Corporation One Glaukos Way Aliso Viejo, CA 92656	csteel@glaukos.com Tel: 813-459-9638, mobile www.glaukos.com
M. Fernanda Suarez, PhD Stamer Lab Duke University Durham, NC	maria.suarez523@duke.edu
Preeti Subramanian, PhD Director of Scientific Programs, Vision Science BrightFocus Foundation 22512 Gateway Center Drive Clarksburg, MD 20871	psubramanian@brightfocus.org Tel: 301-556-9359 www.brightfocus.org
Benjamin Thomson, PhD Assistant Professor of Ophthalmology Northwestern University Feinstein School of Medicine 259 E. Erie St., Suite 1520 Chicago, IL, 60611	benjamin.thomson@northwestern.edu Tel: 312-292-8691
Carol B. Toris, PhD Professor, Havener Eye Institute Dept. of Ophthalmology and Visual Sciences The Ohio State University Wexner Medical Center 915 Olentangy River Rd, Suite 3010B Columbus, OH 43212	carol.toris@osumc.edu ctoris@unmc.edu carol.toris@osumc.edu
Judith West-Mays, PhD Professor Dept. of Pathology and Molecular Medicine Asst. Dean, Medical Sciences Graduate Program McMaster University 1200 Main St. West, HSC Rm 4H17 Hamilton, Ontario, Canada, L8N 3Z5	westmayj@mcmaster.ca Tel: 905-525-9140 x26237 Fax: 905-525-7400
Colin Willoughby, MD, PhD School of Biomedical Sciences Ulster University, Coleraine Campus Room W1033, Cromore Rd., Coleraine, Co. Londonderry, PT52 1SA Northern Ireland	c.willoughby@ulster.ac.uk Tel: +44-38-7012-3381

Hao Zhang, PhD Professor of Biomedical Engineering McCormick School of Engineering Northwestern University Tech M335 2145 Sheridan Rd. Chicago, IL 60208-3107	hzhang@northwestern.edu Tel: 847-491-2946, Office Tel: 847-491-7167, Lab Fax: 847-491-4928 Twitter: @visibleOCT
Steven Zhang, MD, PhD EVP Medical Affairs & Pharmacovigilance Théa Pharma Inc 303 Wyman St, Suite 205 Waltham, Massachusetts 02451 United States	steven.zhang@theapharma.com Tel: +01 781-816-5011, office Tel: +01 626-476-0261, mobile Fax: +01 781-816-5019 www.theapharmainc.com